

**TARGETING THE TUMOUR MICROENVIRONMENT:
CHARACTERIZING THE ANTI-VASCULAR EFFECTS OF
THE HYPOXIC CYTOTOXIN TIRAPAZAMINE**

by

JENNIFER HAZEL ELIZABETH BAKER

B.Sc., Simon Fraser University, 2004

A THESIS SUBMITTED IN PARTIAL FULFILLMENT OF THE REQUIREMENTS FOR
THE DEGREE OF

DOCTOR OF PHILOSOPHY

in

THE FACULTY OF GRADUATE STUDIES

(Interdisciplinary Oncology)

THE UNIVERSITY OF BRITISH COLUMBIA
(Vancouver)

March 2010

© Jennifer Hazel Elizabeth Baker, 2010

ABSTRACT

Tirapazamine (TPZ) is a bioreductive prodrug with greater toxicity to hypoxic cells *in vitro*, and anti-vascular activity in tumours grown *in vivo* in mice. Considerable inter- and intra-tumour heterogeneity occurs in response to the anti-vascular effects of TPZ. The main hypothesis for the work described in this thesis is that features of the tumour microenvironment confer tumour sensitivity to TPZ-mediated vascular dysfunction.

Tumours exhibiting less sensitivity to the anti-vascular effects of TPZ had evidence of greater pre-treatment vascular function, including greater blood flow or permeability measured using DCE-MRI derived biomarkers and tumour mapping data of high molecular weight fluorescent dyes injected intravenously. Modulation of nitric oxide (NO) levels decreased the density of perfused blood vessels and sensitized tumours to the anti-vascular effects of TPZ. Additional vascular phenotype features such as relatively poor vascular maturity were also found to correlate with greater tumour sensitivity to TPZ-mediated vascular dysfunction.

Greater toxicity of TPZ to hypoxic cells *in vitro* led to the hypothesis that blood oxygenation may have an impact on tumour sensitivity to TPZ-mediated vascular dysfunction *in vivo*. Tumours from mice that had moderate bleeding-induced anemia or that were breathing lowered (7-10%) oxygen were sensitized to the anti-vascular effects of TPZ. *In vitro* assays showed that human microvascular tube structures are sensitive to damage by TPZ at clinically relevant concentrations and oxygen levels.

TPZ may be reduced by cellular nitric oxide synthase (NOS), and NOS is competitively inhibited by TPZ to result in decreased amounts of NO. Enhanced anti-cancer effects have previously been observed for other vascular disrupting agents (VDAs) and hypoxic cytotoxins when combined with NOS inhibitors. These findings led to studies presented in this thesis, which show that TPZ-mediated vascular dysfunction is enhanced by co-administration with a NOS inhibitor, and this combined activity can lead to reduced cancer growth.

Results from this thesis suggest that features of the tumour microenvironment, including tumour vascular phenotype, blood oxygenation and tumour hypoxia impact tumour sensitivity to TPZ-mediated vascular dysfunction. In addition, inhibiting NOS in combination with TPZ is a therapeutically advantageous strategy that merits further investigation.

TABLE OF CONTENTS

ABSTRACT	ii
TABLE OF CONTENTS	iii
LIST OF TABLES	vi
LIST OF FIGURES	vii
LIST OF ABBREVIATIONS	ix
ACKNOWLEDGEMENTS	xiii
CO-AUTHORSHIP STATEMENT	xiv

CHAPTER 1 1

1.1 INTRODUCTION.....	2
1.2 TPZ AS A HYPOXIC CYTOTOXIN.....	4
1.3 TPZ HAS ANTI-VASCULAR ACTIVITY <i>IN VIVO</i>	6
1.4 TUMOUR HYPOXIA.....	8
1.5 HYPOXIC VASCULATURE IN TUMOURS.....	9
1.6 ABNORMAL TUMOUR BLOOD VESSELS.....	11
1.7 VASCULAR DISRUPTING AGENTS (VDAs).....	13
1.8 COMBINING NOS INHIBITION WITH HYPOXIC CYTOTOXINS AND VASCULAR TARGETING AGENTS.....	15
1.9 THESIS OVERVIEW	19
1.9.1 Research hypothesis and objectives.....	20
1.10 CHAPTER SUMMARIES	21
1.10.1 Chapter 2 summary - Detecting vascular-targeting effects of the hypoxic cytotoxin tirapazamine in tumour xenografts using magnetic resonance imaging.....	21
1.10.2 Chapter 3 summary – Decreased blood oxygen tension sensitizes tumours to the anti- vascular effects of tirapazamine.....	22
1.10.3 Chapter 4 summary – Inhibition of nitric oxide synthase enhances tirapazamine- mediated vascular dysfunction in pre-clinical tumours.....	23
1.11 IMPACT OF THE RESEARCH	24
1.12 REFERENCES	26

CHAPTER 2 31

2.1 INTRODUCTION	32
2.1.1 Tirapazamine (TPZ) as a hypoxic cytotoxin with anti-vascular activity	32
2.1.2 Dynamic Contrast Enhanced Magnetic Resonance Imaging (DCE-MRI).....	32
2.1.3 Current study outline	33
2.2 METHODS.....	35
2.2.1 Mice, fiducial markers and tumours	35
2.2.2 Treatments.....	36
2.2.3 DCE-MRI	36
2.2.4 Immunohistochemical staining and image acquisition.....	36
2.2.5 Image analysis.....	37

2.2.6	Scoring vascular dysfunction response.....	37
2.2.7	DCE-MRI analysis	40
2.2.8	Radial analysis.....	40
2.2.9	Statistics	41
2.3	RESULTS	42
2.3.1	Histological analysis identifies tumours with an increase in necrosis or a decrease in perfusion in response to TPZ	42
2.3.2	BrdUrd data not included	45
2.3.3	DCE-MRI analysis shows decreases in IAUC and K^{trans} for TPZ-treated tumours with central vascular dysfunction	46
2.3.4	Microregional heterogeneity of response to TPZ	48
2.4	DISCUSSION.....	51
2.4.1	DCE-MRI parameters IAUC and K^{trans}	51
2.4.2	Analysis of DCE-MRI and histological images.....	52
2.4.3	Pre-treatment perfusion as indicator of non-response	53
2.5	CONCLUSIONS	55
2.6	REFERENCES	56
CHAPTER 3		58
3.1	INTRODUCTION.....	59
3.1.1	Tirapazamine (TPZ) as a hypoxic cytotoxin with anti-vascular activity	59
3.1.2	Tumour vasculature as a target for TPZ	59
3.2	METHODS	61
3.2.1	Mice and tumours	61
3.2.2	Treatments	61
3.2.3	Immunohistochemistry (IHC)	62
3.2.4	Image acquisition and analysis	62
3.2.5	Vascular Dysfunction Score (VDS).....	63
3.2.6	Endothelial Tube Assay	63
3.2.7	Statistics.....	64
3.3	RESULTS	64
3.3.1	HT29 colorectal xenograft tumours are resistant to vascular dysfunction effects of TPZ.....	64
3.3.2	Microenvironmental differences between HCT116 and HT29 colorectal xenografts ...	67
3.3.3	Differences in vascular permeability between HCT116 and HT29 colorectal xenografts	69
3.3.4	Differences in vascular phenotype between HCT116 and HT29 colorectal xenografts	69
3.3.5	10% O ₂ breathing or induction of anemia enhances the anti-vascular effects of TPZ in HCT116 colorectal xenografts	73
3.3.6	7% O ₂ breathing enhances the anti-vascular effects of TPZ in HT29 colorectal xenografts	76
3.3.7	Tirapazamine mediates damage to endothelial tube structures <i>in vitro</i> in a time, concentration and oxygen-dependent manner.....	76
3.4	DISCUSSION.....	78
3.4.1	Tumour vasculature and TPZ sensitivity.....	78
3.4.2	Tumour hypoxia and TPZ sensitivity	79
3.5	CONCLUSIONS	81
3.6	REFERENCES	82

CHAPTER 4	85
4.1 INTRODUCTION.....	86
4.1.1 Tirapazamine (TPZ) as a hypoxic cytotoxin with anti-vascular activity <i>in vivo</i>	86
4.1.2 TPZ reduced by Nitric Oxide Synthase (NOS).....	86
4.2 METHODS	88
4.2.1 Reagents	88
4.2.2 Mice and tumours	88
4.2.3 Immunohistochemistry	89
4.2.4 Image acquisition and overlay	89
4.2.5 Image analysis.....	89
4.2.6 Vascular Dysfunction Score (VDS).....	90
4.2.7 Statistics.....	91
4.3 RESULTS	92
4.3.1 L-NNA enhances TPZ-mediated vascular dysfunction in HCT116 xenografts	92
4.3.2 Excess NO enhances the vascular dysfunction effects of TPZ in HCT116 xenografts	95
4.3.3 Decrease in proliferating cells in response to NOS inhibition in combination with TPZ	97
4.3.4 L-NNA enhances growth inhibition effects of TPZ in HCT116 xenografts.....	98
4.3.5 L-NNA enhances the vascular dysfunction effects of TPZ in SCCVII murine but not in HT29 xenografts.....	99
4.3.6 L-NNA and spermine NONOate effects on hypoxia in colorectal xenografts	103
4.3.7 Differential NOS expression in colorectal xenografts that are sensitive (HCT116) and resistant (HT29) to TPZ mediated vascular dysfunction.....	104
4.4 DISCUSSION.....	106
4.4.1 Effects of NO modulation in tumours	106
4.4.2 Hypothesis for role of NOS in mechanism for TPZ mediated vascular dysfunction ...	108
4.4.3 Bioreductive hypoxic cytotoxic targeting of tumour vasculature enhanced by NOS inhibition	110
4.5 CONCLUSIONS	111
4.6 REFERENCES	112
CHAPTER 5	114
5.1 RESEARCH HYPOTHESIS.....	115
5.2 ASSESSING THE ANTI-VASCULAR EFFECTS OF TPZ.....	115
5.3 TUMOUR BLOOD VESSELS – IMPACT ON SENSITIVITY TO TPZ.....	119
5.4 HYPOXIA – IMPACT ON SENSITIVITY TO TPZ.....	120
5.5 NO - IMPACT ON SENSITIVITY TO TPZ	123
5.6 CONCLUSIONS	125
5.7 REFERENCES	127
APPENDIX	129
A LIST OF PUBLICATIONS	129
B BIOHAZARD APPROVAL CERTIFICATE B06-0187	132
C ANIMAL CARE CERTIFICATE A06-1454	133
D ANIMAL CARE CERTIFICATE A07-0404	134

LIST OF TABLES

CHAPTER 3

Table 3.1 TPZ-mediated vascular dysfunction in HT29 and HCT116 colorectal xenografts.....	67
Table 3.2 Impact of modulation of blood oxygenation on TPZ-mediated vascular dysfunction in HCT116 and HT29 colorectal xenografts.....	74

CHAPTER 4

Table 4.1 Impact of modulation of NO on TPZ-mediated vascular dysfunction in HCT116 colorectal xenografts	93
Table 4.2 Impact of NOS inhibition on TPZ-mediated vascular dysfunction in SCCVII and HT29 tumours.	100

LIST OF FIGURES

CHAPTER 1

Figure 1.1 Hypoxic cells in the tumour microenvironment.	3
Figure 1.2 Model for TPZ metabolism.	4
Figure 1.3 Vascular dysfunction visualized using tumour mapping.	8
Figure 1.4 NO synthesized by nitric oxide synthase (NOS).	16

CHAPTER 2

Figure 2.1 Experiment overview.	34
Figure 2.2 Fiducial markers.	35
Figure 2.3 Rationale for combined Vascular Dysfunction Score (VDS).	39
Figure 2.4 Compartmental modeling of DCE-MRI contrast agent	41
Figure 2.5 DCE-MRI and histological parameter maps of HCT116 tumour	43
Figure 2.6 DCE-MRI and histological parameter maps of HCT116 tumour	44
Figure 2.7 Tirapazamine-mediated changes in vascular function measured using histological analysis.	45
Figure 2.8 Tirapazamine-mediated changes in vascular function measured using DCE-MRI parameters IAUC and K^{trans}	47
Figure 2.9 Tumour mapping microregional heterogeneity in response to TPZ.	48
Figure 2.10 MRI microregional heterogeneity in response to tirapazamine.	49
Figure 2.11 Correlation of MRI and histology features.	50

CHAPTER 3

Figure 3.1 HT29 and HCT116 colorectal xenograft sensitivity to anti-vascular effects of TPZ.	65
Figure 3.2 HT29 tumour maps.	66
Figure 3.3 Tumour microenvironment of HCT116 and HT29 colorectal xenografts.	68
Figure 3.4 Vascular function in HCT116 and HT29 colorectal xenografts.	70
Figure 3.5 CD31 and α SMA staining in HCT116 and HT29 colorectal xenografts.	71
Figure 3.6 CD31 and Collagen Type IV (CIV) staining in HCT116 and HT29 colorectal xenografts.	72
Figure 3.7 Modulation of tumour hypoxia in HCT116 and HT29 colorectal xenografts.	74
Figure 3.8 Hypoxia enhances anti-vascular effects of TPZ in HCT116 and HT29 xenografts.	75
Figure 3.9 TPZ mediates damage to endothelial tube structures in a concentration, time and oxygen dependent manner.	77

CHAPTER 4

Figure 4.1 NOS inhibition enhances anti-vascular effects of TPZ in HCT116 tumours; quantitative data.....	93
Figure 4.2 NOS inhibition enhances anti-vascular effects of TPZ in HCT116 tumours; tumour maps.....	94
Figure 4.3 Excess NO enhances anti-vascular effects of TPZ in HCT116 tumours.	96
Figure 4.4 Decrease in S-phase cells when TPZ combined with NO modulation.	97
Figure 4.5 Inhibition of NOS by L-NNA enhances the growth inhibition effects of TPZ in HCT116 tumours.	98
Figure 4.6 NOS inhibition enhances the anti-vascular effects of TPZ in SCCVII tumours.	101
Figure 4.7 NOS inhibition does <i>not</i> enhance anti-vascular effects of TPZ in HT29 tumours.....	102
Figure 4.8 Modulation of NO effects on hypoxia in HCT116 and HT29 tumour	103
Figure 4.9 NOS expression variation between HCT116 and HT29 tumour	105

LIST OF ABBREVIATIONS

α SMA	alpha smooth muscle actin
BrdUrd	5-bromo-2-deoxy-uridine
BTZ	benzotriazine
Ca ²⁺	calcium
CA-4-P	combretastatin-A-4-phosphate
CFU	colony forming units
CIV	collagen type IV
CO ₂	carbon dioxide
DAB	diamino benzidine
DCE-MRI	dynamic contrast enhanced magnetic resonance imaging
DMSO	di-methyl sulfoxide
DMXAA	5,6-dimethylxanthenone-4-acetic acid
DNA	deoxy-ribonucleic acid
ECM	extra-cellular matrix
EF5	2-(2-nitro-1H-imidazol-1-yl)-N-(2,2,3,3,3-pentafluoropropyl)acetamide
EGF	epidermal growth factor
eNOS	endothelial nitric oxide synthase
ETC	electron transport chain
FBS	foetal bovine serum
FITC	fluorescein isothiocyanate
FLASH	fast low-angle shot sequence

Gd-DTPA	gadolinium-diethylene-triamine-penta-acetate
H ₂ O	water
H ₂ O ₂	hydrogen peroxide
HbO ₂	hemoglobin saturation
HER2	human epidermal growth factor receptor 2
HI	heterogeneity index
HMEC	human microvascular endothelial cell
IAUC	initial area under the concentration time curve
IDL	interactive data language
IFP	interstitial fluid pressure
IHC	immunohistochemistry
iNOS	inducible nitric oxide synthase
i.p.	intraperitoneal
i.v.	intravenous
kDa	kilo dalton
K ^{trans}	volume transfer coefficient
L-NNA	N-omega-nitro-L-arginine
MAb	monoclonal antibody
MCDB-131	molecular cellular developmental biology
MEM/EBSS	minimum essential media with Earle's balanced salts solution
min	minutes
MRI	magnetic resonance imaging
N ₂	nitrogen

NaCl	sodium chloride
NADPH	nicotinamide adenine dinucleotide phosphate
NaOH	sodium hydroxide
NIH	national institutes of health
nNOS	neural nitric oxide synthase
NO	nitric oxide
NOD/SCID	non-obese diabetic/severe combined immunodeficient
NOS	nitric oxide synthase
O ₂	oxygen
O ₂ • ⁻	superoxide radical
OH	hydroxyl
OH•	hydroxyl radical
PAb	polyclonal antibody
PDT	photodynamic therapy
PECAM (CD31)	platelet/endothelial cell adhesion marker
PET	positron emission tomography
PF	perfused fraction
pO ₂	partial pressure of oxygen
RBC	red blood cell
ROS	reactive oxygen species
s.c.	subcutaneous
SD	standard deviation
s.e.	standard error

SOD	superoxide dismutase
TPZ	tirapazamine
TR	repetition time
uNOS	universal nitric oxide synthase
VDA	vascular disrupting agent
VDS	vascular dysfunction score
VF	viable fraction
VEGF	vascular endothelial growth factor
VTA	vascular targeting agent

ACKNOWLEDGEMENTS

I would like to thank my supervisor Dr. Andrew Minchinton for providing me with the opportunity to pursue graduate school and for creating a fantastic laboratory and working environment. It is truly a pleasure coming to the lab every day, and I am so grateful.

Thank you to Dr. Alastair Kyle for building so many useful things and for always having insightful, cheerful advice. Thank you to Dr. Lynsey Huxham for guidance, making tirapazamine and for doing great work with tirapazamine prior to this project. Alastair and Lynsey have been wonderful mentors and I greatly appreciate their impact on my research and experience as a graduate student.

Many thanks to the undergraduate co-op students who have participated on this project or who have been involved in the Minchinton laboratory: Kirsten Bartels, Erin Flanagan, Stephen Methot, Firas Moosvi, Andrew Balbirnie, Melissa Woodward, Erin Gabriel and Jordan Cran. Thanks also to Kirstin Lindquist, a fellow graduate student at *aimLab*.

Thank you to Dr. Stefan Reinsberg and Lauren Bains who provided expertise and contributed much of the work with DCE-MRI. Thank you to my supervisory committee Drs. Marcel Bally, Aly Karsan and Sylvia Ng for helpful comments, advice and encouragement. Special thanks to Dr. Ng for her thorough reading of this thesis. Thank you also to Dr. Don Yapp for useful imaging advice and collaborations. Thank you to Wil Cottingham for always being so helpful and supportive, to the department of Medical Biophysics for general support and encouragement, and to the many other BC Cancer graduate students who have become friends.

Finally, I owe a huge thank you to my wonderful family and great friends who have been so important in my motivation and ability to do this work. You have been so patient, supportive and above all enthusiastic - I am so very grateful! Special mention to my loving parents Brian & Janette, my wonderful husband Mark, my awesome siblings Melissa & Simon, and to Courtney, Hugh, *et al.*

Financial support for my graduate work was provided by a senior graduate studentship from the Michael Smith Foundation for Health Research. I have also been the grateful recipient of travel awards from the American Association of Cancer Research, the Tumour Microenvironment Society, the Interdisciplinary Oncology Program, and the European School of Hematology.

CO-AUTHORSHIP STATEMENT

CHAPTER 2

A version of this chapter has been published:

Bains* LJ, Baker* JHE, Kyle AH, Minchinon AI and Reinsberg SA. (2009). International Journal of Radiation Oncology Biology Physics 74 (3) pp. 957-965. (*Bains and Baker are co-first authors of this publication).

Author contributions: **Baker JHE** designed and carried out experiments and wrote 50% of the manuscript including designing and creating figures. **Bains LJ** designed and carried out experiments and wrote 20% of the manuscript; parts of this work contributed to the MSc work of LBains. **Kyle AH** designed and built the robotic microscope and image analysis software. **Minchinton AI** is the principal investigator and supervisor of JBaker and AKyle, and contributed in experiment design, data interpretation and editing of the manuscript. **Reinsberg SA** is the principal investigator and supervisor of LBains, and contributed by designing and carrying out experiments and writing 30% of the manuscript.

CHAPTER 3

A version of this chapter has been submitted for publication and is under review.

Author list: Baker JHE, Kyle AH, Flanagan E, Methot S, Bartels K and Minchinton AI.

Author contributions: **Baker JHE** designed and carried out all the experiments, performed all data analysis and interpretation of results, and authored 100% of the manuscript including design and creation of figures. **Kyle AH** designed and built the robotic microscope and image analysis software. **Flanagan E**, **Methot S** and **Bartels K** were all undergraduate student assistants who helped carry out mouse handling and histological processing for experiments. **Minchinton AI** is the principal investigator and supervisor of all the authors in this manuscript.

CHAPTER 4

A version of this chapter will be submitted for publication.

Author list: Baker JHE, Kyle AH, Balbirnie A, Gabriel E, Cran J and Minchinton AI.

Author contributions: **Baker JHE** designed and carried out all the experiments in this paper, performed all data analysis and interpretation of results, and authored 100% of the manuscript including design and creation of figures. **Kyle AH** designed and built the robotic microscope and image analysis software. **Balbirnie A, Gabriel E** and **Cran J** were all undergraduate assistants who helped carry out mouse handling and histological processing for experiments. **Minchinton AI** is the principal investigator and supervisor of all other authors in this manuscript.

Please see Appendix A for a complete list of publications by Jennifer H.E. Baker.

CHAPTER 1

Introduction

1.1 Introduction

The treatment of cancer relies on three principal strategies: surgery, radiotherapy and chemotherapy. Localized tumours may often be effectively treated with one or a combination of these strategies, but eradication of occult metastases must be achieved by systemically administered chemotherapies. Most anti-cancer chemotherapies work by killing cells that are rapidly dividing, and are described as cytotoxic anti-proliferative drugs. Other, normal tissues of the body such as the bone marrow, hair follicles and epithelial cells lining the gastrointestinal tract also have rapidly proliferating cells, therefore cytotoxic anti-proliferatives can lead to dose-limiting side effects (Tannock 1998). Considerable drug development efforts have therefore shifted from broad-spectrum, poorly selective cytotoxic anti-proliferative drugs towards more cancer-specific, targeted treatments that should have an improved therapeutic index.

While targeted treatment strategies continue to be developed for cancer-specific proteins at the molecular and cellular level, there are also tissue level or pathophysiological, cancer-specific features that may be targeted for therapy (Brown and Giaccia 1998). In addition to cancer cells, tumours may contain blood, immune cells, fibroblasts and cells that make up the tumour vasculature, all of which are collectively described as the tumour stroma. A solid tumour therefore contains a mix of cancer cells, stromal cells, non-cellular material such as ECM, and soluble signaling molecules. These individual components may be abnormal relative to healthy tissues, and their organization is highly heterogeneous. Microregional variations in tumour components result in subpopulations of cells that may be described based on their location within the tumour microenvironment. For example, tumour microenvironments may have a varying availability of nutrients, oxygen and signaling molecules, as well as a distinct local pH, interstitial fluid pressure or reducing environments (Vaupel *et al.* 1989; Brown and Giaccia 1998; Dewhirst 2003). Figure 1.1 shows tissue from a human colorectal carcinoma xenograft where the inter-vessel distances cause cells distal to the vasculature to become hypoxic (shown in green).

The purpose of work presented in this thesis is to investigate the mechanism for activity of an experimental targeted anti-cancer agent, tirapazamine (TPZ), which has greater toxicity in conditions of low oxygen and is therefore described as a *hypoxic cytotoxin*. TPZ is

in clinical trials for the treatment of various cancers including head and neck, lung and cervical cancers alone or in combination with radiotherapy or chemotherapy (Marcu and Olver 2006; Reddy and Williamson 2009). While the principal mechanism for tissue-level targeted toxicity of TPZ to tumours is thought to be its selective activation in hypoxic cells, TPZ has also been observed to damage tumour blood vessels *in vivo* (Huxham *et al.* 2006; Huxham *et al.* 2008). The mechanism for TPZ-mediated vascular dysfunction in solid tumours is the subject of this thesis, where features of the tumour microenvironment such as hypoxia and blood vessels are investigated for their impact on tumour sensitivity to the anti-vascular effects of TPZ.

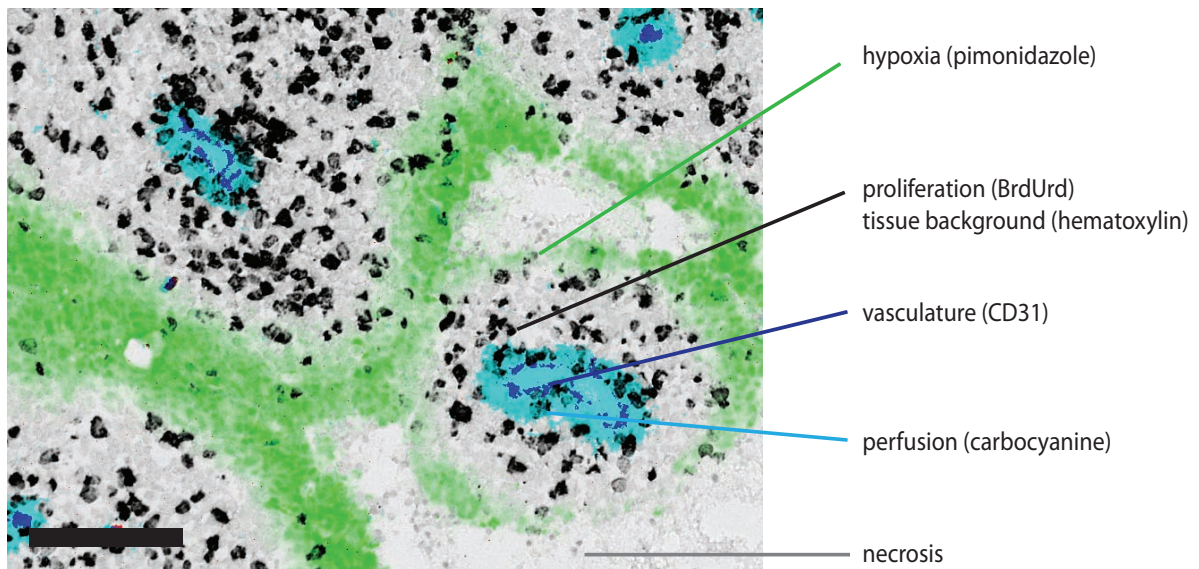


Figure 1.1 Hypoxic cells in the tumour microenvironment.

In this HCT116 human colorectal xenograft model the tumour cells are arranged around blood vessels in a corded structure. Staining illustrates vasculature (blue) labeled with perfusion marker (cyan) surrounded by tumour cells stained lightly with hematoxylin (grey), some of which are labeled for incorporated BrdUrd as an indicator of S-phase (black). At distances far from vasculature cells label positively for pimonidazole (green), a bioreductive marker of hypoxia, before becoming necrotic at distances greater than the diffusion limit of oxygen. Scale bar 150 μm .

1.2 TPZ as a hypoxic cytotoxin

Tirapazamine (TPZ; SR 4233; 3-amino-1,2,4-benzotriazine-1,4-di-N-oxide; WIN 59075; Tirazone®) is a prodrug that is reduced and bioactivated by cellular, one-electron reductases and has greater toxicity to hypoxic cells *in vitro* (Zeman *et al.* 1986). Cytotoxic TPZ radical formation occurs at < 5 % oxygen and the toxicity of TPZ is oxygen dependent (Koch 1993). In the presence of oxygen, the reduced prodrug (TPZ•) is back oxidized to its parental form, producing superoxide ($O_2^{\bullet-}$) as a byproduct (Figure 1.2). Further metabolism of the TPZ• radical in the absence of oxygen yields additional reactive oxygen species that cause DNA damage. The radical intermediate responsible for mediating hypoxic cytotoxicity via topoisomerase II poisoning or DNA double strand breaks is thought to be a hydroxyl ($OH\bullet$) or benzotriazinyl oxidizing radical (BTZ•) (Anderson *et al.* 2005).

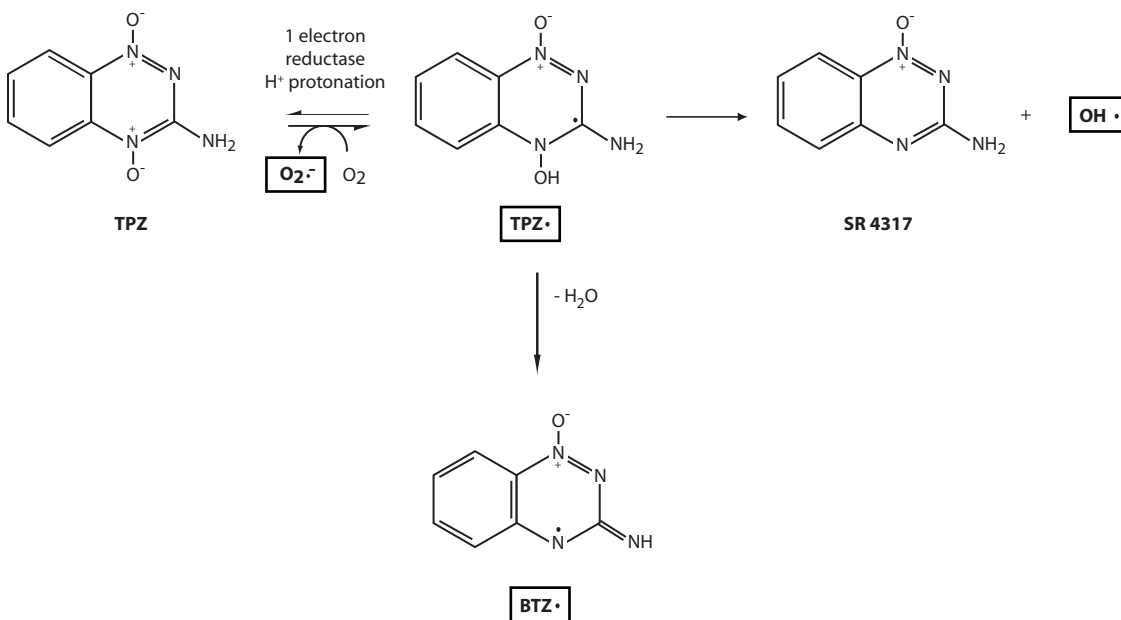


Figure 1.2 Model for TPZ metabolism.

A one electron reduction results in a TPZ radical (TPZ•) that may be back-oxidized to its original form (TPZ) in the presence of oxygen, producing a superoxide radical as a byproduct ($O_2^{\bullet-}$). In the absence of oxygen, TPZ• may further decay to produce oxidizing radicals $OH\bullet$ or BTZ•, either of which may effect DNA damage. Boxes highlight oxidizing radicals that may cause damage. Figure modified from (Siim *et al.* 2004; Anderson *et al.* 2005).

The *in vivo* efficacy of TPZ has typically been assessed using growth delay or clonogenic survival assays. Growth delay studies measure tumour volumes over time and assess if a treatment reduces the volume or rate of growth of tumours. Clonogenic survival assays involve harvesting tumours following treatment and dissociating the tissues to single cell suspensions that are then plated in culture. The number of detectable colonies after several days of growth in culture is a reflection of the number of cells recovered from the tumours that are capable of proliferating through several generations. Data from clonogenic survival studies may be described as the number of colonies per gram of tissue or per number of viable cells at time of plating. While both of these assays are capable of demonstrating anti-cancer activity, neither specifically confirm the microregional location or microenvironmental status of cells that were killed. Therefore, neither the growth delay nor the clonogenic assay are able to specifically confirm selective cytotoxicity of TPZ directly to *hypoxic tumour cells* as the mechanism for its anti-cancer activity *in vivo*.

Growth delay and clonogenic assays have been used to demonstrate that TPZ has anti-cancer effects *in vivo*. TPZ significantly enhances cell kill of both radiotherapy and cisplatin (Zeman *et al.* 1986; Brown and Lemmon 1990; Dorie and Brown 1993). Radiotherapy is effective at killing oxygenated cells, while hypoxic cells are more resistant by a factor of three and often survive to repopulate irradiated tumours (Gray, Conger *et al.* 1953). The synergistic activity of TPZ in combination with radiotherapy, where more cells are killed than with radiation alone, is therefore often attributed to complementary killing of radioresistant hypoxic cells by TPZ and is suggested as evidence of selective toxicity of TPZ to hypoxic cells *in vivo* (Zeman *et al.* 1986; Zeman *et al.* 1988; Brown and Lemmon 1990; Brown and Lemmon 1991). However, as described above, clonogenic survival studies are unable to provide specific detail regarding the microregional or microenvironmental location of cells that were killed. It is therefore an assumption that the cells killed by TPZ when combined with radiotherapy were killed by selective hypoxic cytotoxic activity, and an indirect effect such as vascular dysfunction cannot be excluded. Indeed vascular damage would not be anticipated in response to TPZ, as the tumour endothelium would typically be regarded as the most well oxygenated population of cells in a tumour due to their proximity to the blood supply, and specific investigations regarding an anti-vascular effect for hypoxic cytotoxins are not typically conducted.

Additional support for the hypothesis that TPZ kills hypoxic cells *in vivo* has been determined in experiments of low oxygen breathing in mice. Greater cell kill is achieved by TPZ when more cells within tumours are made hypoxic through low oxygen breathing (Sun and Brown 1989; Minchinton and Brown 1992a; Minchinton and Brown 1992b; Minchinton *et al.* 2002). Again, these data suggest that TPZ is more effective in hypoxic tumours, but were not able to specifically confirm selective toxicity to hypoxic *tumour cells* in lieu of an alternate mechanism such as indirect tumour cell kill via vascular damage.

While the above mentioned studies provide evidence of anti-cancer activity of TPZ *in vivo*, data from three dimensional tissue model systems such as spheroids (Durand and Olive 1992) and multi-layered cell cultures (Hicks *et al.* 1998; Kyle and Minchinton 1999) suggest that TPZ does not penetrate well through tissue and may be consumed at intermediate oxygen levels. In animal models, TPZ is delivered to the tumour by blood vessels and must distribute through tumour tissue to reach target hypoxic cells located far from the blood supply (Figure 1.1). The poor tissue penetration profile of TPZ suggests that it will have difficulty reaching hypoxic cells located far from vasculature at concentrations sufficient to be effective.

1.3 TPZ has anti-vascular activity *in vivo*.

Studies showing limited penetration of TPZ through multi-layered tissue culture models in the Minchinton laboratory at the BC Cancer Agency Research Centre led to the question of how TPZ has anti-cancer activity *in vivo* if it does not efficiently penetrate through tissue to reach hypoxic cells (Kyle and Minchinton 1999). The activity of TPZ *in vivo* was assessed using tumour mapping analysis whereby tumours grown subcutaneously in mice were excised for cryosectioning and staining at several time points following treatment. Layered immunohistochemical staining permits identification of cytotoxicity damaged tumour cells in the context of the tumour microenvironment, including the presence of hypoxia. A hypothesis of the tumour mapping studies was that TPZ would cause damage to hypoxic cells located far from vasculature. However, results showed a surprising effect whereby TPZ-treated HCT116 tumours had evidence of central vascular damage (Huxham *et al.* 2006). TPZ mediated vascular dysfunction was characterized as an irreversible loss of perfusion in the centre of tumours at 12-24 hours; by 48-72 hours large areas of necrosis develop. Blood vessels at the tumour periphery appear to be unaffected by TPZ, leaving a

viable rim of tumour tissue. TPZ-mediated vascular dysfunction effects are dose-dependent, with approximately 65 % of tumours responding at the near maximum tolerated dose of 60 mg/kg (0.34 mmol/kg) and the remaining 35 % of treated tumours showing no signs of central vascular dysfunction.

Vascular dysfunction detected by tumour mapping studies is illustrated in Figure 1.3. Hypoxia is labeled using immunohistochemical (IHC) staining for bound pimonidazole, a bioreductive marker that is administered by intraperitoneal (i.p.) injection 2 hours prior to tumour excision. Pimonidazole is reduced by reductases in areas of low oxygen and binds cellular proteins. The nucleotide analogue BrdUrd is co-administered with pimonidazole 2 hours prior to excision and labels S-phase cells. Vasculature is stained using antibodies for CD31 and perfused blood vessels are labeled with a fluorescent dye (DiOC₇(3); carbocyanine) injected intravenously 5 minutes prior to recovering the tumour. An HCT116 tumour with central vascular dysfunction (Figure 1.3B) shows unperfused vessels in the central regions, with tumour margins staining positive for vasculature, perfusion, proliferation and hypoxia. Because BrdUrd and pimonidazole are exogenously administered markers, negative staining in unperfused regions is likely to be an experimental artifact due to vascular dysfunction and consequent poor delivery of the agents. Mapping the entire tumour section using a custom-built robotic microscope enabled analysis of effects on whole tumours, whereas most IHC studies are typically limited to fewer markers and smaller microscope fields. Composite tumour map images of BrdUrd, pimonidazole, carbocyanine and CD31 create an easily identifiable visual representation of central vascular dysfunction in tumours, as shown in Figure 1.3.

Additional tumour models are also sensitive to the anti-vascular effects of TPZ. HCT116 tumours are characterized by relatively low vascular density, with hypoxia located at distances far from vasculature (Figure 1.1). SiHa cervical carcinoma xenografts have a similar pattern of vasculature and hypoxia, and TPZ causes a similar vascular dysfunction effect in these tumours (Huxham *et al.* 2008). However, murine SCCVII squamous carcinoma tumours have a relatively high density of blood vessels, with some areas of vascularized and perfused tumour tissue that is hypoxic, and these tumours are also sensitive to the anti-vascular effects of TPZ (Huxham *et al.* 2008).

A) Control HCT116

B) Central vascular dysfunction in HCT116

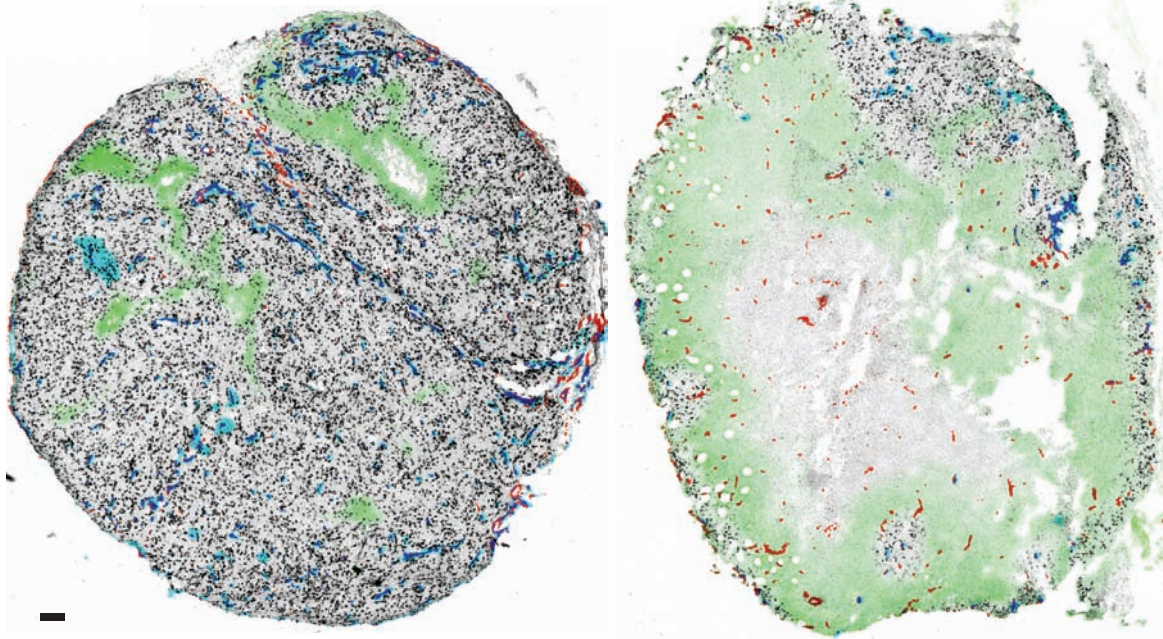


Figure 1.3 Vascular dysfunction visualized using tumour mapping.

An untreated control HCT116 colorectal xenograft tumour (A) is compared to a tumour exhibiting vascular dysfunction 24 h following anti-vascular treatment (B). Vascular dysfunction is easily observed by loss of perfusion in central areas indicated by the large number of unperfused CD31 vasculature (red), with a hallmark viable rim of perfused vessels (blue). The peripheral rim also stains positively for exogenously administered markers of hypoxia (green) and S-phase (black) that are only delivered to the perfused tumour tissues. Scale bar 150 μm .

1.4 Tumour hypoxia

While the patterns of vasculature and hypoxia are different between HCT116 and SCCVII tumour models, both are similarly sensitive to the anti-vascular effects of TPZ. Poorly oxygenated cells are a common characteristic of solid tumours, indicating that the demand for oxygen in tumours often exceeds supply. Cellular oxygen consumption rates and the availability of blood, which is dependent on the distribution of blood vessels and the blood oxygen carrying capacity, dictate tissue oxygenation levels. Tumours consume oxygen at an intermediate rate that is greater than tissues with low metabolic rates, but lower than tissues with high metabolic rates (Vaupel *et al.* 1989). Tumour vascular abnormalities (further discussed below in section 1.5) cause poor blood flow and large inter-vascular

distances and result in heterogeneous oxygenation of tumour tissue. Normal tissues have considerable variation in tissue oxygenation and hypoxia is defined as oxygen levels that are less than normal. Normal arterial pO₂ is typically at 80-100 mmHg, and the median pO₂ for tissues ranges from 24 mmHg in the brain to 66 mmHg in the spleen (Vaupel *et al.* 1989). The median pO₂ for tumours is < 20 mmHg and the ratio of normal tissue pO₂ to tumour tissue pO₂ is almost always >1, with considerable inter-tumour heterogeneity (Vaupel *et al.* 1989; Brown and Wilson 2004).

Causes for tumour hypoxia include severe structural and functional microvessel abnormalities that can cause slow, poor or even static blood flow (*perfusion-limited hypoxia; acute hypoxia*). Large inter-vascular distances result in tumour cells located far from their nearest blood vessel that are consequently hypoxic (*diffusion-limited hypoxia; chronic hypoxia*). Cancer patients can be tumour-associated or therapy-associated anemic, which results in reduced oxygen carrying capacity of the blood (*anemic hypoxia*). Other more minor contributors to tumour hypoxia include reduced oxygen carrying capacity of hemoglobin in smokers due to carbon monoxide binding to hemoglobin (*toxic hypoxia*). Lower blood oxygen content can also arise from pulmonary diseases or high altitude. Tumour blood vessel supply from the hepatic portal vein system in the liver may also have lower blood oxygen content that can result in tissue hypoxia (*hypoxemic hypoxia*). For a review of definitions regarding hypoxia see Höckel and Vaupel (2001).

1.5 Hypoxic vasculature in tumours

As described above (section 1.2), TPZ is a prodrug that is reduced to a cytotoxic agent in conditions of hypoxia. It therefore appears counter-intuitive that it can cause damage to vascular endothelial cells, likely the most well oxygenated cell population in solid cancers. Evidence for intravascular hypoxia in tumours comes from cryospectrophotometric studies measuring hemoglobin saturation (HbO₂), which directly measure the oxygenation of blood. HbO₂ has been measured as low as 0 % and as high as 100 % in tumours (Fenton *et al.* 1988; Fenton *et al.* 2001; Måseide and Rofstad 2001). In window chamber models, microelectrode measurements of pO₂ found that 25 % of functioning, patent blood vessels had pO₂ levels that were indistinguishable from 0 (Dewhirst *et al.* 1992). Observation of hypoxic perivascular tumour cells despite patency of the blood vessels is indirect evidence of

intravascular hypoxia and has been observed in tissues using oxygen-dependent phosphorescence quenching microscopy of tumours in window chambers (Helmlinger *et al.* 1997). Similar observations of hypoxic perivascular tumour cells have also been made in clinical glioblastoma tumours stained with EF5, a bioreductive marker that labels hypoxic cells similarly to pimonidazole, where tumour cells proximal to some vessels were more hypoxic than those located farther from vasculature (Evans *et al.* 2008).

Considerable inter- and intra- tumour heterogeneity is observed in tumour cell and vascular hypoxia measurements. A trend of lower oxygenation in the central tumour regions relative to the more well oxygenated periphery has been consistently reported (Fenton *et al.* 1988; Dewhirst *et al.* 1992; Måseide and Rofstad 2001). Several contributing factors are likely to be responsible for intravascular hypoxia in tumour blood vessels. Evans *et al.* (2008) have suggested that some regions of tumours are supplied with blood vessels that are functioning similarly to the veins of normal tissues and actually act as oxygen ‘sinks’. In window chamber models where it is possible to track the supplying arteriolar vessels in the relatively small, two-dimensional tumours, a longitudinal oxygen gradient has been observed, where oxygen is removed from the blood as it travels through the tumour from the oxygenated periphery to the more hypoxic central core (Dewhirst *et al.* 1992; Dewhirst *et al.* 1999). The hypoxic vasculature in the central regions of tumours in window chambers have also been reported to be less sensitive to modulation of tumour hypoxia by high oxygen breathing (Erickson *et al.* 2003). Slow and static blood flow is a likely culprit for vascular hypoxia and is likely underestimated in routine histological analyses of tumour perfusion that cannot reflect blood flow rates. Heterogeneous blood flow is often reported in tumours and may be responsible for tumour and intravascular hypoxia (Kimura *et al.* 1996; Lyng *et al.* 2001; Dewhirst 2003; Lanzen *et al.* 2006; Cárdenas-Navia *et al.* 2007; Brurberg *et al.* 2008).

The presence of hypoxic vasculature is likely to be a feature that is relatively uncommon in healthy tissues and therefore represents a pathophysiological feature that is highly cancer-specific. If cytotoxic drugs could be targeted to damage hypoxic vasculature a high therapeutic ratio could potentially be expected.

There is currently no direct evidence that TPZ mediates anti-vascular damage through a hypoxic cytotoxic mechanism to hypoxic vasculature. The pattern of central vascular dysfunction and a remaining viable rim in response to TPZ is consistent with the reports of

greater tumour and vascular hypoxia in the central regions of tumours. Data presented in Chapter 2 uses dynamic contrast enhanced magnetic resonance imaging (DCE-MRI) to investigate the impact of vascular function and therefore indirectly, hypoxia, on the sensitivity of tumours to the anti-vascular effects of TPZ. Further studies in Chapter 3 look more directly at the effects of hypoxia, investigating the effects of modulation of blood oxygenation and hypoxia on tumour response to TPZ.

1.6 Abnormal tumour blood vessels

In addition to vascular hypoxia, tumour vasculature has many abnormal phenotypic and functional features that could contribute to tumour sensitivity to TPZ. A characteristic of TPZ-mediated vascular dysfunction is the heterogeneity in response. Some tumour blood vessels are sensitive, responding with loss of perfusion, while others are resistant and maintain blood flow despite high doses of TPZ. As described in section 1.3, inter-tumour heterogeneity in response to TPZ is observed in all sensitive tumour models. Approximately 65 % of TPZ-treated tumours respond with central vascular dysfunction and the remaining 35 % are non-responders. This rate of response is similar in each of the HCT116, SiHa and SCCVII tumour models previously examined (Huxham *et al.* 2006; Huxham *et al.* 2008). Intra-tumour heterogeneity is reflected by the persistence of a viable rim of undamaged blood vessels even in responding tumours. The inter- and intra-tumour heterogeneity of tumour blood vessel sensitivity to the anti-vascular effects of TPZ is seen despite tumour endothelial cells all deriving from genetically identical host animals, and despite the identical nature of the immortalized tumour models.

Because the cells that make up tumour blood vessels originate from normal tissues, they are hypothesized to be more genetically stable than tumour cells, and should consequently be less likely than tumour cells to develop resistance to chemotherapies (Folkman 2006). Despite the relative *genetic* normalcy of blood vessel cells, the *function* and *phenotype* of tumour blood vessels is affected by the tumour microenvironment, and the resulting tumour vasculature is far from normal. A balance of pro- and anti-angiogenic signalling molecules arising from tumour cells typically initiates growth of blood vessels from neighbouring host tissues in a process known as angiogenesis (Folkman 1971; Ferrara and Kerbel 2005; Folkman 2006). The exact pattern for blood vessel growth varies between

tumour types and is highly heterogeneous. Though there are exceptions, like normal tissue vessels, tumour blood vessels are typically comprised of endothelial cells in a tubular structure and the outside of the tubes may be associated with mural support cells such as pericytes (Morikawa *et al.* 2002) and layers of basement membrane (Baluk *et al.* 2003). All of these components, in addition to the structure, size, shape, branching pattern, organization and hierarchy can be highly abnormal in tumours (Baluk *et al.* 2005; Tozer *et al.* 2005). Severe structural aberrations lead to functional abnormalities such as slow or even static blood flow, as well as high permeability and leakiness due to poor endothelial junctional complexes and large fenestrations (Hashizume *et al.* 2000; Dewhirst 2003). Tumours also have poor or absent lymphatic systems for drainage of the large volumes of fluid that leak from the sluggish, leaky vessels, and this deficiency can result in a relatively high interstitial fluid pressure (Leu *et al.* 2000).

A central hypothesis presented in this thesis is that cancer-specific features of the tumour vasculature and microenvironment confer sensitivity or resistance to the anti-vascular effects of TPZ in tumours. Tumour vascular function is investigated as a predictor of response to TPZ using DCE-MRI in Chapter 2 of this thesis. Additional functional and phenotype characteristics of blood vessels in tumours that are sensitive or resistant to TPZ-mediated vascular dysfunction are compared and investigated in Chapters 3 and 4.

1.7 Vascular disrupting agents (VDAs)

As described above, the tumour microenvironment is highly heterogeneous due in large part to the abnormal organization and function of tumour blood vessels. Abnormal vascular features of solid tumours represent tissue-level, targetable features for anti-cancer therapeutics (Baluk *et al.* 2005). Vascular disrupting agents (VDAs), previously described as vascular damaging agents or vascular targeting agents (VTAs), are a relatively new class of anti-cancer compounds that are distinct to angiogenesis inhibitors. Instead of inhibiting the growth of new vessels, VDAs target and destroy existing tumour vasculature (Thorpe 2004; Tozer *et al.* 2005). The overall pattern of effect by VDAs is similar to that seen for TPZ. VDA-mediated loss of perfusion is followed by death of dependent tumour cells and the effect is primarily limited to the central regions of tumours with a persisting rim of viable, undamaged tissue at the tumour margins. A flavone acetic acid-derived compound, DMXAA (5,6-Dimethylxanthenone-4-acetic acid, ASA404), is a VDA that interferes with the actin cytoskeleton principally through induction of cytokines (McKeage *et al.* 2009). Combretastatin phosphate (CA-4-P, ZybrestatTM) is a small molecule VDA that disrupts the cellular cytoskeleton via binding to tubulin (Pettit *et al.* 1989). A mechanism for VDA-mediated vascular dysfunction proposed by Tozer *et al.* (2001) describes the effects as similar to those seen in acute inflammatory reactions. The initial action of small molecule VDAs that disrupt the cytoskeleton results in the rounding up of vascular endothelial cells. Inter-endothelial cell gaps result in a substantial, rapid change in vascular permeability. Leaking plasma proteins, edema, leukocyte interactions and infiltration, and an increase in interstitial fluid pressure, all result in blood vessel narrowing and a decrease in blood flow rates.

The similar pattern of vascular damage in tumours by both VDAs and TPZ suggests that there may be some overlap in their mechanisms of action. However, *in vitro* studies examining the effects of TPZ on endothelial cell cytoskeletal structures showed no effect in hypoxic or normoxic conditions (Huxham *et al.* 2008). The specific mechanism for TPZ-mediated damage to the tumour vasculature is therefore likely to be distinct to that of the small molecule VDAs. However, the pattern of sensitivity of central tumour blood vessels and insensitivity of the peripheral rim of tumour vessels suggests there may be some overlap in the mechanism for sensitivity of tumour blood vessels to both TPZ and VDAs.

A precise mechanism for the specificity of small molecule VDA-mediated damage in tumour vasculature (vs. normal tissue vasculature) remains somewhat unclear, but an overview of hypotheses and supporting data is presented in a review by Tozer *et al.* (2008). In addition to cell-based mechanisms for selectivity in tumour endothelium, including tubulin modifications and defective inter-cellular junctions, a series of tissue level mechanisms are suggested. These tissue level mechanisms include micro-regional instabilities in blood flow that may sensitize some vessels such that further pharmacologically-induced reductions are catastrophic (Tozer *et al.* 2001). In addition, high vascular permeability and the resulting high interstitial fluid pressure in tumours may sensitize vessels to collapse following any further disruption in permeability (Beauregard *et al.* 2001; Tozer *et al.* 2001; Beauregard *et al.* 2002) or change in fluid pressure (Boucher *et al.* 1990). Vascular maturity may also play an important role, as inefficient or inadequate association of mural support cells such as pericytes with tumour blood vessels may reduce vascular stability and the ability of tumour vessels to withstand or recover from vascular damage (Tozer *et al.* 2008).

The proliferation rate of tumour vascular endothelial cells can be up to 20x greater than in the vasculature elsewhere in the body (Denekamp 1982; Denekamp and Hobson 1982). Proliferating endothelial cells may therefore represent a targetable feature of tumours for anti-cancer drugs, and small molecule VDAs such as CA-4-P are toxic to proliferating endothelial cells *in vitro* (Kanthou *et al.* 2004). However, inhibiting proliferation and inducing apoptosis in endothelial cells is likely too slow a process to be responsible for the anti-vascular effects observed within minutes of CA-4-P administration *in vivo*; disruption of interphase cytoskeletal structures is likely the more important mechanism of action of CA-4-P (Kanthou *et al.* 2004; Tozer *et al.* 2005).

Anti-microtubule vinca alkaloid anti-cancer drugs also show vascular targeting effects, though only at near maximum tolerated doses (Hill *et al.* 1993; Chaplin *et al.* 1996). Hyperthermia also causes widespread vascular damage in some tumours and the tumour selectivity of these effects have been attributed to the same vascular abnormalities described above (Song 1984). Other strategies for targeting tumour vasculature include targeted antibodies or peptides that use tumour vasculature-specific ligands for delivering toxic payloads to tumours (Thorpe 2004). Photodynamic therapy (PDT) also causes tumour vascular damage, achieving tumour-specificity due to the intravascular nature of the injected

prodrug compounds that become activated and cytotoxic only upon exposure to light, which can be limited to tumour regions of interest (Dolmans *et al.* 2003).

Three main strategies for targeting the tumour vasculature are represented by the examples described above: a) using tumour vascular specific expressions of antigen to which ligands or agents are targeted; b) selective activation of cytotoxic agents when they are located within the tumour region of interest; and c) small molecule VDAs that exploit tumour microenvironmental differences to effect vascular damage. All three strategies work on a similar principal of achieving tumour cell kill through deprivation of oxygen and nutrients via damage to the tumour blood supply. Targeting the tumour vasculature with anti-cancer drugs is a particularly useful strategy due to the accessibility of the target cells to systemically delivered agents. In addition, a relatively small number of affected cells results in the death of a high number of cancer cells that were otherwise dependent on the damaged blood vessels.

As has been described, the hallmark effects of TPZ mediated vascular dysfunction, including loss of central perfusion and persistence of the viable rim, are very similar to those seen with other vascular targeting strategies. While the mechanism of action for TPZ-mediated damage to the tumour vascular endothelium is likely to be distinct to any of the other described anti-vascular strategies, the similarity in pattern of damage suggests some overlap in vessel sensitivity. All or any of the three main targeting strategies described may have relevance to the anti-vascular effects of TPZ.

As mentioned in Section 1.6, studies in Chapters 2 and 3 of this thesis investigate aspects of vascular function and phenotype in tumour models that have differential sensitivity to the anti-vascular effects of TPZ. These data may also have relevance to the efficacy and mechanisms for tumour vascular selectivity of the other vascular targeting strategies described here.

1.8 Combining NOS inhibition with hypoxic cytotoxins and vascular disrupting agents (VDAs)

While the pattern of TPZ-mediated vascular dysfunction is similar to that of other anti-vascular strategies, the mechanism for damage requires further investigation. A mechanism for TPZ mediated damage in or proximal to endothelial cells may be related to the location of

its bioactivation and redox cycling. Many cellular reductases can reduce TPZ, including cytosolic enzymes such as NADPH:cytochrome c reductase (P450R) (Walton *et al.* 1992; Saunders *et al.* 2000) and intranuclear enzymes (Evans *et al.* 1998). TPZ is also reduced by and competitively inhibits nitric oxide synthase (NOS), which has a reductase domain with homology to that of P450R; in conditions of hypoxia TPZ reduction by NOS can result in DNA damage (Garner *et al.* 1999; Chinje *et al.* 2003). Neuronal NOS (nNOS, NOSI) and endothelial NOS (eNOS, NOSIII) isoforms of NOS are constitutively expressed and are dependent on calcium/calmodulin for regulation. A third isoform is inducible NOS (iNOS, NOSII). Several studies have identified a correlation between iNOS activity in tumours and poor prognosis, greater metastatic activity or higher tumour grade, including in gastric (Song *et al.* 2002), head and neck (Gallo *et al.* 1998) and colorectal carcinoma (Lagares-Garcia *et al.* 2001; Cianchi *et al.* 2003). Non-isoform specific NOS expression has also been linked to higher grade tumours in gynecological (Thomsen *et al.* 1994), breast (Thomsen *et al.* 1995) and central nervous system tumour studies (Cobbs *et al.* 1995). NOS has been proposed as a potential therapeutic target for cancer treatment (Fukumura *et al.* 2006; Fitzpatrick *et al.* 2008).

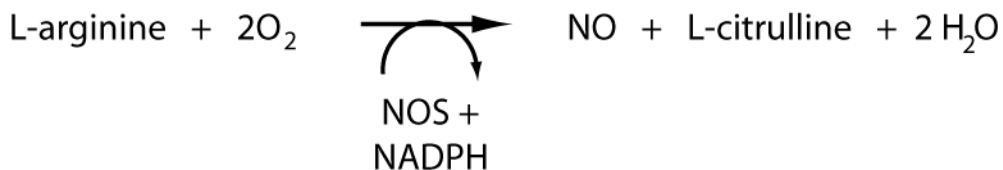


Figure 1.4 NO synthesized by nitric oxide synthase (NOS).

Competitive inhibition of NOS by TPZ results in reduced production of nitric oxide (NO), an important messenger molecule synthesized by NOS in a two step oxidation of L-arginine to L-citrulline in the presence of oxygen (Figure 1.4). NO is highly reactive and has a wide array of actions and therefore NOS inhibition has an equally wide array of impacts; for a comprehensive review of the role of NO in tumour biology, see Fukumura *et al.* (2006). Chronic stimulation by NO from endothelial cells has an important role in recruiting pericytes and is involved in vessel remodeling and maturation (Kashiwagi *et al.* 2005; Yu *et al.* 2005). NO can also have a more acute impact on tumour vascular function. Studies

pharmacologically inhibiting NOS have resulted in reduced tumour blood flow and decreased tumour vessel diameters (Andrade *et al.* 1992; Fukumura *et al.* 1997; Tozer *et al.* 1997; Ng *et al.* 2007). Inter- and intra-tumour heterogeneity in vessel response to NOS inhibition has been suggested to be the result of microregional variations in both regional NO production and the inconsistent presence of smooth muscle cells adjacent to tumour vasculature for vasodilatory control (Fukumura *et al.* 1997).

Reduced tumour blood flow as a consequence of NOS inhibition can cause an increase in tumour hypoxia, and as a result NOS inhibition has been proposed as a complementary treatment for hypoxic cytotoxins *in vivo* (Wood *et al.* 1993; Wood *et al.* 1994). The suggested mechanism for the combination strategy is that an increase in hypoxia due to NOS inhibition will result in greater reduction and bioactivation of the hypoxic cytotoxins, which would ultimately enhance tumour cell kill. Given the observation that TPZ is both a hypoxic cytotoxin and a competitive inhibitor of NOS, Garner *et al.* (1999) have proposed that TPZ may potentiate itself via this mechanism.

The anti-cancer activity of the hypoxic cytotoxin RB6145 was increased when combined with a NOS inhibitor (Wood *et al.* 1994; Butler *et al.* 1997). No added systemic toxicity was seen with this combination, suggesting that inhibition of NOS in combination with a bioreductive hypoxic cytotoxin may be therapeutically advantageous. The efficacy of combining RB6145 with NOS inhibition was demonstrated in these studies using growth delay and clonogenic survival assays. As described in section 1.2, using growth delay and clonogenic survival assays it is difficult to conclude with certainty that the mechanism for potentiation of RB6145 by NOS inhibition is an increase in hypoxia and subsequently greater bioactivation of RB6145. The authors noted a time-dependence for cell kill in their clonogenic survival studies. When tumour excision was delayed to 24 hours post treatment with RB6145 or RB6145 in combination with NOS inhibition, a greater cell kill was observed than if tumours were excised at 12 hours (Butler *et al.* 1997). The timing of tumour excision post treatment is of critical importance if an anti-vascular effect were to have occurred. If tumours are excised and cultured after sustaining loss of perfusion, but prior to onset of tissue death due to the loss of blood vessel supply, then most tumour cells will be rescued by the culture conditions and a high survival rate would be observed. However, if tumours are excised at longer times post treatment, then more cells will have died due to lack

of oxygen and nutrient delivery and a dramatically lower number of colonies per gram of tumour tissue would result. The delay in peak cell death measured using clonogenic survival observed in the studies combining RB6145 with NOS inhibition is consistent with an anti-vascular effect. Therefore, a central vascular dysfunction effect, though not assessed in these studies combining the hypoxic cytotoxin RB6145 with a NOS inhibitor, may explain both the time-dependent clonogenic survival results as well as the unexpectedly high rates of cell kill noted by the authors (Butler *et al.* 1997).

NOS inhibition has also been successfully combined with VDAs in pre-clinical studies. Small molecule VDAs cause losses in perfusion through a mechanism similar to that of an acute inflammatory reaction (as described in section 1.7), whereas NOS inhibition in tumours primarily results in decreased blood vessel diameters. Therefore, through a mechanism distinct from that seen for VDAs themselves, NOS inhibition enhances the loss of perfusion in tumours treated with a combretastatin (Parkins *et al.* 2000; Tozer *et al.* 2009). A protective effect of NO is also suggested by studies overexpressing NOS in tumour models; NOS overexpression attenuates the anti-vascular response of tumours treated with ZD6126, an analogue of colchicine with microtubule destabilizing effects similar to those seen with the combretastatins (Cullis *et al.* 2006).

There is evidence of TPZ having activity both as a hypoxic cytotoxin and as VDA. Enhancement of both hypoxic cytotoxins and VDAs by inhibition of NOS has therefore led to the work presented in Chapter 4 of this thesis where the anti-cancer activity of TPZ in combination with modulation of NO levels is investigated in multiple tumour models.

1.9 Thesis Overview

Tirapazamine (TPZ) is a hypoxic cytotoxin that has anti-vascular activity in tumour models grown in mice. The effect of TPZ on tumour vasculature is incomplete, typically leaving a viable rim of undamaged vessels at the tumour periphery. Anti-vascular activity of TPZ has been observed in several tumour types, and in all of these types the effect occurs in 65 % of treated tumours, leaving 35 % unaffected despite identical animal and tumour origins. A mechanism for TPZ damage to select tumour blood vessels remains unclear and represents an important research question.

The purpose of the research presented in this thesis is to explore the mechanism of action of the anti-vascular activity of TPZ, and to investigate features of the tumour microenvironment that confer sensitivity to these effects.

Experiments in Chapter 2 explore the utility of dynamic contrast enhanced magnetic resonance imaging (DCE-MRI) to observe the effects of TPZ on vascular function *in vivo*. DCE-MRI derived biomarkers of vascular function are also examined as potential predictors for tumour response to TPZ-mediated vascular dysfunction.

Chapter 3 specifically investigates tumour hypoxia as a relevant microenvironmental feature for tumour vascular sensitivity to TPZ. Tumour mapping analyses are used to examine the *in vivo* effects of TPZ in combination with decreasing blood vessel oxygenation. IHC staining is also used to compare features of the tumour microenvironment and blood vessels in tumours characterized as either sensitive or resistant to TPZ mediated vascular damage.

The effect of changes in tumour vascular function on tumour sensitivity to TPZ-mediated vascular damage are further examined in tumour mapping studies in Chapter 4. TPZ in combination with NOS inhibition or excess NO supply is investigated in order to determine whether NO has an effect on the anti-vascular activity of TPZ, and whether this activity can be translated to reduced tumour growth.

1.9.1 Research hypothesis and objectives

The overall hypothesis of this research is that features of the tumour microenvironment confer sensitivity to the anti-vascular activity of tirapazamine.

The main objectives of the work presented in this thesis were to:

1. Use dynamic contrast enhanced magnetic resonance imaging (DCE-MRI) to observe TPZ-mediated vascular dysfunction *in vivo*.
2. Identify tumour microenvironmental features that confer tumour sensitivity for TPZ.
3. Investigate the impact of modulation of NO in combination with TPZ in tumours.

1.10 Chapter summaries

1.10.1 Chapter 2 summary - *Detecting vascular-targeting effects of the hypoxic cytotoxin tirapazamine in tumour xenografts using magnetic resonance imaging*

Purpose: Previous investigations of the anti-vascular activity of tirapazamine (TPZ) have been limited to two-dimensional histological techniques that are invasive and static. The purpose of the studies presented in Chapter 2 is to determine whether vascular-targeting effects of TPZ can be detected *in vivo* using magnetic resonance imaging (MRI).

Methods: MR images of subcutaneously implanted HCT116 xenografts in mice were acquired at 7 Tesla before and 24 hours after intraperitoneal injections of TPZ. Quantitative dynamic contrast-enhanced MRI (DCE-MRI) analyses were performed to evaluate changes in tumour vascular function using two biomarkers: the volume transfer constant (K^{trans}) and the initial area under the concentration-time curve (IAUC). Novel implanted fiducial markers were used to obtain highly reproducible imaging planes for longitudinal MR imaging and selection of corresponding histological sections. Quantitative immunohistochemical mapping of tumour vasculature, perfusion and necrosis enabled correlative analysis between these and MR images. A Vascular Dysfunction Score (VDS) was developed and reported to enable objective, quantitative assessment of anti-vascular effects.

Results: Conventional histological analysis showed lower fractions of perfused vessels or lower proportions of viable tissue in the central regions of five of eight TPZ-treated tumours, with three treated tumours showing no vascular dysfunction response. MRI data reflected this result and a striking decrease in both K^{trans} and IAUC values was seen with the responsive tumours. Loss of perfusion was found to be microregionally variable, with greater changes observed in the central areas of tumours in both DCE-MRI and histological parameter analyses. Retrospective evaluation of pretreatment MRI parameters revealed that those tumours that did not respond to the vascular-targeting effects of tirapazamine had significantly higher pretreatment K^{trans} and IAUC values.

Conclusions: MRI-derived parameter maps showed good agreement with histological tumour maps. MRI was found to be an effective tool for non-invasively monitoring tirapazamine-mediated central vascular dysfunction and for predicting tumour sensitivity.

1.10.2 Chapter 3 summary – Decreased blood oxygen tension sensitizes tumours to the anti-vascular effects of tirapazamine

Purpose: The hypoxic cytotoxin tirapazamine (TPZ) mediates central vascular dysfunction in several pre-clinical tumour models. MRI data from Chapter 2 suggested vascular function as a predictor for tumour sensitivity to the anti-vascular effects of TPZ. The purpose of studies presented in Chapter 3 is to evaluate features of the tumour microenvironment that may confer sensitivity to TPZ, including hypoxia and vascular phenotype.

Methods: Quantitative immunohistochemical (IHC) based tumour mapping was used to evaluate the response to TPZ in a variety of conditions in HCT116 and HT29 colorectal xenograft tumours grown subcutaneously in mice. Markers of vasculature, perfusion, permeability, hypoxia, S-phase, basal lamina and smooth muscle cells were stained and imaged to evaluate vascular dysfunction and characteristics of tumours that are sensitive or resistant to the anti-vascular effects of TPZ. The effect of hypoxia on tumour sensitivity to TPZ was investigated via induction of moderate anemia and exposure of mice to 7-10% oxygen during treatment. Dependence of microvessel sensitivity on oxygenation and TPZ concentration was evaluated using human microvascular endothelial cells (HMECs) grown as tubular structures on Matrigel coated plates.

Results: HT29 colorectal xenografts were resistant to anti-vascular effects of TPZ, compared to sensitive HCT116 colorectal xenografts. Tumour mapping analyses of the two models revealed quantifiable differences, where HT29 tumours exhibited greater microvessel density and permeability, with thicker layers of CIV and α SMA proximal to vasculature. Decreasing tumour oxygen levels via anemia or low oxygen breathing enhanced TPZ mediated vascular dysfunction, even in otherwise resistant HT29 tumours. HMEC tube structures show evidence of damage at 8h following exposure to clinically relevant TPZ concentrations at 2% oxygen.

Conclusions: These data establish a direct link between the anti-vascular effects of TPZ and hypoxia. Additional tumour specific features of the microenvironment such as vascular architecture and phenotype may also play a role in tumour sensitivity to TPZ mediated vascular dysfunction.

1.10.3 Chapter 4 summary – Inhibition of nitric oxide synthase enhances tirapazamine-mediated vascular dysfunction in pre-clinical tumours

Purpose: A mechanism for the ability of tirapazamine (TPZ) to mediate central vascular dysfunction in solid tumours remains unclear. Data from Chapters 2 and 3 established hypoxia as a sensitizer to the effect and have implicated vascular function and phenotype as additional, potential predictors for sensitivity. The purpose of studies in Chapter 4 is to evaluate the activity of nitric oxide (NO) on tumour sensitivity to the anti-vascular effects of TPZ.

Methods: HCT116 and HT29 colorectal xenografts and SCCVII murine tumours were grown subcutaneously in mice. TPZ was administered alone or in combination with the non-specific NOS inhibitor L-NNA or with NO donor spermine NONOate. Tumour mapping analyses of vasculature, perfusion, hypoxia, S-phase and NOS expression were used to evaluate TPZ mediated vascular dysfunction. Enhancement of anti-cancer activity of TPZ by NOS inhibition was evaluated by monitoring the growth of HCT116 tumours.

Results: Administration of NOS inhibitor L-NNA in combination with TPZ at lower than maximum tolerated doses resulted in reduced HCT116 tumour growth. NOS inhibition in combination with TPZ results in enhanced anti-vascular activity in both HCT116 and SCCVII tumours where the magnitude and frequency of vascular dysfunction were increased. No vascular dysfunction effects were seen in HT29 xenografts treated with the combination of TPZ and L-NNA. Administration of excess NO in combination with TPZ did not protect against TPZ mediated anti-vascular damage, but instead enhanced the vascular dysfunction response.

Conclusions: Combining NOS inhibition with TPZ enhances the anti-vascular activity of TPZ and this translates into reduced growth rates in HCT116 tumours. Excess NO also enhances tumour sensitivity to TPZ mediated vascular dysfunction. These data suggest that NO or tumour vascular phenotype may play an important role in tumour sensitivity to TPZ, and that combining TPZ with NOS inhibition warrants further investigation as a therapeutic strategy.

1.11 Impact of the Research

Data from this thesis provides further evidence of the anti-vascular activity of TPZ in solid tumours and provides direct links between the tumour microenvironment and sensitivity to these effects. Data from Chapters 2 and 3 demonstrate that pre-treatment vascular function or hypoxia can predict the anti-vascular effects of TPZ. These data are evidence of TPZ affecting tumour vasculature through its activity as a hypoxic cytotoxin for therapeutic benefit. Intentionally targeting hypoxic tumour vasculature would represent a novel therapeutic strategy in cancer treatment. This result has relevance to drug development strategies in the field of bioreductive hypoxic cytotoxins, where specific and comprehensive *in vivo* screening of candidate hypoxic cytotoxins for both anti-vascular and hypoxic cytotoxicity should be undertaken. In addition, pursuit of hypoxic cytotoxic agents that could be limited to and bioactivated within the intra-vascular compartment may represent a useful anti-cancer agent development strategy.

No studies to date have investigated whether TPZ or other hypoxic cytotoxins mediate vascular damage in clinical patients. Experiments in Chapter 2 demonstrate DCE-MRI as a practical technique for observing TPZ mediated vascular dysfunction. DCE-MRI is a method that is translatable to the clinic, and trials examining the activity of TPZ or other hypoxic cytotoxins may consider DCE-MRI for assessment of vascular function in response to treatment. If vascular dysfunction occurs in response to TPZ in the clinic, DCE-MRI would also have useful application in assessing patient response to therapy and may provide applicable biomarkers for predicting response to TPZ.

In addition to DCE-MRI biomarkers of vascular function as potential predictors for response, data from Chapter 3 suggest that pre-treatment vascular function, tumour hypoxia or blood oxygenation can have an impact on the frequency and magnitude of the anti-vascular effects of TPZ. These results suggest that in addition to screening candidate patients for tumour hypoxia, it may be useful to assess peripheral blood oxygen levels as potential predictors for sensitivity to TPZ. Other potentially useful predictors of sensitivity to the anti-vascular effects of TPZ suggested in Chapters 3 and 4 include vascular phenotype characteristics such as NOS expression or the maturity of tumour blood vessels.

Experiments in Chapter 4 demonstrate that combining TPZ with a NOS inhibitor enhances the anti-cancer activity of TPZ through greater vascular dysfunction effects. These

data provide supporting evidence to the hypothesis that combining bioreductive hypoxic cytotoxins with NOS inhibition is an effective therapeutic strategy, and demonstrate that the mechanism for this effect may involve damage to the tumour vasculature.

Overall, this work emphasizes the importance of specifically examining the effects of anti-cancer drugs on whole tumours *in vivo*, as the tumour microenvironment is complex and can have a significant impact on drug efficacy and tumour response to treatment.

1.12 REFERENCES

- Anderson, R. F., S. S. Shinde, *et al.* (2005). "Radical properties governing the hypoxia-selective cytotoxicity of antitumor 3-amino-1,2,4-benzotriazine 1,4-dioxides." Org Biomol Chem **3**(11): 2167-74.
- Andrade, S. P., I. R. Hart, *et al.* (1992). "Inhibitors of nitric oxide synthase selectively reduce flow in tumor-associated neovasculature." British Journal of Pharmacology **107**(4): 1092-5.
- Baluk, P., H. Hashizume, *et al.* (2005). "Cellular abnormalities of blood vessels as targets in cancer." Curr Opin Genet Dev **15**(1): 102-11.
- Baluk, P., S. Morikawa, *et al.* (2003). "Abnormalities of basement membrane on blood vessels and endothelial sprouts in tumors." Am J Pathol **163**(5): 1801-15.
- Beauregard, D. A., S. A. Hill, *et al.* (2001). "The susceptibility of tumors to the antivascular drug combretastatin A4 phosphate correlates with vascular permeability." Cancer Res **61**(18): 6811-5.
- Beauregard, D. A., R. B. Pedley, *et al.* (2002). "Differential sensitivity of two adenocarcinoma xenografts to the anti-vascular drugs combretastatin A4 phosphate and 5,6-dimethylxanthenone-4-acetic acid, assessed using MRI and MRS." NMR in biomedicine **15**(2): 99-105.
- Boucher, Y., L. T. Baxter, *et al.* (1990). "Interstitial pressure gradients in tissue-isolated and subcutaneous tumors: implications for therapy." Cancer Res **50**(15): 4478-84.
- Brown, J. M. and A. J. Giaccia (1998). "The unique physiology of solid tumors: opportunities (and problems) for cancer therapy." Cancer Res **58**(7): 1408-16.
- Brown, J. M. and M. J. Lemmon (1990). "Potentiation by the hypoxic cytotoxin SR 4233 of cell killing produced by fractionated irradiation of mouse tumors." Cancer Res **50**(24): 7745-9.
- Brown, J. M. and M. J. Lemmon (1991). "Tumor hypoxia can be exploited to preferentially sensitize tumors to fractionated irradiation." Int J Radiat Oncol Biol Phys **20**(3): 457-61.
- Brown, J. M. and W. R. Wilson (2004). "Exploiting tumour hypoxia in cancer treatment." Nature Reviews Cancer **4**(6): 437-47.
- Brurberg, K. G., J. V. Gaustad, *et al.* (2008). "Temporal heterogeneity in blood supply in human tumor xenografts." Neoplasia **10**(7): 727-35.
- Butler, S. A., P. J. Wood, *et al.* (1997). "Enhancement of bioreductive drug toxicity in murine tumours by inhibition of the activity of nitric oxide synthase." Br J Cancer **76**(4): 438-44.
- Cárdenas-Navia, L. I., T. W. Secomb, *et al.* (2007). "Effects of fluctuating oxygenation on tirapazamine efficacy: Theoretical predictions." Int J Radiat Oncol Biol Phys **67**(2): 581-6.
- Chaplin, D. J., G. R. Pettit, *et al.* (1996). "Antivascular approaches to solid tumour therapy: evaluation of tubulin binding agents." Br J Cancer Suppl **27**: S86-8.
- Chinje, E. C., R. L. Cowen, *et al.* (2003). "Non-nuclear localized human NOSII enhances the bioactivation and toxicity of tirapazamine (SR4233) in vitro." Mol Pharmacol **63**(6): 1248-55.
- Cianchi, F., C. Cortesini, *et al.* (2003). "Inducible nitric oxide synthase expression in human colorectal cancer: correlation with tumor angiogenesis." Am J Pathol **162**(3): 793-801.
- Cobbs, C. S., J. E. Brenman, *et al.* (1995). "Expression of nitric oxide synthase in human central nervous system tumors." Cancer Res **55**(4): 727-30.
- Cullis, E. R., T. L. Kalber, *et al.* (2006). "Tumour overexpression of inducible nitric oxide synthase (iNOS) increases angiogenesis and may modulate the anti-tumour effects of the vascular disrupting agent ZD6126." Microvasc Res **71**(2): 76-84.
- Denekamp, J. (1982). "Endothelial cell proliferation as a novel approach to targeting tumour therapy." Br J Cancer **45**(1): 136-9.

- Denekamp, J. and B. Hobson (1982). "Endothelial-cell proliferation in experimental tumours." Br J Cancer **46**(5): 711-20.
- Dewhurst, M. W. (2003). "Mechanisms underlying hypoxia development in tumors." Adv Exp Med Biol **510**: 51-6.
- Dewhurst, M. W., E. T. Ong, *et al.* (1999). "Quantification of longitudinal tissue pO₂ gradients in window chamber tumours: impact on tumour hypoxia." Br J Cancer **79**(11-12): 1717-22.
- Dewhurst, M. W., E. T. Ong, *et al.* (1992). "Perivascular oxygen tensions in a transplantable mammary tumor growing in a dorsal flap window chamber." Radiation Research **130**(2): 171-82.
- Dolmans, D. E., D. Fukumura, *et al.* (2003). "Photodynamic therapy for cancer." Nature Reviews Cancer **3**(5): 380-7.
- Dorie, M. J. and J. M. Brown (1993). "Tumor-specific, schedule-dependent interaction between tirapazamine (SR 4233) and cisplatin." Cancer Res **53**(19): 4633-6.
- Durand, R. E. and P. L. Olive (1992). "Evaluation of bioreductive drugs in multicell spheroids." Int J Radiat Oncol Biol Phys **22**(4): 689-92.
- Erickson, K., R. D. Braun, *et al.* (2003). "Effect of longitudinal oxygen gradients on effectiveness of manipulation of tumor oxygenation." Cancer Res **63**(15): 4705-12.
- Evans, J. W., K. Yudoh, *et al.* (1998). "Tirapazamine is metabolized to its DNA-damaging radical by intranuclear enzymes." Cancer Res **58**(10): 2098-101.
- Evans, S. M., K. W. Jenkins, *et al.* (2008). "Imaging and analytical methods as applied to the evaluation of vasculature and hypoxia in human brain tumors." Radiation Research **170**(6): 677-90.
- Fenton, B. M., E. M. Lord, *et al.* (2001). "Intravascular HBO(2) saturations, perfusion and hypoxia in spontaneous and transplanted tumor models." Int J Cancer **93**(5): 693-8.
- Fenton, B. M., E. K. Rofstad, *et al.* (1988). "Cryospectrophotometric determination of tumor intravascular oxyhemoglobin saturations: dependence on vascular geometry and tumor growth." J Natl Cancer Inst **80**(20): 1612-9.
- Ferrara, N. and R. S. Kerbel (2005). "Angiogenesis as a therapeutic target." Nature **438**(7070): 967-74.
- Fitzpatrick, B., M. Mehibel, *et al.* (2008). "iNOS as a therapeutic target for treatment of human tumors." Nitric Oxide **19**(2): 217-24.
- Folkman, J. (1971). "Tumor angiogenesis: therapeutic implications." N Engl J Med **285**(21): 1182-6.
- Folkman, J. (2006). "Angiogenesis." Annu Rev Med **57**: 1-18.
- Fukumura, D., S. Kashiwagi, *et al.* (2006). "The role of nitric oxide in tumour progression." Nature Reviews Cancer **6**(7): 521-34.
- Fukumura, D., F. Yuan, *et al.* (1997). "Role of nitric oxide in tumor microcirculation. Blood flow, vascular permeability, and leukocyte-endothelial interactions." Am J Pathol **150**(2): 713-25.
- Gallo, O., E. Masini, *et al.* (1998). "Role of nitric oxide in angiogenesis and tumor progression in head and neck cancer." J Natl Cancer Inst **90**(8): 587-96.
- Garner, A. P., M. J. Paine, *et al.* (1999). "Nitric oxide synthases catalyze the activation of redox cycling and bioreductive anticancer agents." Cancer Res **59**(8): 1929-34.
- Gray, L. H., *et al.* (1953). "The concentration of oxygen dissolved in tissues at the time of irradiation as a factor in radiotherapy." Br J Radiol **26**(312): 638-48.
- Hashizume, H., P. Baluk, *et al.* (2000). "Openings between defective endothelial cells explain tumor vessel leakiness." Am J Pathol **156**(4): 1363-80.
- Helmlinger, G., F. Yuan, *et al.* (1997). "Interstitial pH and pO₂ gradients in solid tumors in vivo: high-resolution measurements reveal a lack of correlation." Nat Med **3**(2): 177-82.
- Hicks, K. O., Y. Fleming, *et al.* (1998). "Extravascular diffusion of tirapazamine: effect of metabolic consumption assessed using the multicellular layer model." Int J Radiat Oncol Biol Phys **42**(3): 641-9.

- Hill, S. A., S. J. Lonergan, *et al.* (1993). "Vinca alkaloids: anti-vascular effects in a murine tumour." *Eur J Cancer* **29A**(9): 1320-4.
- Höckel, M. and P. Vaupel (2001). "Tumor hypoxia: definitions and current clinical, biologic, and molecular aspects." *J Natl Cancer Inst* **93**(4): 266-76.
- Huxham, L. A., A. H. Kyle, *et al.* (2006). "Tirapazamine causes vascular dysfunction in HCT-116 tumour xenografts." *Radiotherapy and oncology : journal of the European Society for Therapeutic Radiology and Oncology* **78**(2): 138-45.
- Huxham, L. A., A. H. Kyle, *et al.* (2008). "Exploring vascular dysfunction caused by tirapazamine." *Microvasc Res* **75**(2): 247-55.
- Kanthou, C., O. Greco, *et al.* (2004). "The tubulin-binding agent combretastatin A-4-phosphate arrests endothelial cells in mitosis and induces mitotic cell death." *Am J Pathol* **165**(4): 1401-11.
- Kashiwagi, S., Y. Izumi, *et al.* (2005). "NO mediates mural cell recruitment and vessel morphogenesis in murine melanomas and tissue-engineered blood vessels." *J Clin Invest* **115**(7): 1816-27.
- Kimura, H., R. D. Braun, *et al.* (1996). "Fluctuations in red cell flux in tumor microvessels can lead to transient hypoxia and reoxygenation in tumor parenchyma." *Cancer Res* **56**(23): 5522-8.
- Koch, C. J. (1993). "Unusual oxygen concentration dependence of toxicity of SR-4233, a hypoxic cell toxin." *Cancer Res* **53**(17): 3992-7.
- Kyle, A. H. and A. I. Minchinton (1999). "Measurement of delivery and metabolism of tirapazamine to tumour tissue using the multilayered cell culture model." *Cancer Chemotherapy and Pharmacology* **43**(3): 213-20.
- Lagares-Garcia, J. A., R. A. Moore, *et al.* (2001). "Nitric oxide synthase as a marker in colorectal carcinoma." *Am Surg* **67**(7): 709-13.
- Lanzen, J., R. D. Braun, *et al.* (2006). "Direct demonstration of instabilities in oxygen concentrations within the extravascular compartment of an experimental tumor." *Cancer Res* **66**(4): 2219-23.
- Leu, A. J., D. A. Berk, *et al.* (2000). "Absence of functional lymphatics within a murine sarcoma: a molecular and functional evaluation." *Cancer Res* **60**(16): 4324-7.
- Lyng, H., A. O. Vorren, *et al.* (2001). "Intra- and intertumor heterogeneity in blood perfusion of human cervical cancer before treatment and after radiotherapy." *Int J Cancer* **96**(3): 182-90.
- Marcu, L. and I. Olver (2006). "Tirapazamine: from bench to clinical trials." *Current clinical pharmacology* **1**(1): 71-9.
- Måseide, K. and E. K. Rofstad (2001). "Intratumor heterogeneity in microvessel oxyhaemoglobin saturations." *Cancer Lett* **162**(2): 245-51.
- McKeage, M. J., M. Reck, *et al.* (2009). "Phase II study of ASA404 (vadimezan, 5,6-dimethylxanthenone-4-acetic acid/DMXAA) 1800mg/m² combined with carboplatin and paclitaxel in previously untreated advanced non-small cell lung cancer." *Lung Cancer* **65**(2): 192-7.
- Minchinton, A. I. and J. M. Brown (1992). "Enhancement of the cytotoxicity of SR 4233 to normal and malignant tissues by hypoxic breathing." *Br J Cancer* **66**(6): 1053-8.
- Minchinton, A. I. and J. M. Brown (1992). "Improving the effectiveness of the bioreductive antitumor agent SR 4233 by induced hypoxia." *Adv Exp Med Biol* **317**: 177-81.
- Minchinton, A. I., D. A. Tonn, *et al.* (2002). "Carbogen breathing after irradiation enhances the effectiveness of tirapazamine in SiHa tumors but not SCCVII tumors in mice." *Radiat Res* **158**(1): 94-100.
- Morikawa, S., P. Baluk, *et al.* (2002). "Abnormalities in pericytes on blood vessels and endothelial sprouts in tumors." *Am J Pathol* **160**(3): 985-1000.
- Ng, Q., V. Goh, *et al.* (2007). "Effect of nitric-oxide synthesis on tumour blood volume and vascular activity: a phase I study." *The Lancet Oncology* **8**(2): 111-118.
- Parkins, C. S., A. L. Holder, *et al.* (2000). "Determinants of anti-vascular action by combretastatin A-4 phosphate: role of nitric oxide." *Br J Cancer* **83**(6): 811-6.

- Pettit, G. R., S. B. Singh, *et al.* (1989). "Isolation and structure of the strong cell growth and tubulin inhibitor combretastatin A-4." Experientia **45**(2): 209-11.
- Reddy, S. B. and S. K. Williamson (2009). "Tirapazamine: a novel agent targeting hypoxic tumor cells." Expert opinion on investigational drugs **18**(1): 77-87.
- Saunders, M. P., A. V. Patterson, *et al.* (2000). "NADPH:cytochrome c (P450) reductase activates tirapazamine (SR4233) to restore hypoxic and oxycytotoxicity in an aerobic resistant derivative of the A549 lung cancer cell line." Br J Cancer **82**(3): 651-6.
- Siim, B. G., F. B. Pruijn, *et al.* (2004). "Selective potentiation of the hypoxic cytotoxicity of tirapazamine by its 1-N-oxide metabolite SR 4317." Cancer Res **64**(2): 736-42.
- Song, C. W. (1984). "Effect of local hyperthermia on blood flow and microenvironment: a review." Cancer Res **44**(10 Suppl): 4721s-4730s.
- Song, Z. J., P. Gong, *et al.* (2002). "Relationship between the expression of iNOS, VEGF, tumor angiogenesis and gastric cancer." World J Gastroenterol **8**(4): 591-5.
- Sun, J. R. and J. M. Brown (1989). "Enhancement of the antitumor effect of flavone acetic acid by the bioreductive cytotoxic drug SR 4233 in a murine carcinoma." Cancer Res **49**(20): 5664-70.
- Tannock, I. F. (1998). "Conventional cancer therapy: promise broken or promise delayed?" Lancet **351** Suppl 2: S119-16.
- Thomsen, L. L., F. G. Lawton, *et al.* (1994). "Nitric oxide synthase activity in human gynecological cancer." Cancer Res **54**(5): 1352-4.
- Thomsen, L. L., D. W. Miles, *et al.* (1995). "Nitric oxide synthase activity in human breast cancer." Br J Cancer **72**(1): 41-4.
- Thorpe, P. E. (2004). "Vascular targeting agents as cancer therapeutics." Clin Cancer Res **10**(2): 415-27.
- Tozer, G. M., S. Akerman, *et al.* (2008). "Blood vessel maturation and response to vascular-disrupting therapy in single vascular endothelial growth factor-A isoform-producing tumors." Cancer Res **68**(7): 2301-11.
- Tozer, G. M., S. M. Ameer-Beg, *et al.* (2005). "Intravital imaging of tumour vascular networks using multi-photon fluorescence microscopy." Adv Drug Deliv Rev **57**(1): 135-52.
- Tozer, G. M., C. Kanthou, *et al.* (2005). "Disrupting tumour blood vessels." Nature Reviews Cancer **5**(6): 423-35.
- Tozer, G. M., C. Kanthou, *et al.* (2008). "Tumour vascular disrupting agents: combating treatment resistance." The British journal of radiology **81** Spec No 1: S12-20.
- Tozer, G. M., V. E. Prise, *et al.* (1997). "Inhibition of nitric oxide synthase induces a selective reduction in tumor blood flow that is reversible with L-arginine." Cancer Res **57**(5): 948-55.
- Tozer, G. M., V. E. Prise, *et al.* (2009). "Nitric oxide synthase inhibition enhances the tumor vascular-damaging effects of combretastatin a-4 3-o-phosphate at clinically relevant doses." Clin Cancer Res **15**(11): 3781-90.
- Tozer, G. M., V. E. Prise, *et al.* (2001). "Mechanisms associated with tumor vascular shut-down induced by combretastatin A-4 phosphate: intravital microscopy and measurement of vascular permeability." Cancer Res **61**(17): 6413-22.
- Vaupel, P., F. Kallinowski, *et al.* (1989). "Blood flow, oxygen and nutrient supply, and metabolic microenvironment of human tumors: a review." Cancer Res **49**(23): 6449-65.
- Walton, M. I., C. R. Wolf, *et al.* (1992). "The role of cytochrome P450 and cytochrome P450 reductase in the reductive bioactivation of the novel benzotriazine di-N-oxide hypoxic cytotoxin 3-amino-1,2,4-benzotriazine-1,4-dioxide (SR 4233, WIN 59075) by mouse liver." Biochem Pharmacol **44**(2): 251-9.
- Wood, P. J., J. M. Sansom, *et al.* (1994). "Induction of hypoxia in experimental murine tumors by the nitric oxide synthase inhibitor, NG-nitro-L-arginine." Cancer Res **54**(24): 6458-63.
- Wood, P. J., I. J. Stratford, *et al.* (1993). "Modification of energy metabolism and radiation response of a murine tumour by changes in nitric oxide availability." Biochem Biophys Res Commun **192**(2): 505-10.

- Yu, J., E. D. deMunck, *et al.* (2005). "Endothelial nitric oxide synthase is critical for ischemic remodeling, mural cell recruitment, and blood flow reserve." Proc Natl Acad Sci USA **102**(31): 10999-1004.
- Zeman, E. M., J. M. Brown, *et al.* (1986). "SR-4233: a new bioreductive agent with high selective toxicity for hypoxic mammalian cells." Int J Radiat Oncol Biol Phys **12**(7): 1239-42.
- Zeman, E. M., V. K. Hirst, *et al.* (1988). "Enhancement of radiation-induced tumor cell killing by the hypoxic cell toxin SR 4233." Radiotherapy and oncology : journal of the European Society for Therapeutic Radiology and Oncology **12**(3): 209-18.

CHAPTER 2

Detecting vascular-targeting effects of the hypoxic cytotoxin tirapazamine in tumour xenografts using magnetic resonance imaging.¹

¹ A version of this chapter has been published.

Bains* LJ, Baker* JHE, Kyle AH, Minchinton AI, Reinsberg SA. (2009). International Journal of Radiation Oncology Biology Physics 74 (3): 957-965.

*Bains and Baker are co-first authors of this publication.

2.1 INTRODUCTION

2.1.1 *Tirapazamine (TPZ) as a hypoxic cytotoxin with anti-vascular activity*

The presence of hypoxic cells within tumours reduces the effectiveness of radiotherapy and is a known mechanism for tumour radioresistance (Brown and Wilson 2004). One strategy to combat this resistance is to utilize bioreductive cytotoxins, prodrugs that are reduced under low oxygen conditions to cytotoxic metabolites. Selective toxicity to hypoxic cells complements the preferential toxicity of radiotherapy to oxygenated tumour cells. Tirapazamine (TPZ; 3-amino-1,2,4-benzotriazine-1,4-di-N-oxide; SR 259075; formerly SR 4233) is the most advanced hypoxic cytotoxin under clinical development (for a review of tirapazamine, see Marcu and Olver (2006)).

Tirapazamine (TPZ) is reduced by cellular reductases to an oxidizing species that under conditions of low oxygen is further metabolized to oxidizing radicals that cause DNA damage (Anderson *et al.* 2005). *In vivo* experiments have shown anti-cancer activity of TPZ in multiple tumour models and in combination with radiotherapy (Zeman *et al.* 1988; Dorie *et al.* 1994). However, the anti-cancer activity of TPZ is something of a paradox, as compelling evidence using spheroids and multi-cellular cultures suggests that TPZ is unable to penetrate efficiently through tumour tissue to reach chronically hypoxic cells located far from vasculature (Durand and Olive 1992; Durand and Olive 1997; Hicks *et al.* 1998; Kyle *et al.* 1999). This poor penetration of TPZ has been attributed to bioreductive activation at intermediate oxygen tensions more proximal to vasculature (Kyle *et al.* 1999; Cárdenas-Navia *et al.* 2007).

We have previously reported an observation of the unexpected ability of TPZ to mediate central vascular dysfunction in murine syngeneic and human xenograft tumours grown in mice (Huxham *et al.* 2006; Huxham *et al.* 2008). This anti-vascular activity of TPZ could have a significant impact on its application if found to be clinically relevant.

2.1.2 *Dynamic Contrast Enhanced Magnetic Resonance Imaging (DCE-MRI)*

Monitoring drug effects on tumour blood volume, flow and permeability non-invasively can be accomplished using magnetic resonance imaging (MRI). It has been used extensively in both pre-clinical and clinical situations investigating the effects of vascular

disrupting agents (VDAs) such as combretastatin (Galbraith *et al.* 2003), ZD6126 (Robinson *et al.* 2003) and DMXAA (McPhail *et al.* 2006). MRI has also been employed in clinical investigations of vascular disrupting agents (for a review see (O'Connor *et al.* 2007)). This chapter presents a method for evaluating the effects of TPZ non-invasively using two dynamic contrast-enhanced MRI (DCE-MRI)-derived biomarkers for assessment of anti-vascular agents: initial area under the curve (IAUC) and K^{trans} .

2.1.3 Current study outline

The experiments presented in this chapter follow the schematic presented in Figure 2.1. HCT116 tumour-bearing mice received baseline MR scans, were subsequently treated with TPZ, and received a follow-up scan at 24 hours. Cryosections of tumour slices corresponding to MR imaging regions of interest were obtained using fiducial markers. Tumours were evaluated for TPZ-mediated vascular dysfunction using staining data for vasculature, perfusion and necrosis. These histological tumour mapping analyses were used to confirm and validate observations seen in DCE-MRI data and parameter maps. DCE-MRI has the potential to be highly beneficial for determining whether TPZ-mediated loss of perfusion occurs in patients, and whether this is a contributing mechanism for the clinical anti-cancer activity of TPZ.

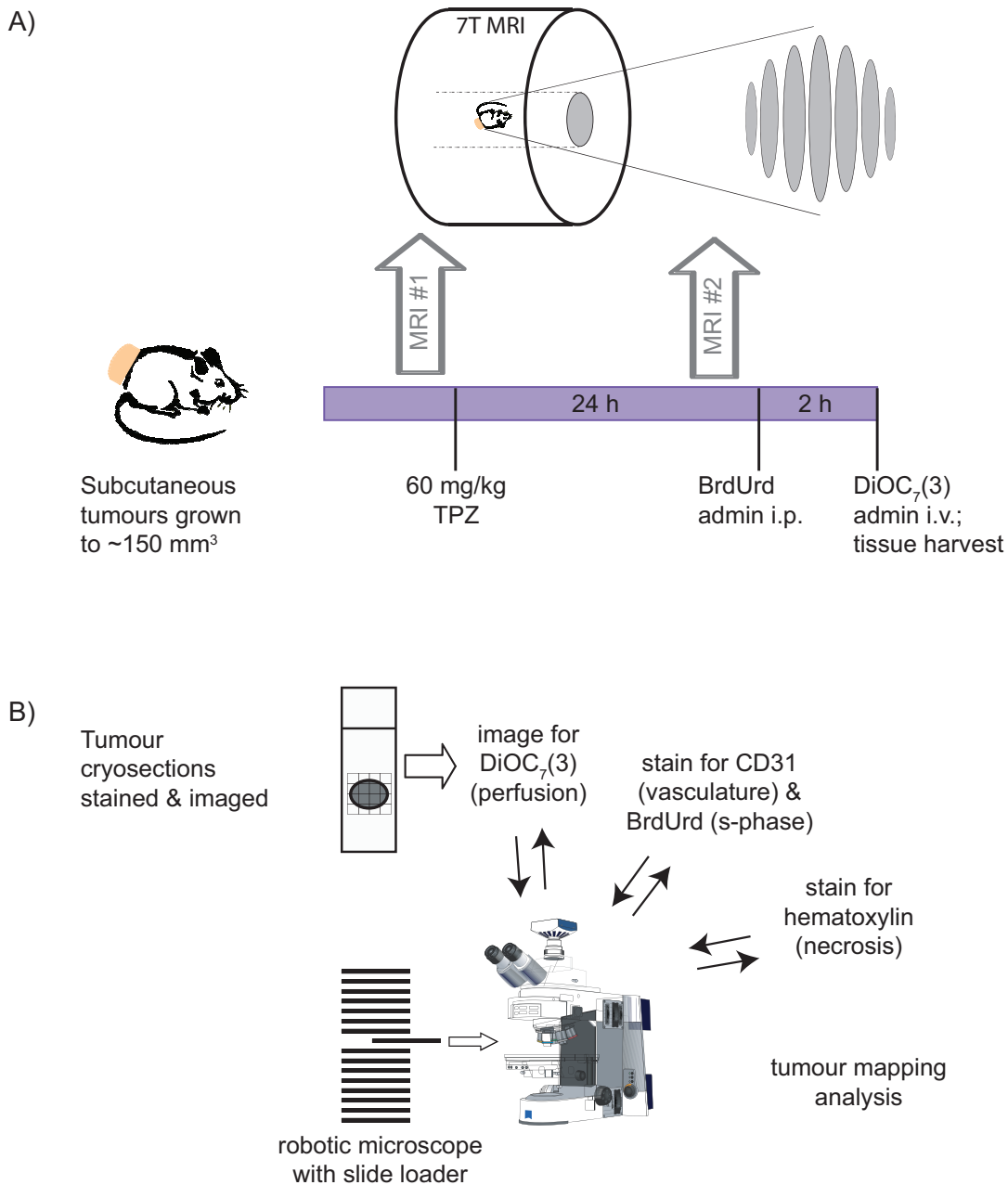


Figure 2.1 Experiment overview.

A) HCT116 tumours grown subcutaneously in the dorsal region of mice were imaged using a 7T MR scanner. A second MR scan was obtained 24 h following 60 mg/kg treatment with TPZ. S-phase marker BrdUrd was administered 2 h prior to an intravenous injection of perfusion marker DiOC₇(3) administered 5min prior to euthanasia. Tumour tissues were excised with fiducial markers attached. (B) A robotic microscope with automated slide loader obtains tiled images of whole tumour cryosections at a resolution of $1.5 \mu\text{m}/\text{pixel}$. Fluorescent images of DiOC₇(3) were obtained prior to staining and imaging for CD31 (vasculature), BrdUrd (S-phase cells) and hematoxylin. Overlaid images were cropped and analyzed; corresponding MR images and histological images were compared.

2.2 METHODS

2.2.1 Mice, fiducial markers and tumours

NOD/SCID mice aged 8 - 11 weeks, weighing 19 to 24 g, were bred in our institutional animal facility; experiments in this chapter were approved by the University of British Columbia and its Animal Care Committee (Appendices B, C, D). Fiducial markers (Figure 2.2) were constructed of polyethylene tubing (inner diameter 0.58 mm) and filled with paraffin wax and saline creating an MR-visible interface that was also detectable in cryosections. Marker tubes were implanted subcutaneously (s.c.) in the sacral region of mice, craniocaudal orientation, two days prior to s.c. implantation of 8×10^6 HCT116 cells. Histological sections and MRI slices were taken such that the fiducial marker lay perpendicular to the imaging plane of each slice; the fixed nature of the marker ensured small angular differences between sectioning planes for histological and serial MR slices. The mean weight \pm standard error (s.e.) of excised tumours was 512 ± 68 mg.

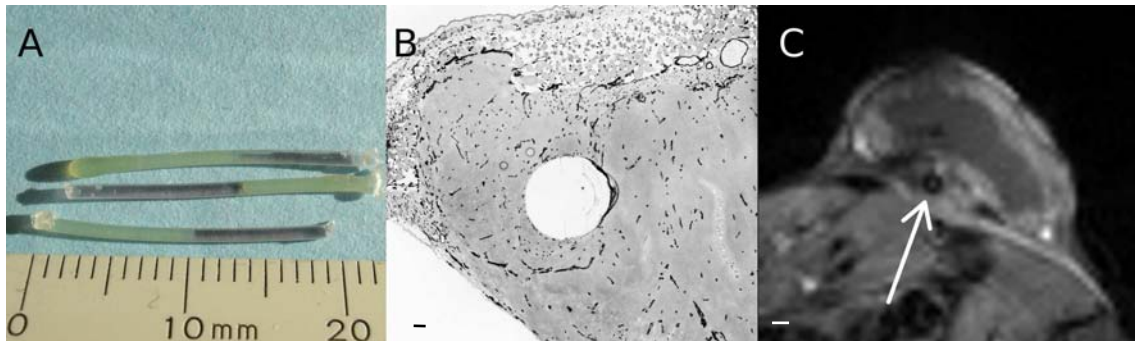


Figure 2.2 Fiducial markers.

A) 2 cm sections of tubing were filled with paraffin (green) and saline (purple), and implanted subcutaneously in the sacral region of mice. 2 days later, 8×10^6 HCT116 cells were implanted in the same region. Tumours typically grew around tubes and could be identified in histological sections, as shown in a magnified CD31 image (B) (scale bar $150 \mu\text{m}$) and MR images, white arrow (C) (scale bar $500 \mu\text{m}$). The locations of fiducial markers are also indicated in Figure 2.5 and Figure 2.6 by blue stars.

2.2.2 Treatments

Mice were anaesthetized with isoflurane, received an MRI scan and were administered either TPZ or vehicle one hour after removal from anaesthesia. TPZ (synthesized by Dr. L.A. Huxham (Huxham *et al.* 2006)) was administered by intraperitoneal (i.p.) injection at 60 mg/kg (0.34 mmol/kg) using a 1.25 mg/ml solution in saline. A second MRI scan was obtained 24 hrs after treatment; mice awakened promptly following anaesthesia, however some TPZ-treated mice required longer periods to recover to their pre-anaesthesia fitness. No correlation was found between length of recovery time and response to TPZ treatment. Mice that recovered within 35 min post-anesthesia received 500 mg/kg i.p. 5-bromo-2-deoxyuridine (BrdUrd, Sigma Chemical, Oakville, ON) as a back-up perfusion marker (Janssen *et al.* 2005), with tumour excision one hour post-BrdUrd administration. All mice received a 35 μ l intravenous dose of 0.6 mg/ml carbocyanine, DiOC₇(3), (Molecular Probes, Eugene, OR) in 75 % DMSO 5 minutes before euthanasia. Excised tumours were embedded and frozen with fiducial markers at -20°C.

2.2.3 DCE-MRI

MR images were acquired using a 7T horizontal-bore Bruker BioSpec 65/35 with a transmit/receive solenoid coil. A fast low-angle shot sequence (FLASH) (6 slices, 1mm thickness, 0.5 mm gap, 312.5 μ m in-plane resolution) with a repetition time TR = 226 ms was performed, followed by a FLASH with a TR of 113 ms; both used a flip angle of 75°. Contrast agent (35 mM Gd-DTPA, 10 μ l/g) was injected via tail vein catheter at 18 μ l/s using a power injector. Ten pre-contrast and 124 post-contrast image stacks were acquired at time resolution of 14.5 s.

2.2.4 Immunohistochemical staining and image acquisition

Serial step 10 μ m cryosections were cut at 0.5 mm intervals, imaged for carbocyanine fluorescence and fixed in acetone-methanol for 10 min. Vasculature and proliferation were stained using antibodies for CD31 and incorporated BrdUrd respectively (Kyle *et al.* 2003) and slides were counterstained with hematoxylin. Whole tumour sections were imaged as previously reported (Kyle *et al.* 2007) using a system which allowed for tiling of adjacent

microscope fields of view such that images of entire tumour cryosections were captured at a resolution of 1.5 μm per pixel.

2.2.5 Image analysis

Similar image analysis methods have been previously reported with additional detail provided below (Huxham *et al.* 2006; Huxham *et al.* 2008). Using both fiducial and anatomical landmarks, six cryosections per tumour were identified that matched the MRI slices. Using NIH-Image and user-supplied algorithms, digital images were superimposed. Tumours were manually cropped to tumour tissue boundaries with staining artefacts removed; necrosis was subsequently cropped from hematoxylin images. The viable fraction (VF) is derived from the proportions of necrotic and whole tissue. Values reported in this thesis reflect the proportion of necrosis as (1-VF). Positive fluorescence for CD31 and carbocyanine images was obtained by applying a threshold (>5 SDs above background) with neighbouring positive pixels grouped as 'objects'. The perfused vessel fraction (PF) was calculated as the proportion of CD31 positive objects that were also at minimum 20 % overlapped with positive carbocyanine pixels on the overlaid image.

Each histological section was manually aligned with the corresponding MR slice using custom IDL software (Interactive Data Language, 2007). For MRI/histological image correlative analyses, carbocyanine images with a pixel size of 1.5 μm x 1.5 μm were thresholded and the number of carbocyanine positive objects in an area corresponding to an MRI pixel (0.3125 mm x 0.3125 mm) was calculated. A 0.3 mm x 0.3 mm resolution 'carbocyanine map' depicting pixels at intensities representative of the number of perfused vessels in the histological sections was produced. Data for individual tumours are displayed as means for six analyzed slices per tumour \pm s.e.

2.2.6 Scoring vascular dysfunction response

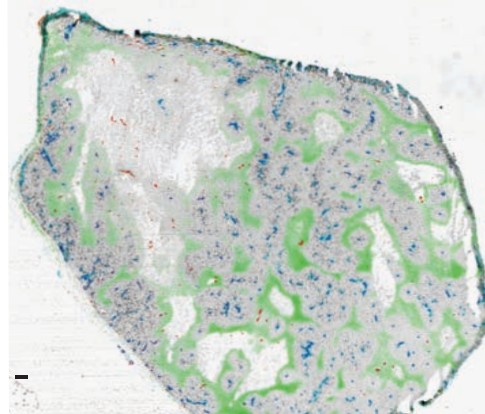
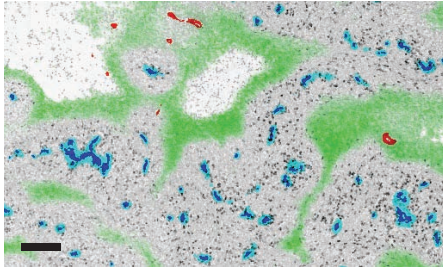
A combined Vascular Dysfunction Score (VDS) was used to determine an objective, quantifiable assessment of vascular dysfunction response to TPZ; see Figure 2.3 for a rationale for the VDS.

The VDS reported here incorporates both the viable fraction (VF) and perfused fraction (PF) within a tumour section:

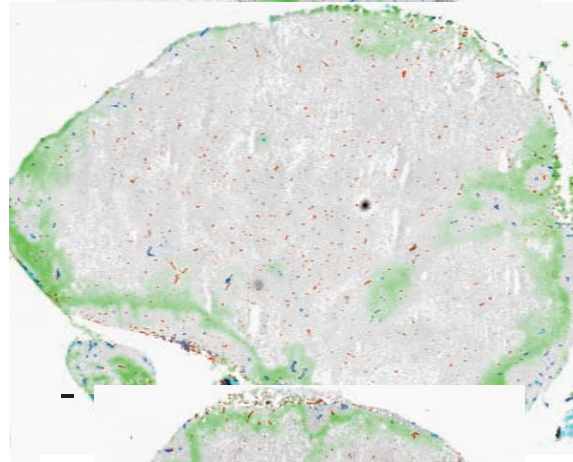
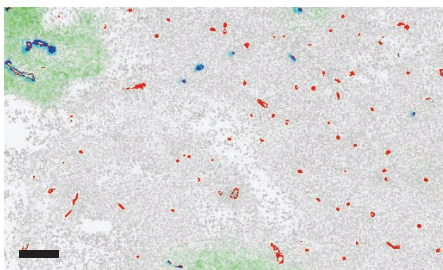
$$\text{VDS} = 1 - (\text{VF} \times \text{PF}_c)$$

The PF_c was calculated as the proportion of perfused vessels for a tumour (PF; see above) divided by the maximum proportion of perfused vessels as observed in controls. For individual tumours a VDS will be 0 if all the tumour tissue is viable ($\text{VF} = 1$) and vessels are all perfused ($\text{PF} = 1$). It will be higher for cases of increased necrosis or reduced perfusion. This objective score permits quantitative evaluation of tumours that may have loss of perfusion measurable using either CD31 staining combined with a perfusion marker, or necrosis in tumours that have no remaining CD31. Tumours with a VDS of > 2 SDs higher than the mean control score (VDS_{min}) are considered strong-responders to TPZ and remaining tumours are described as non-responders.

A) Control HCT116



B) Vascular dysfunction in HCT116:
lots of unperfused CD31



C) Vascular dysfunction in HCT116:
unperfused tissue becoming necrotic

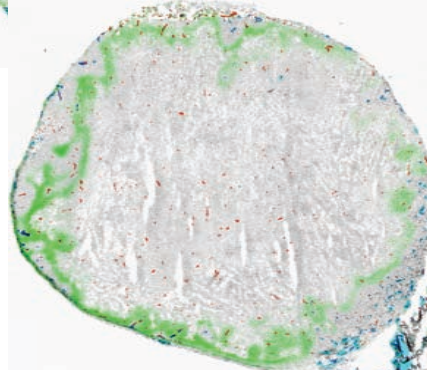
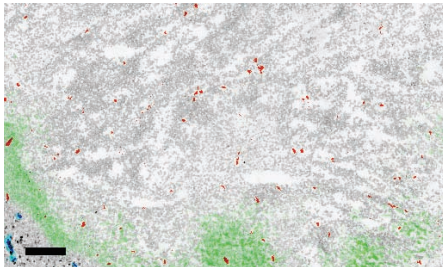


Figure 2.3 Rationale for combined Vascular Dysfunction Score (VDS)

Images of a representative HCT116 control tumour (A) show typical corded architecture with perfusion marker DiOC₇(3) labeling of CD31 stained vasculature (blue) surrounded by BrdUrd labeled S-phase cells (black) and regions of hypoxia labeled with pimonidazole (green). Vascular dysfunction may manifest as in tumour (B) where unperfused CD31 stained vascular objects (red) remain in central areas of otherwise viable tissue identified using hematoxylin counterstaining (grey). An alternate manifestation of vascular dysfunction may appear as in tumour (C) where CD31 staining is disappearing and tissue is becoming necrotic. Quantification of the proportion of perfused vessels (PF) would indicate vascular dysfunction for tumour (B). However, fewer CD31 stained objects may remain in a tumour (C), and describing both the loss of perfusion and the proportion of viable tissue (VF) more robustly represents vascular dysfunction.

2.2.7 DCE-MRI analysis

Custom IDL software was used to calculate change in T1 using signal intensity images from pre-injection (TR = 226ms) and baseline (TR = 113ms) scans to create concentration time curves. Relaxivity of the contrast agent was determined in a phantom study using diluted contrast agent samples. Initial Areas under the Concentration Time Curves (IAUCs) were calculated by integrating the concentration time curves from the beginning of enhancement to the fourth frame (60 s post contrast arrival). A two-compartment (Figure 2.4) Kety model was used to find the transfer constant (K^{trans}) describing movement of contrast agent from blood plasma (V_p) into the extravascular extracellular tissue space (V_e) (Tofts and Kermode 1991). The relationship between the concentrations of contrast agent in the tissue and the blood plasma are described by the equation ,

$$C_t(t) = K^{trans} \int_0^t C_p(\tau) e^{-\frac{K^{trans}}{v_e}(t-\tau)} d\tau$$

where $C_t(t)$ and $C_p(t)$ are the time-dependent concentration of contrast agent in the tissue and vascular plasma, respectively.

2.2.8 Radial analysis

Custom radial intensity analysis IDL software was created to quantify each parameter as a function of distance from the tumour edge. Starting from the outside edge, 312.5 μm rims were created and parameter means pooled for all six slices in a tumour. As a measure of tumour radial heterogeneity, a heterogeneity index (HI) was calculated as the percent difference between two weighted means: the outer 1/3 and the inner 2/3 of the tumour.

2.2.9 Statistics

All statistical analyses were performed using the GraphPad Prism software (Version 4.0c for Macintosh, 2005). Non-parametric tests were used in all instances: typically a Kruskal-Wallis analysis of variance rank test, followed by Dunn's post tests between groups. P values < 0.05 (*) and < 0.01 (**) are reported. A Spearman's rank correlation was used for IAUC mean values and a Pearson's correlation coefficient with 95 % confidence intervals is reported for regression analyses for IAUC radial profiles vs. carbocyanine fluorescence.

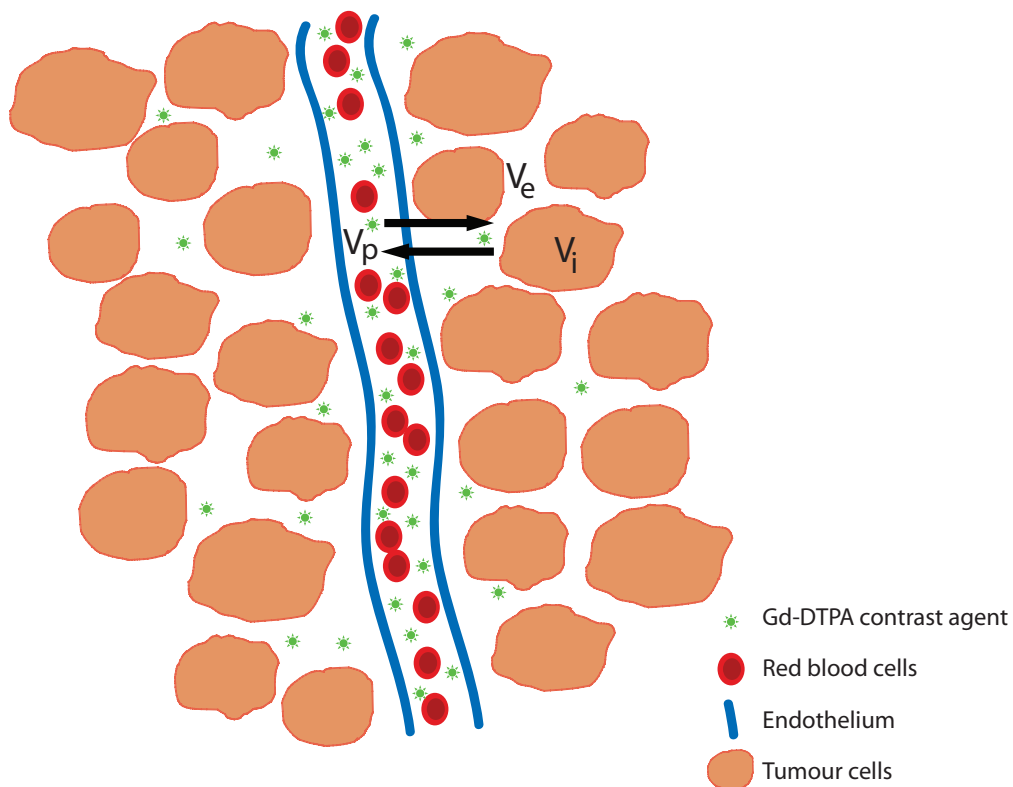


Figure 2.4 Compartmental modeling of DCE-MRI contrast agent.

The two compartment Kety model of contrast agent delivery comprises the vascular plasma volume (V_p), and the extravascular extracellular tissue volume (V_e). Gd-DTPA does not penetrate the cellular membrane and is therefore excluded from the intracellular compartment (V_i). A single intravenous bolus administration of contrast agent (Gd-DTPA, green stars) is delivered to the tumour via the vasculature (blue). The amount of contrast agent in either of the compartments depends on the surface area and permeability of the endothelium, the concentration difference between the two compartments, as well as blood flow, heart rate and blood pressure.

2.3 RESULTS

HCT116 tumour bearing mice were examined using DCE-MRI before and after treatment with TPZ, and immunohistochemistry based tumour mapping was subsequently performed on the same tumours. Figure 2.5 contains images of both MRI and tumour mapping modalities, and displays sample tumours from untreated control (tumour 4) and TPZ-treated mice that either did (tumour 12) or did not (tumour 7) respond with central vascular dysfunction following TPZ treatment.

Figure 2.6 illustrates further examples of TPZ-treated tumours, including one tumour classed as a non-responder (tumour 9) and two tumours with evidence of strong central vascular dysfunction (tumours 13, 14).

2.3.1 Histological analysis identifies tumours with an increase in necrosis or a decrease in perfusion in response to TPZ

Response to TPZ was assessed by examining both the amount of necrosis (1-VF), Figure 2.7A, and the number of perfused vessels, Figure 2.7B. Combined vascular dysfunction scores (VDS) were calculated for all tumours, Figure 2.7C, with controls showing a mean VDS of 0.386 ± 0.203 (mean \pm SD). VDS's for tumours 7, 8 and 9 were $< VDS_{\min}$ (0.792) and are subsequently classed as 'non-responders', whereas tumours 10 to 14 had $VDS > VDS_{\min}$ and were objectively classified as 'responders'. This proportion of responder (63 %) and non-responder (37%) HCT116 tumours treated with tirapazamine is consistent with previous studies examining vascular dysfunction response using tumour mapping data (Huxham *et al.* 2006).

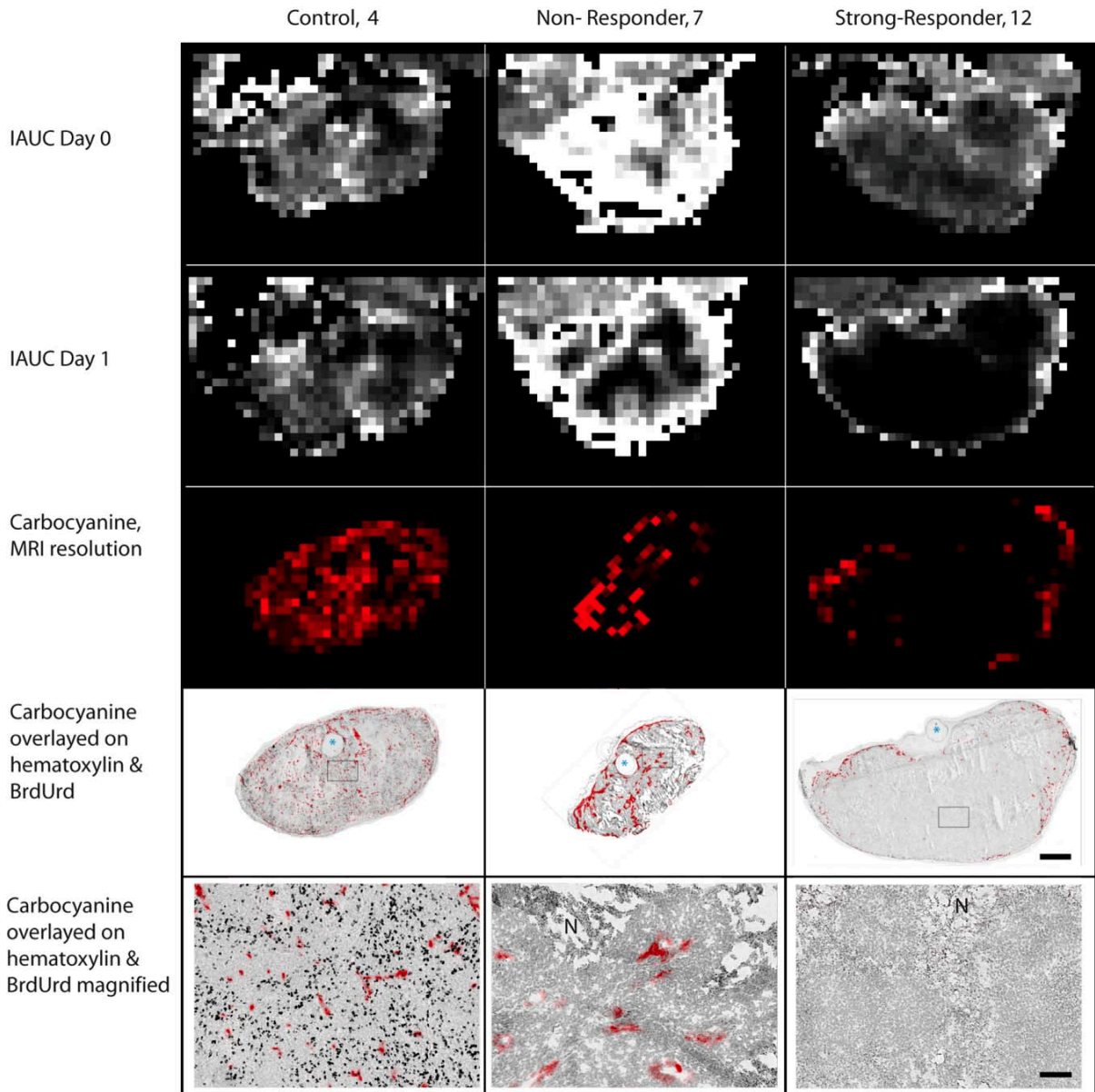


Figure 2.5 DCE-MRI and histological parameter data maps and images of HCT116 tumours.

Parameter data maps reflect the calculated IAUC values for individual voxels for baseline day 0 (row 1) and day 1 (row 2), and the fraction of perfused vessels measured using histology displayed at MR resolution (row 3). Histological tumour maps are shown as composite images of carbocyanine fluorescence (red) overlaid on the hematoxylin counter-stained tissue background (grey), with BrdUrd staining in black (row 4). Boxed areas indicate magnified regions (row 5); N = necrotic; blue stars = fiducial markers. Row 4 scale bar is 1250 μm , row 5 is 125 μm .

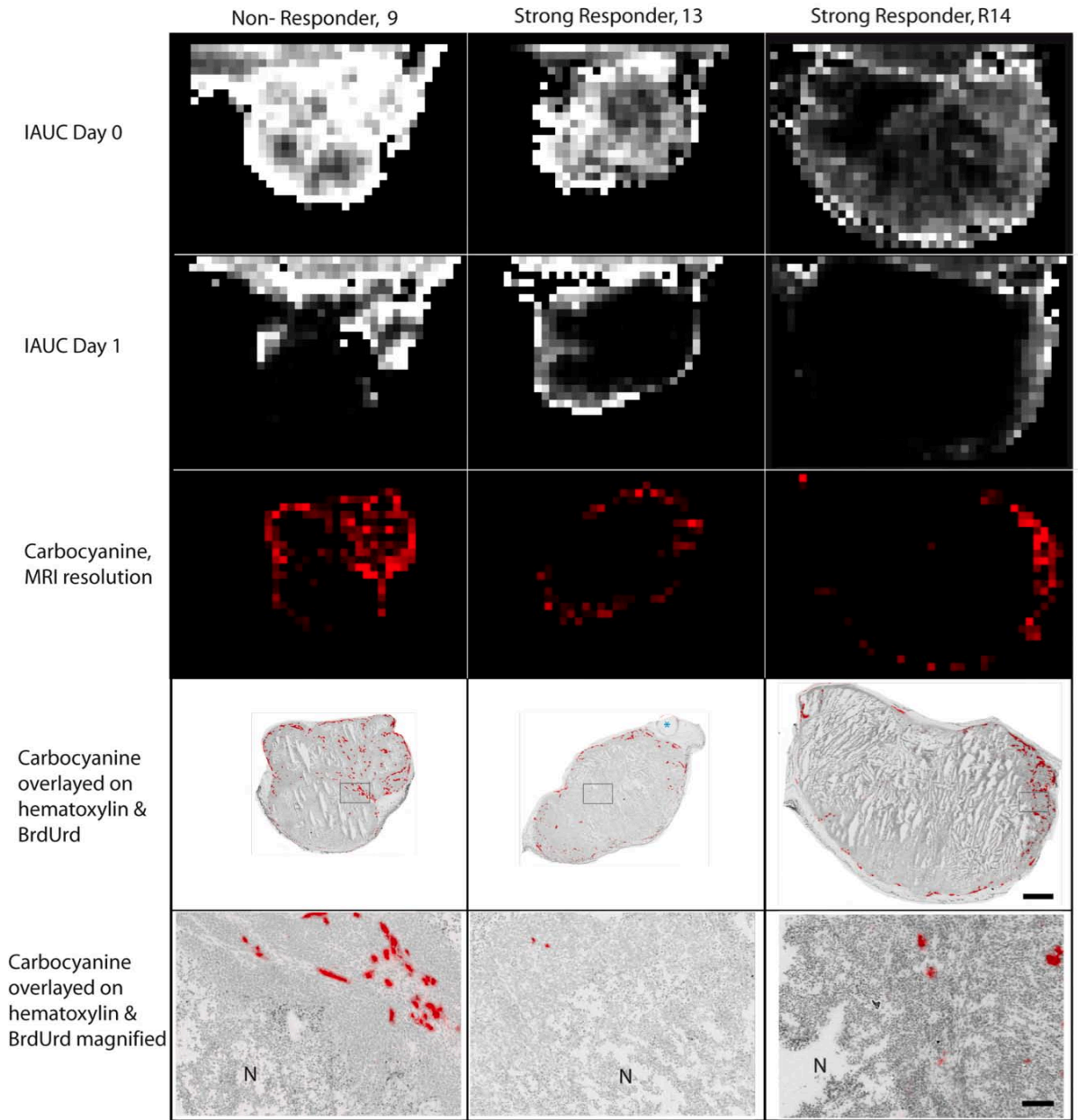


Figure 2.6 DCE-MRI and histological parameter data maps and images of HCT116 tumours

Parameter data maps reflect the calculated IAUC values for individual voxels for baseline day 0 (row 1) and day 1 (row 2), and the fraction of perfused vessels measured using histology displayed at MR resolution (row 3). Histological tumour maps are shown as composite images of carbocyanine fluorescence (red) overlaid on the hematoxylin counter-stained tissue background (grey), with BrdUrd staining in black (row 4). Boxed areas indicate magnified regions (row 5); N = necrotic; blue stars = fiducial markers. Row 4 scale bar is 1250 μm , row 5 is 125 μm .

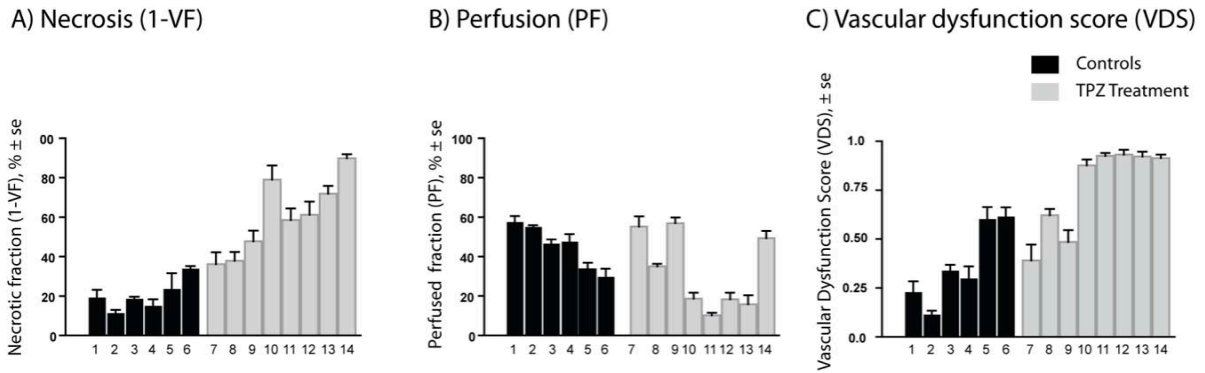


Figure 2.7 Tirapazamine -mediated changes in vascular function measured using histological analysis.

Amounts of necrosis (1-VF) (A) and perfusion (PF) (B) in sections of individual control and tirapazamine treated tumours. Vascular Dysfunction Scores (VDS) are reported (C), incorporating both necrosis and perfusion values. Tumours 7-9 are classed as non-responders; tumours 10-14 are strong-responders.

2.3.2 *BrdUrd* data not included

BrdUrd is a nucleotide analogue that is useful as a marker of cells in S-phase. BrdUrd is delivered to tumour tissue via tumour blood vessels, which means that it can function as a perfusion marker (Janssen *et al.* 2005). However, in cases of vascular dysfunction, it is difficult to differentiate between poor delivery of the marker and a decrease in proliferation in areas of low BrdUrd incorporation. In our previous studies, low BrdUrd staining reflected a decrease in proliferation in areas around perfused blood vessels following TPZ administration, with large areas of unperfused tissue also showing a complete lack of BrdUrd incorporation, likely due to a combination of decreased proliferation and poor delivery of the marker (Huxham *et al.* 2006; Huxham *et al.* 2008). In data presented in the current chapter, BrdUrd was administered at a lower dose to some mice to assist in determination of large areas of perfusion loss using the tumour mapping images, however carbocyanine was successfully injected intravenously in every animal, providing a more reliable marker for perfusion assessment. Our MR imaging protocol is unable to evaluate proliferation for useful comparisons between tumour mapping and imaging, making proliferation data of relatively low value for this study and it is consequently not included.

2.3.3 DCE-MRI analysis shows decreases in IAUC and K^{trans} for TPZ-treated tumours with central vascular dysfunction

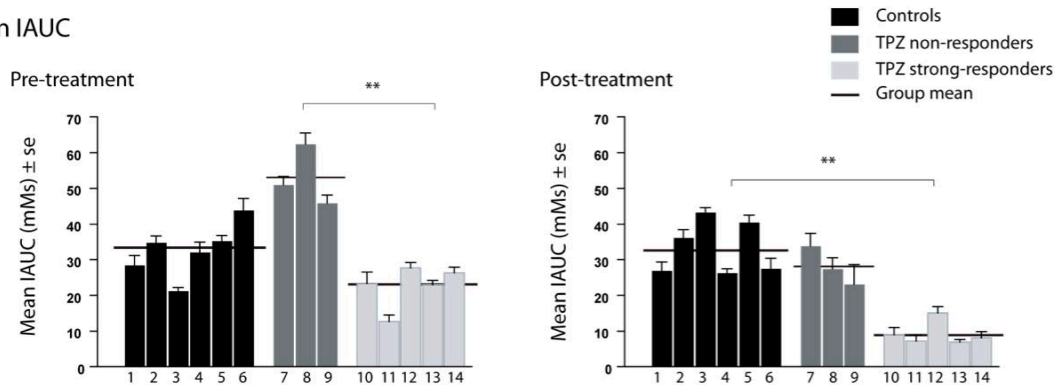
Control tumours show no significant changes in their pre- and 24h post-treatment IAUC values, while TPZ-treated tumours show a combined average reduction. Whole tumour mean IAUCs for all tumours are shown in Figure 2.8A, with retrospective classification of TPZ-treated tumours into non- and strong- responders based on histological data (VDS). Strong-responding tumours have significantly lower post-treatment IAUC values relative to controls whereas non-responders are similar to controls (Figure 2.8C).

Non-responders have greater *pre-treatment* IAUC values relative to strong-responders. Pre-treatment IAUC and VDS in response to TPZ are correlated using the Spearman's rank test ($R = -0.667$, one-sided $p = 0.042$) (Figure 2.11B). Spearman's rank correlation is also significant between pre- and post- treatment IAUC values in all treated tumours ($R = 0.929$, one-sided $p = 0.001$) (Figure 2.11A). These data indicate that higher pre-treatment IAUC predicts for higher post-treatment IAUC and for a low VDS score. Note that, prior to retrospective separation into non-and strong- responders, the mean baseline IAUC value of the treated group is not significantly different from the control group.

Mean K^{trans} values exhibit similar trends; strong-responders show marked reduction of average K^{trans} (73 % reduction) while non-responders show a non-significant ($p = 0.1$) average loss from pre-treatment values (59 % reduction). As shown in Figure 2.8B, elevated pre-treatment K^{trans} values are seen in those tumours that did not respond to TPZ treatment relative to the strong responders, and only the strong-responders have a significantly lower post-treatment K^{trans} value relative to controls.

Therefore, both DCE-MRI derived biomarkers IAUC and K^{trans} assessed prior to TPZ treatment predicted which HCT116 colorectal xenografts responded with vascular dysfunction.

A) Mean IAUC



B) Mean K^{trans}

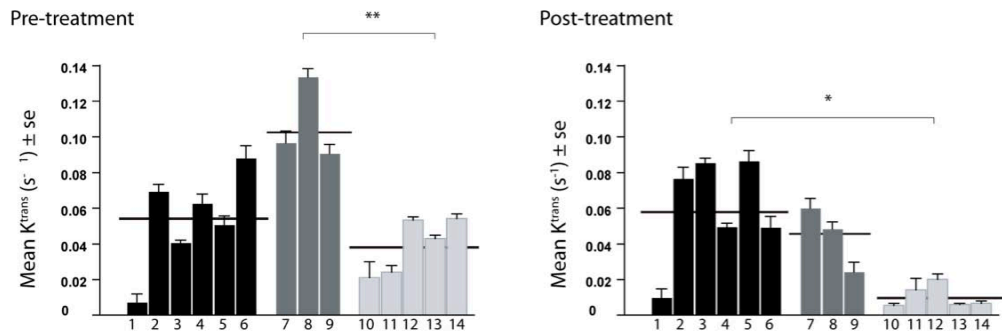


Figure 2.8 Tirapazamine-mediated changes in vascular function measured using DCE-MRI parameters IAUC and K^{trans} .

DCE-MRI derived biomarkers IAUC (A) and K^{trans} (B) are shown where bars represent individual tumours, horizontal lines indicate group means. TPZ-treated groups were retrospectively classed as non- and strong- responders based on histological data (* $p < 0.05$) (** $p < 0.01$).

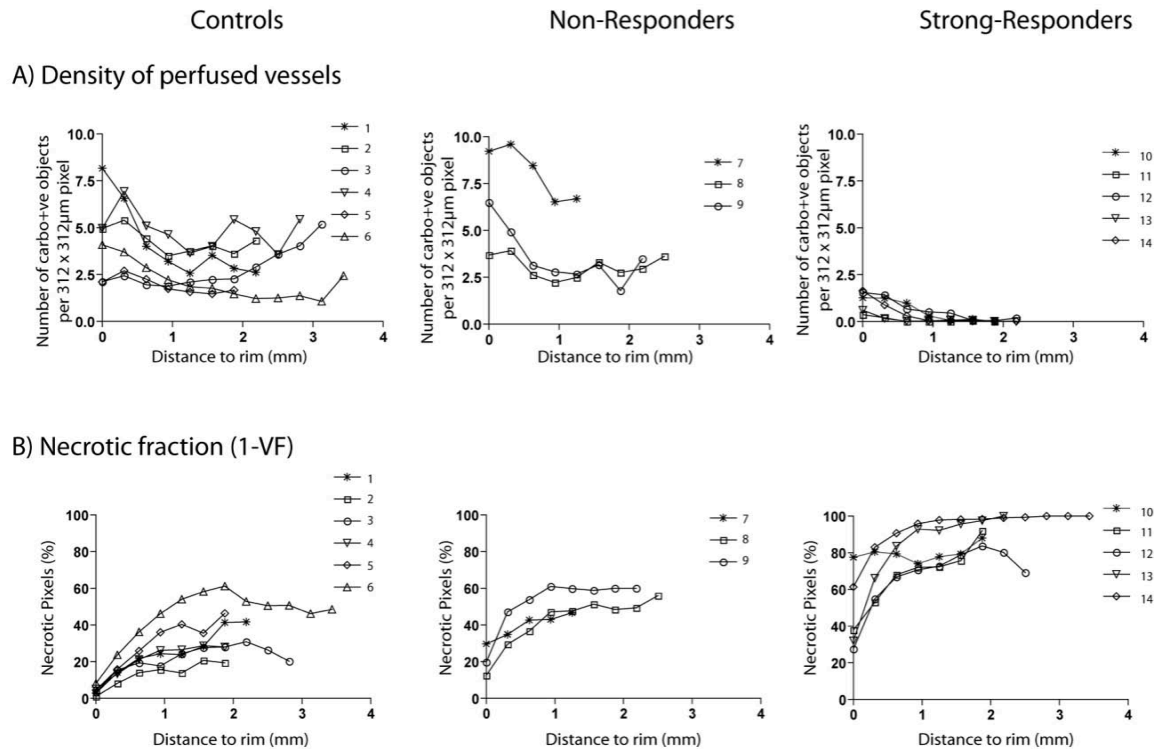


Figure 2.9 Tumour mapping microregional heterogeneity in response to TPZ.

Radial analyses of images show small amounts of perfusion (A) and large amounts of necrosis (B) in the central regions of TPZ-treated strong responding tumours.

2.3.4 Microregional heterogeneity of response to TPZ

MRI and histological maps (Figures 2.4, 2.5) illustrate that some TPZ-treated tumours experienced a loss of perfusion in central regions but retained a peripheral rim of perfused tissue. Figure 2.9A shows the average density of carbocyanine-positive vessels as a function of distance from the tumour margin. Control (left) and non-responders (middle) show comparable amounts of carbocyanine throughout their tissues, while strong-responders (right) show only a few remaining perfused vessels at the rim. Figure 2.9B shows the radial distribution of necrotic tissue; as is typical for HCT116 xenografts, necrosis is observed in treatment-naïve tumours (left), particularly in the central regions. This necrosis is elevated slightly for non-responders (middle) and is increased dramatically in strong-responders (right), reaching nearly 100 % as close as 1 mm to the tumour margin in some tumours.

Similar analysis for IAUC is shown in Figure 2.10 where the radial distribution of IAUC in all tumours before treatment (A) exhibits a slight gradient with higher values at the periphery relative to distances further from the margin. After treatment with TPZ, tumours classified as strong-responders (B, right) show mean IAUCs approaching zero towards the centre of tumours, while non-responders show IAUCs which are reduced from pre-treatment levels but do not reach zero (B, middle). MRI parameter maps were compared with histology tumour maps to determine whether data and images were successfully obtained from similar areas of tumours. In addition to visual confirmation of co-registration (Figures 2.5, 2.6), a quantitative comparison was done by correlating the heterogeneity indices (HI) for post-treatment IAUC parameter maps and carbocyanine histological maps (Figure 2.11C) where a positive correlation was observed (Pearson correlation $R = 0.79$, with 95 % confidence intervals 0.45 - 0.93).

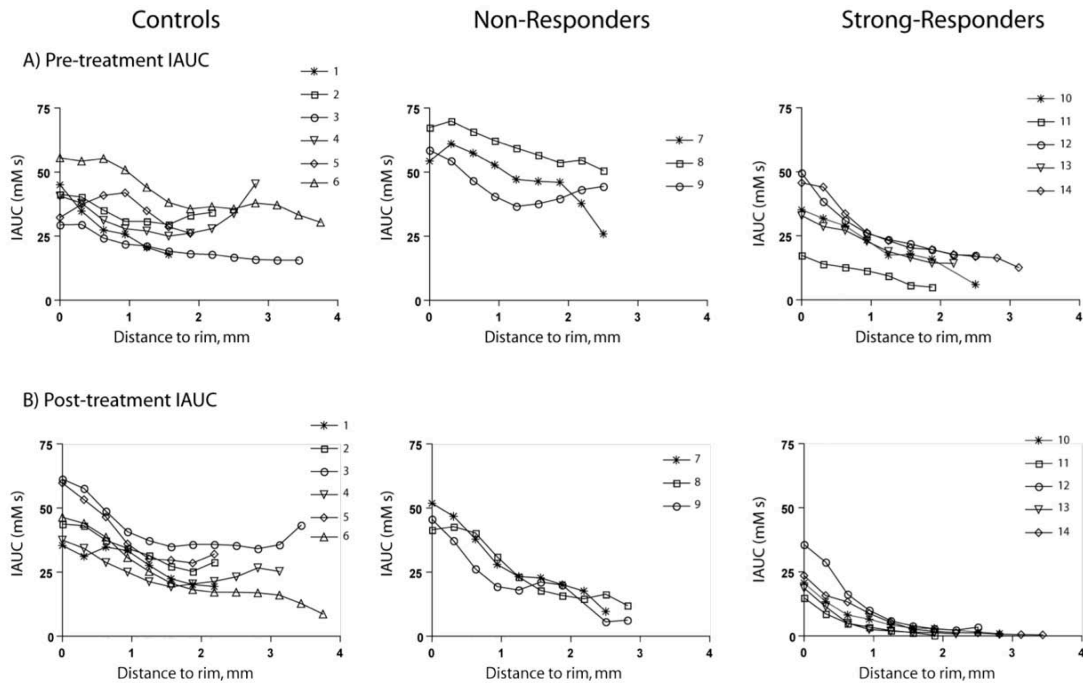
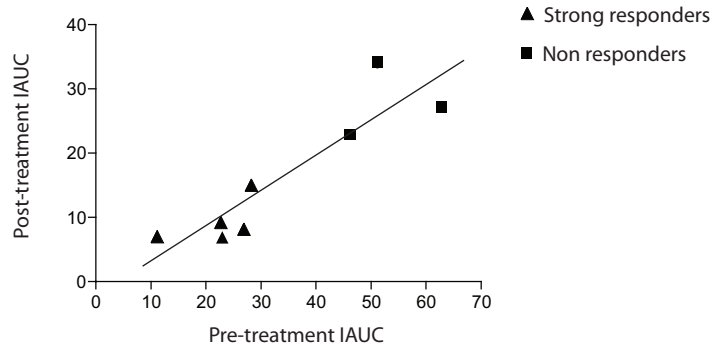


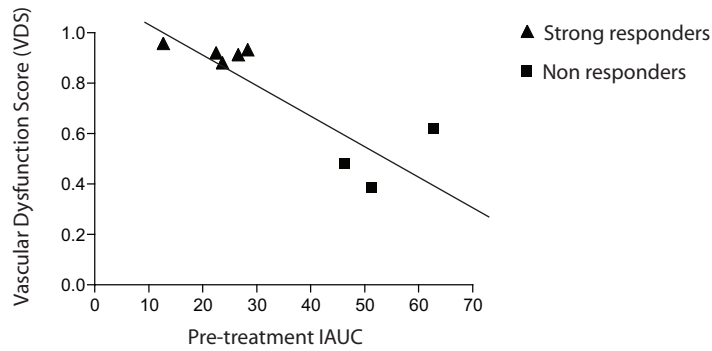
Figure 2.10 MRI microregional heterogeneity in response to tirapazamine.

Losses in perfusion occur predominantly in the central regions of strong responding tumours, as shown with radial analyses of IAUC parameter maps before (A) and after (B) treatment with TPZ.

A) Pre-treatment IAUC vs Post-treatment IAUC



B) Pre-treatment IAUC vs Vascular Dysfunction Score



C) Heterogeneity Index Correlation: Post-IAUC values vs carbocyanine

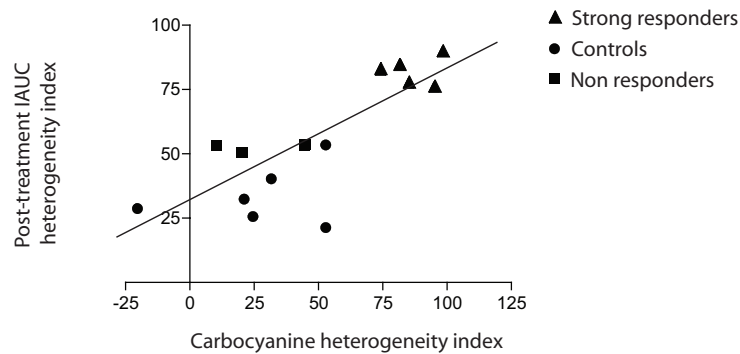


Figure 2.11 Correlation of MRI and histology features.

Evidence for pre-treatment MRI parameter IAUC as a useful predictor for tumour response to TPZ comes from correlations of pre- and post-treatment IAUC values (A) and of pre-treatment IAUC values with the Vascular Dysfunction Score (B). Successful co-registration of MRI and histological parameter maps is suggested by positive correlation of post-treatment IAUC heterogeneity index with the carbocyanine heterogeneity index (C).

2.4 DISCUSSION

Although the effectiveness of tirapazamine (TPZ) has been attributed to its cytotoxicity to hypoxic tumour cells, its poor tissue penetration profile (Durand and Olive 1992; Durand and Olive 1997; Hicks *et al.* 1998; Kyle *et al.* 1999) presents a paradox regarding its mechanism for anti-cancer activity *in vivo*. Using immunohistochemistry (IHC) based tumour mapping, we have previously shown that TPZ has an unexpected vascular-targeting effect in multiple tumour models (Huxham *et al.* 2006; Huxham *et al.* 2008), leading to the question of whether this effect also occurs in patients. Studies in this chapter investigate the use of DCE-MRI as a clinically relevant tool for observing TPZ-mediated vascular dysfunction.

Studies followed three major steps: a baseline DCE-MRI scan followed by TPZ treatment, a follow up scan at 24 h post-treatment, and finally, tumour excision and histological analysis.

2.4.1 DCE-MRI parameters IAUC and K^{trans}

DCE-MRI is a noninvasive method of quantitatively measuring vascular function by monitoring tumour uptake of a systemically administered contrast agent. Interpretation of DCE-MRI-derived data is complex and sensitive to several physiological parameters, including blood flow, vascular surface area, vascular permeability, tumour extravascular space and patient physiological values such as heart rate and blood pressure (Figure 2.4) (O'Connor *et al.* 2007). Initial Area Under the contrast agent Concentration time-curve (IAUC) is a model-free value that reflects uptake of the contrast agent in tumours. The volume transfer coefficient (K^{trans}) reflects the transfer of contrast agent from the blood vessels and the extravascular space, and is interpreted as an indication of vascular permeability or tumour blood flow depending on whether contrast agent delivery is limited by blood flow or permeability (Tofts *et al.* 1999). IAUC and K^{trans} are distinct biomarkers that are reasonably reproducible and are used in assessing tumour vascular function in both pre-clinical and clinical studies (Roberts *et al.* 2006). Unfortunately, standardized methods for the use of DCE-MRI are not yet agreed upon. Methods for measurement, analysis and interpretation of DCE-MRI data that would be useful in multiple centres and for use in

clinical trials to provide meaningful, biologically validated endpoints continue to be developed (Leach *et al.* 2005; Roberts *et al.* 2006; O'Connor *et al.* 2007).

Several pre-clinical studies have used MRI in the investigation of vascular disrupting agents (VDAs), including examinations of ZD6126 (Breidahl *et al.* 2006), DMXAA (McPhail *et al.* 2006) and CA-4-P (Beauregard *et al.* 2001). MRI has also been employed in clinical investigations of VDAs (see (O'Connor *et al.* 2007) for a review of MRI evaluation of VDAs in the clinic). Post-treatment examination of TPZ-mediated vascular dysfunction was done at 24h, in contrast to other VDAs where follow up MR imaging may be done much earlier, at 30 min to 3h following administration of the compounds. The anti-vascular effects of TPZ do not manifest in HCT116 tumours for several hours post-treatment, with peak loss of perfusion occurring at 24h, making this timepoint a rational choice for the present studies (Huxham *et al.* 2006). While most experimental designs involve pre- and post-treatment evaluations of T1 weighted images, the application of contrast agents and the use of calculated biomarkers varies considerably between studies. Data presented here in Chapter 2 reports TPZ-treatment induced changes in vascular function using biomarkers IAUC and K^{trans} derived from the two-compartment model (Figure 2.8) (Tofts *et al.* 1999). These data were obtained using a pre- and post- imaging strategy that was facilitated by an implanted fiducial marker. Positive correlation of post-treatment IAUC values with the biological treatment response indicator, VDS, validates DCE-MRI biomarkers as useful indicators of TPZ mediated vascular dysfunction. These data therefore suggest IAUC and K^{trans} as useful biomarkers of TPZ effect that can be used in the clinic. Additionally, new data analysis techniques including microregional analysis of parameter maps and the creation of the vascular dysfunction score (VDS) were developed and reported in these studies.

2.4.2 Analysis of DCE-MRI and histological images

The use of simple implanted fiducial markers (Figure 2.2) greatly reduced variations in MR image slice angulation and position which were observed in preliminary studies using a detachable external marker. This suggests that internal markers are a more reliable solution for longitudinal studies of tissue that moves as easily as a subcutaneous tumour. With the assistance of these fiducial markers, tumour cryosections were obtained to closely approximate the MRI slices, and histological tumour maps for vascular perfusion and tumour

necrosis were analyzed. The visual correlations between the three measurements of perfusion are quite striking (Figures 2.5, 2.6) particularly in light of the experimental difficulties inherent in such a comparison.

In all of the tumour models reported in previous studies, the typical rate of vascular dysfunction response to TPZ seen is approximately 65 %, with remaining tumours having little or no obvious centralized loss of perfusion effects measurable with the static tumour maps (Huxham *et al.* 2006; Huxham *et al.* 2008). Tumours classed as "strong-responders" to TPZ treatment exhibit a significant loss of perfused vessels or greater levels of necrosis in the central regions of tissue. "Non-responders" are tumours that may have sustained a decrease in measurable vascular function using DCE-MRI or histological analysis, but those changes were either insufficient in degree or too heterogeneously distributed through the tumour tissues to result in a sustained, centralized loss of perfusion to a large tissue area. If damage occurs in a single vessel, but nearby vessels continue to function and are able to supply the tumour cells with adequate nutrients and oxygen, then the vascular damage may not result in death of tumour cells. When many neighbouring vessels are damaged, in a centralized region, then the tumour cells may more effectively be deprived of their oxygen and nutrients and will not survive. A combined vascular dysfunction score (VDS) provides an objective, quantitative measure of the vascular disrupting effects of TPZ and identified tumours 7, 8 and 9 as non-responders and the remaining tumours 10 - 14 as responders, with qualitative examination of the tumour maps confirming these observations (Figure 2.7C).

MRI and histological parameter maps qualitatively depict vascular changes occurring preferentially in the centre regions of tumours and quantitative radial analyses confirmed these observations for IAUC, K^{trans} , necrosis and histologically assessed perfusion analyses (Figure 2.9, Figure 2.10). The heterogeneity index created by comparing peripheral and central regions of tumours permitted a comparison between the two imaging modalities; parameters from histological tumour mapping (carbocyanine heterogeneity) and MRI (post-treatment IAUC heterogeneity) were found to have a positive correlation (Figure 2.11C).

2.4.3 Pre-treatment perfusion as indicator of non-response

A significant advantage of using MRI is the ability to perform longitudinal measurements. When data from those tumours identified to be non-responders (tumours 7, 8

and 9) based on their histologically-derived VDS were examined retrospectively, it can be seen that prior to TPZ treatment these tumours exhibited greater IAUC and K^{trans} values relative to the rest of the as yet treatment-naïve tumours. A strong correlation is found between pre-treatment IAUC and tumour response (Figure 2.11). Post-treatment MRI data shows that the values for non-responding tumours did decrease, but not to the same degree as seen in the strong-responders. An overall positive correlation was found between pre- and post-treatment measurements for MRI parameter IAUC (Figure 2.11). These data suggest that tumours more likely to be sensitive to the vascular-targeting effects of TPZ may be identified prior to treatment as those which have low levels of vascular function, which may indirectly suggest greater tumour hypoxia. Although the sample size is small in this study, the observation is important considering the hypoxic cytotoxic mechanism of TPZ, and suggests that the vascular targeting mechanism of TPZ may be related to hypoxia.

Support for a hypoxia-associated predictor for the clinical success of TPZ treatment comes from findings by Rischin *et al.* (2006) who found that patients with hypoxic primary tumours, as identified on ^{18}F -fluoromisonidazole positron emission tomography (PET), more often benefit from tirapazamine/cisplatin treatment than do patients with non-hypoxic primaries; 2 of 3 non-hypoxic patients failed locally whereas only 1 of 19 hypoxic patients exhibited loco-regional failure when treated with TPZ. No data were presented to indicate whether or not the anti-cancer activity of TPZ was a consequence of vascular targeting effects.

Gd-based contrast agents are in clinical use and would therefore be practical for determining whether a vascular targeting mechanism for TPZ could be responsible for its clinical efficacy. The MRI protocol used in these experiments is directly transferable to the clinic. The biomarkers for treatment response identified here, IAUC and K^{trans} , are often used in clinical investigations of other vascular disrupting agents, and should be further examined for their diagnostic utility in assessing treatment response to TPZ (O'Connor *et al.* 2007). In particular, trials studying the efficacy of TPZ should be accompanied by DCE-MRI studies with sufficient time and spatial resolution to create IAUC maps and examine heterogeneities in tumour perfusion.

2.5 CONCLUSIONS

Studies in Chapter 2 illustrate that tumour vascular function, determined by IAUC and K^{trans} measurements, is a candidate imaging biomarker for tumour response to treatment with TPZ. The use of novel implanted fiducial markers and analysis of microregional heterogeneity showed that MRI data correspond well with histological findings. Tumours sensitive to the vascular-targeting effects of TPZ sustained measurable losses in perfusion and onset of necrosis in the central regions of tissue, and these effects were also seen in non-invasive, longitudinal DCE-MRI analyses. Those few tumours that did not respond were found to have exhibited significantly higher pretreatment perfusion values as measured by IAUC and K^{trans} .

2.6 REFERENCES

- Anderson, R. F., S. S. Shinde, *et al.* (2005). "Radical properties governing the hypoxia-selective cytotoxicity of antitumor 3-amino-1,2,4-benzotriazine 1,4-dioxides." Org Biomol Chem **3**(11): 2167-74.
- Beauregard, D. A., S. A. Hill, *et al.* (2001). "The susceptibility of tumors to the antivascular drug combretastatin A4 phosphate correlates with vascular permeability." Cancer Res **61**(18): 6811-5.
- Breidahl, T., F. U. Nielsen, *et al.* (2006). "The effects of the vascular disrupting agents combretastatin A-4 disodium phosphate, 5,6-dimethylxanthenone-4-acetic acid and ZD6126 in a murine tumour: a comparative assessment using MRI and MRS." Acta Oncol **45**(3): 356-16.
- Brown, J. M. and W. R. Wilson (2004). "Exploiting tumour hypoxia in cancer treatment." Nature Reviews Cancer **4**(6): 437-47.
- Cárdenas-Navia, L. I., T. W. Secomb, *et al.* (2007). "Effects of fluctuating oxygenation on tirapazamine efficacy: Theoretical predictions." Int J Radiat Oncol Biol Phys **67**(2): 581-6.
- Dorie, M. J., D. Menke, *et al.* (1994). "Comparison of the enhancement of tumor responses to fractionated irradiation by SR 4233 (tirapazamine) and by nicotinamide with carbogen." Int J Radiat Oncol Biol Phys **28**(1): 145-50.
- Durand, R. E. and P. L. Olive (1992). "Evaluation of bioreductive drugs in multicell spheroids." Int J Radiat Oncol Biol Phys **22**(4): 689-92.
- Durand, R. E. and P. L. Olive (1997). "Physiologic and cytotoxic effects of tirapazamine in tumor-bearing mice." Radiation oncology investigations **5**(5): 213-9.
- Galbraith, S. M., R. J. Maxwell, *et al.* (2003). "Combretastatin A4 phosphate has tumor antivascular activity in rat and man as demonstrated by dynamic magnetic resonance imaging." J Clin Oncol **21**(15): 2831-42.
- Hicks, K. O., Y. Fleming, *et al.* (1998). "Extravascular diffusion of tirapazamine: effect of metabolic consumption assessed using the multicellular layer model." Int J Radiat Oncol Biol Phys **42**(3): 641-9.
- Huxham, L. A., A. H. Kyle, *et al.* (2006). "Tirapazamine causes vascular dysfunction in HCT-116 tumour xenografts." Radiotherapy and oncology : journal of the European Society for Therapeutic Radiology and Oncology **78**(2): 138-45.
- Huxham, L. A., A. H. Kyle, *et al.* (2008). "Exploring vascular dysfunction caused by tirapazamine." Microvasc Res **75**(2): 247-55.
- Janssen, H. L., A. S. Ljungkvist, *et al.* (2005). "Thymidine analogues to assess microperfusion in human tumors." Int J Radiat Oncol Biol Phys **62**(4): 1169-75.
- Kyle, A. H., C. T. Chan, *et al.* (1999). "Characterization of three-dimensional tissue cultures using electrical impedance spectroscopy." Biophys J **76**(5): 2640-8.
- Kyle, A. H., L. A. Huxham, *et al.* (2003). "Tumor distribution of bromodeoxyuridine-labeled cells is strongly dose dependent." Cancer Res **63**(18): 5657-11.
- Kyle, A. H., L. A. Huxham, *et al.* (2007). "Limited tissue penetration of taxanes: a mechanism for resistance in solid tumors." Clin Cancer Res **13**(9): 2804-10.
- Leach, M. O., K. M. Brindle, *et al.* (2005). "The assessment of antiangiogenic and antivascular therapies in early-stage clinical trials using magnetic resonance imaging: issues and recommendations." Br J Cancer **92**(9): 1599-610.
- Marcu, L. and I. Olver (2006). "Tirapazamine: from bench to clinical trials." Current clinical pharmacology **1**(1): 71-9.
- McPhail, L. D., D. J. McIntyre, *et al.* (2006). "Rat tumor response to the vascular-disrupting agent 5,6-dimethylxanthenone-4-acetic acid as measured by dynamic contrast-enhanced magnetic resonance imaging, plasma 5-hydroxyindoleacetic acid levels, and tumor necrosis." Neoplasia **8**(3): 199-206.

- O'Connor, J. P., A. Jackson, *et al.* (2007). "DCE-MRI biomarkers in the clinical evaluation of antiangiogenic and vascular disrupting agents." Br J Cancer **96**(2): 189-95.
- Rischin, D., R. J. Hicks, *et al.* (2006). "Prognostic significance of [18F]-misonidazole positron emission tomography-detected tumor hypoxia in patients with advanced head and neck cancer randomly assigned to chemoradiation with or without tirapazamine: a substudy of Trans-Tasman Radiation Oncology Group Study 98.02." J Clin Oncol **24**(13): 2098-104.
- Roberts, C., B. Issa, *et al.* (2006). "Comparative study into the robustness of compartmental modeling and model-free analysis in DCE-MRI studies." Journal of magnetic resonance imaging : JMRI **23**(4): 554-63.
- Robinson, S. P., D. J. McIntyre, *et al.* (2003). "Tumour dose response to the antivascular agent ZD6126 assessed by magnetic resonance imaging." Br J Cancer **88**(10): 1592-7.
- Tofts, P. S., G. Brix, *et al.* (1999). "Estimating kinetic parameters from dynamic contrast-enhanced T(1)-weighted MRI of a diffusable tracer: standardized quantities and symbols." Journal of magnetic resonance imaging : JMRI **10**(3): 223-32.
- Tofts, P. S. and A. G. Kermode (1991). "Measurement of the blood-brain barrier permeability and leakage space using dynamic MR imaging. 1. Fundamental concepts." Magnetic resonance in medicine : official journal of the Society of Magnetic Resonance in Medicine / Society of Magnetic Resonance in Medicine **17**(2): 357-67.
- Zeman, E. M., V. K. Hirst, *et al.* (1988). "Enhancement of radiation-induced tumor cell killing by the hypoxic cell toxin SR 4233." Radiotherapy and oncology : journal of the European Society for Therapeutic Radiology and Oncology **12**(3): 209-18.

CHAPTER 3

Decreased blood oxygen tension sensitizes tumours to the anti-vascular effects of tirapazamine.²

² A version of this chapter has been submitted for publication and is under review. Baker JHE, Kyle AH, Flanagan EJ, Methot SP, Bartels KL and Minchinton AI. Decreased blood oxygen tension sensitizes tumours to the anti-vascular effects of tirapazamine.

3.1 INTRODUCTION

3.1.1 Tirapazamine (TPZ) as a hypoxic cytotoxin with anti-vascular activity

Hypoxia is a common feature of tumours that was first suggested more than 50 years ago (Thomlinson and Gray 1955). The supply of oxygen to tumours is compromised by low microvessel density, abnormal vascular architecture, low blood oxygenation and slow or static blood flow (Dewhirst 2003). Hypoxic tumour cells are resistant to radiotherapy and chemotherapy, but they also represent a target for anti-cancer therapies (Brown and Wilson 2004). Tirapazamine (TPZ; SR4233; 3-amino-1,2,4-benzotriazine 1,4-dioxide) is one of the lead hypoxic cytotoxin compounds in clinical trials, a class of compounds designed to target tumour hypoxia (Marcu and Olver 2006). TPZ is a prodrug that is activated by one-electron reductases, and in the absence of oxygen is further metabolized to oxidizing radicals capable of causing DNA damage (Anderson *et al.* 2005). TPZ shows up to 200x greater toxicity to hypoxic cells *in vitro* compared to oxygenated cells (Zeman *et al.* 1986).

However, despite hypoxic cytotoxicity to tumour cells *in vitro*, studies *in vivo* have shown that TPZ is able to mediate irreversible vascular dysfunction in solid tumours (Huxham *et al.* 2006). The anti-vascular effects of TPZ are characterized by loss of perfusion in the central regions of tumours at 12 – 24 h post administration, leaving a viable rim of undamaged vessels. TPZ-mediated vascular dysfunction is dose dependent, occurring in ~ 65 % of HCT116, SiHa, and SCCVII tumour models treated with 60 mg/kg TPZ; the remaining 35% of treated tumours show no significant loss of perfusion or other signs of vascular dysfunction (Huxham *et al.* 2006; Huxham *et al.* 2008; Bains and Baker *et al.* 2009).

3.1.2 Tumour vasculature as a target for TPZ

It appears counter-intuitive that TPZ can damage vascular endothelial cells, likely the most well oxygenated cell population in solid cancers. The mechanism for anti-vascular activity of TPZ is unclear, however the hypoxic cytotoxicity of TPZ *in vitro* suggests that poorly oxygenated tumour vasculature may represent a target for TPZ damage that results in vascular dysfunction *in vivo*. Evidence for intravascular hypoxia comes from studies directly measuring hemoglobin saturation (HbO₂) (Fenton and Boyce 1994) or microelectrode measurements of pO₂ (Dewhirst *et al.* 1992) within tumour blood vessels, as well as indirect

measurements of hypoxia observed in perivascular tumour cells despite patency of the blood vessels (Helmlinger *et al.* 1997; Olive *et al.* 2002; Evans *et al.* 2008). Considerable inter- and intra- tumour heterogeneity is consistently observed in tumour cell and vascular hypoxia measurements, with a trend of peripheral tumour regions being more oxygenated than the central regions (Fenton *et al.* 1988; Dewhirst *et al.* 1992; Måseide and Rofstad 2001). Peripheral vs central differences in tumour oxygenation is a pattern that is similar to that of vascular damage in response to TPZ, which suggests that hypoxia may play a role in TPZ-mediated vascular dysfunction.

There is another class of compounds that mediates tumour vascular damage in a pattern similar to that seen in TPZ-treated tumours. The vascular disrupting agents (VDAs) cause a decrease in tumour vessel perfusion that is followed by large areas of necrosis in the central regions of tumours, with a surviving viable rim. VDAs typically work either by a ligand-based mechanism that targets toxic drugs to antigens expressed specifically on tumour vascular endothelium, or by interfering with the cytoskeleton of tumour endothelial cells to cause acute changes in tumour vascular permeability (Thorpe 2004; Tozer *et al.* 2005). Tumour blood vessels have features that are a result of their tumour microenvironment, including a higher than normal surrounding interstitial fluid pressure (Boucher *et al.* 1990; Leu *et al.* 2000) and poor vascular architecture that leads to high permeability and low blood flow (Hashizume *et al.* 2000; Dewhirst 2003; Baluk *et al.* 2005). Tumour microenvironment-induced features of blood vessels, as well as the fragility of immature vessels that have poor coverage of mural support cells (Morikawa *et al.* 2002), have been attributed to be at least partially responsible for sensitivity of tumour blood vessels to VDA-mediated vascular dysfunction (Tozer *et al.* 2008; Tozer *et al.* 2008).

Previous studies using DCE-MRI derived biomarkers K^{trans} and IAUC have shown that greater pre-treatment vascular function predicted which HCT116 tumours were more sensitive to the anti-vascular effects of TPZ (Bains and Baker *et al.* 2009). Vascular function as a possible predictor for tumour response to TPZ, as well as the similar patterns of TPZ and VDAs in mediating tumour vascular dysfunction, and the pattern of greater hypoxia in central regions of tumours has prompted the investigations presented here in Chapter 3 regarding the roles of tumour vasculature and hypoxia in conferring tumour sensitivity to TPZ.

3.2 METHODS

3.2.1 *Mice and tumours*

HCT116 and HT29 human colorectal carcinoma cells purchased from American Type Culture Collection were used within 6 months of resuscitation and were maintained using minimum essential media, (MEM/EBSS, HyClone) supplemented with 10% foetal bovine serum (FBS, GIBCO/BRL). Female NOD/SCID mice were bred and maintained in our institutional animal facility in accordance with the Canadian Council on Animal Care guidelines; experiments in this chapter were approved by the University of British Columbia and its Animal Care Committee (Appendices B, C, D). HCT116 (8×10^6) and HT29 (5×10^6) cells were implanted subcutaneously into the sacral region of mice aged 8 to 20 weeks, weighing 20 – 26 g.

3.2.2 *Treatments*

Mice were randomly assigned to treatment groups as tumours grew to an average volume of 100 - 150 mm³. Tirapazamine (TPZ) was synthesized by Dr. L.A. Huxham (Huxham *et al.* 2006) and administered at 60 mg/kg (0.34 mmol/kg) by i.p. injection. Tumour hypoxia was induced in mice breathing humidified 7 or 10% O₂ / 5% CO₂ / balance N₂ for 30 min prior to drug administration and for 6 h post drug administration similar to previously used methods (Minchinton and Brown 1992). Moderate anemia was induced in mice 30 min prior to drug administration via tail vein bleeding (Obara *et al.* 2008). 146.0 ± 61.9 mg of blood was removed from mice weighing 21.1 ± 1.8 g, accounting for 7.0 ± 2.8 % of typical blood volume. Bled mice received a replacement volume of 0.9% NaCl via i.v. injection. The S-phase marker 5-Bromo-2-deoxyuridine (BrdUrd, Sigma Chemical) was administered at 1000 mg/kg along with 60 mg/kg of the hypoxia marker pimonidazole (provided by Dr. J Raleigh) as an i.p. injection 2h prior to tissue harvest. The fluorescent dye DiOC₇(3) (Molecular Probes), administered as a 35 µl of 0.6 mg/ml dissolved in 75%(v/v) dimethyl sulfoxide / 25% sterile H₂O (Trotter *et al.* 1989), or 50 µl of 500 kDa FITC-labeled dextran (Sigma) prepared as a 40 mg/ml solution (Tozer *et al.* 2008), were injected intravenously 5 or 2-20 min prior to euthanasia, respectively.

3.2.3 Immunohistochemistry (IHC)

The general IHC procedure used has been previously reported (Huxham *et al.* 2006). Briefly, 10 μm tumour cryosections were obtained 2-3 mm from the tumour edge, air-dried, imaged for native DiOC₇(3) or FITC-dextran fluorescence and fixed in 50 % (v/v) acetone/methanol. Fluorescent-tagged secondary antibodies were used to visualize vasculature identified using a primary antibody to PECAM/CD31 (BD PharMingen) and bound pimonidazole using HypoxyprobeTM-1 MAb1 (provided by Dr. J. Raleigh). DAB (Sigma) was used for colourimetric visualization of incorporated BrdUrd using a mouse MAb to clone BU33 (Sigma) (Kyle *et al.* 2003), basement membrane using a PAb to CIV (NeoMarkers) and smooth muscle using a MAb to αSMA (NeoMarkers) with light counterstaining using 25 % hematoxylin (Sigma).

3.2.4 Image acquisition and analysis

The imaging system has been previously reported (Kyle *et al.* 2007). Fluorescent images were inverted and grayscale CD31 and DiOC₇(3) images were thresholded and a composite color image was produced (CD31 alone as red, or overlapped with DiOC₇(3) as dark blue prioritized over DiOC₇(3) alone as cyan) using Adobe Photoshop CS (version 8.0). The combined vascular image was then overlaid onto grayscale images of BrdUrd and hematoxylin, where converted grayscale images of pimonidazole (green channel) were then added using the *multiply* mask. Similarly, grayscale images of CD31 were thresholded and prioritized as an overlay (red) on grayscale images of FITC-dextran. CIV and αSMA are shown in original grayscale images with hematoxylin counterstained background.

Using the ImageJ software application and user-supplied algorithms, images from each tumour section were aligned, cropped to tumour tissue boundaries and staining artifacts removed. Necrosis and non-perfused tissue was cropped away to calculate the viable tissue fractions (VF). Percent positive staining reflects the proportion of pixels exceeding a threshold value. The average size of vessels is reported as the number of pixels per object. The average distance for tissue to nearest CD31+ve object is reported as a representation of vascular density. For dual positive staining of CD31 in combination with additional markers, thresholds identified staining above background and a minimum 20 % overlap was required to classify CD31 objects as dual labeled. The proportion of dual labeled vessels was obtained

by dividing the total number of CD31 objects positive for the secondary marker by the total number of CD31 objects. The perfused fraction (PF) is calculated as the % of CD31 objects that are dual positive for DiOC₇(3). The average intensity or proportion of pixels above threshold for overlaid images was determined for individual markers and is reported in 1.5 µm increments from nearest vasculature.

3.2.5 Vascular Dysfunction Score (VDS)

The VDS score has previously been reported in Chapter 2 (Bains and Baker *et al.* 2009) and was used again here with a modification as reported:

$$\text{VDS} = 1 - (\text{VF} \times \text{PF})$$

where VF (viable fraction) and PF (perfused fraction) are calculated as described above. Decreased perfusion (low PF) may be insufficient to report vascular dysfunction in cases where tissue has already proceeded to necrosis and inadequate numbers of CD31 stained vessels remain to reflect loss of functional vasculature (Figure 2.3). Therefore it is necessary to include both the VF and PF in the VDS due to the pathophysiology of vascular dysfunction. Instead of calculating individual tumour VDS using maximal control values (as in Chapter 2), VDS in Chapters 3 and 4 is calculated independently for each tumour using only PF and VF. These independent values are then compared to the VDS_{min} calculated as the control mean plus 2 x SD. A value of 1 indicates complete vascular dysfunction, where both the VF and PF are 0. Tumours from treatment groups scoring higher than their control VDS_{min} and that showed focused areas of vascular dysfunction in tumour maps were considered positive for vascular dysfunction.

3.2.6 Endothelial Tube Assay

24 well plates (Fisher) were coated in 200 µl of 50% Matrigel (BD Pharmingen) in MCDB-131 media and allowed to set at 37 °C for 1 – 2 h. Human microvascular endothelial cells (HMEC; provided by Dr. Aly Karsan (Ades *et al.* 1992; Leong *et al.* 2002)) were authenticated based on *in vitro* culture patterns and behaviour, including their ability to form tubular structures on Matrigel coated plates. Cells were seeded (1 x 10⁵ cells / well) in 1.5 ml MCDB-131 media (Sigma) supplemented with 10 % FBS, 10 µg/ml EGF (Sigma) and 10 ng/ml glutamine (Sigma). Cells formed tubular structures by 24 h post-seeding and were

subsequently treated at indicated concentrations of TPZ; minimum 5 wells per treatment. Plates were brought to indicated gas concentrations in 10.3 min using a custom built aluminum chamber sealed and equilibrated via 8 x 1 min cycles of evacuation and pressurization and final pressure was maintained for 1 h at 37 °C. Wells were then rinsed and replaced with supplemented MCDB-131 and were incubated at 37 °C in 5 % O₂ / 5 % CO₂ / 90 % N₂. For fluorescent imaging Calcein AM (Invitrogen), 10 µM in media, was added 1 h prior to endpoint and was rinsed with phosphate buffered saline (PBS, HyClone) prior to fixation in 10 % formalin (Sigma) overnight.

3.2.7 Statistics

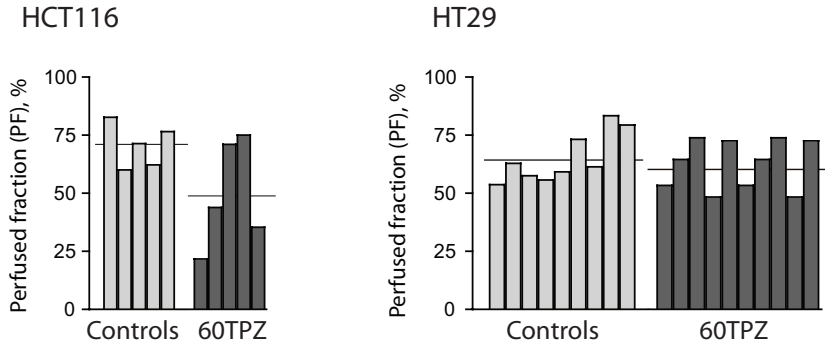
All statistical analyses were performed using GraphPad Prism software (version 4.0e for Macintosh). Nonparametric Mann-Whitney U tests were used for comparisons between groups; p values *<0.05, **<0.01 and ***<0.001 are reported. Where appropriate charts display values for individual tumours as means for analysis of whole tumour sections; combined means are reported for 4-8 tumours per group ± standard error (s.e.).

3.3 RESULTS

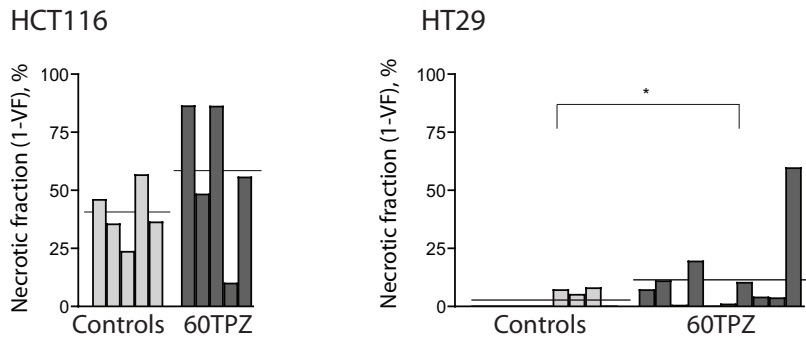
3.3.1 HT29 colorectal xenograft tumours are resistant to vascular dysfunction effects of TPZ

HT29 tumours treated with TPZ show no difference in their proportion of perfused vasculature (PF), however a small but significant increase in the proportion of non-viable tissue (1-VF) is seen (Figure 3.1A, B; Table 3.1). Only 1 of 10 HT29 tumours scored a VDS value greater than the VDS_{min} (0.505) (Figure 3.1C). HT29 tumour maps confirm no evidence of central vascular damage in response to TPZ, with exception to the single tumour scoring >VDS_{min} which has a central area of necrosis; representative images are shown (Figure 3.2). TPZ treatment in HCT116 tumours resulted in 3 of 5 tumours exhibiting vascular dysfunction and scoring greater than the VDS_{min} (0.782), although no significant differences were found in PF and 1-VF values between groups (Figure 3.1C, Table 3.1).

A) Perfused vasculature (PF)



B) Non-viable fraction (1-VF)



C) Vascular Dysfunction Score (VDS)

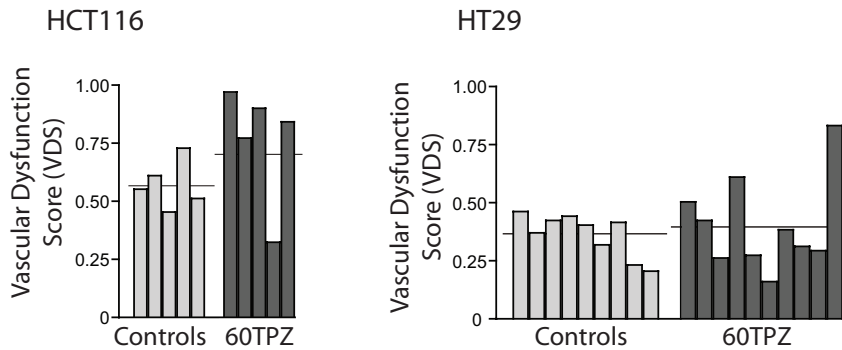
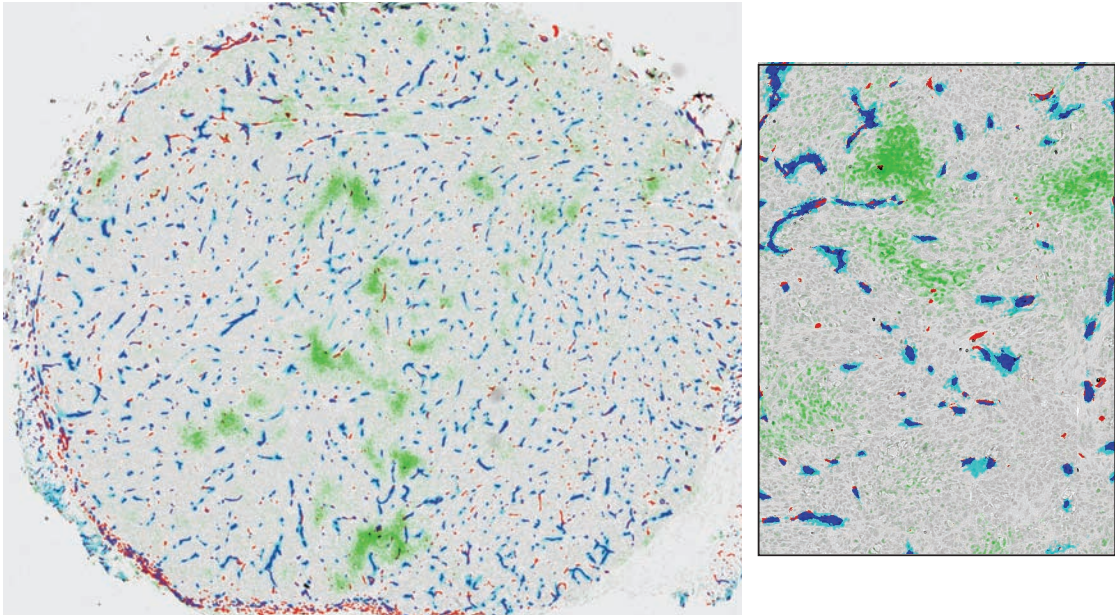


Figure 3.1 HT29 and HCT116 colorectal xenograft sensitivity to anti-vascular effects of TPZ.

Quantitative histological data displays the perfused fraction (PF) (A), non-viable fraction (1-VF) (B) and a combined VDS (C) for HCT116 and HT29 colorectal xenografts treated with 60 mg/kg TPZ. Individual tumours represented by bars and group means by horizontal lines; *p<0.05.

A) HT29, Untreated control



B) HT29, 60 mg/kg TPZ, 24h

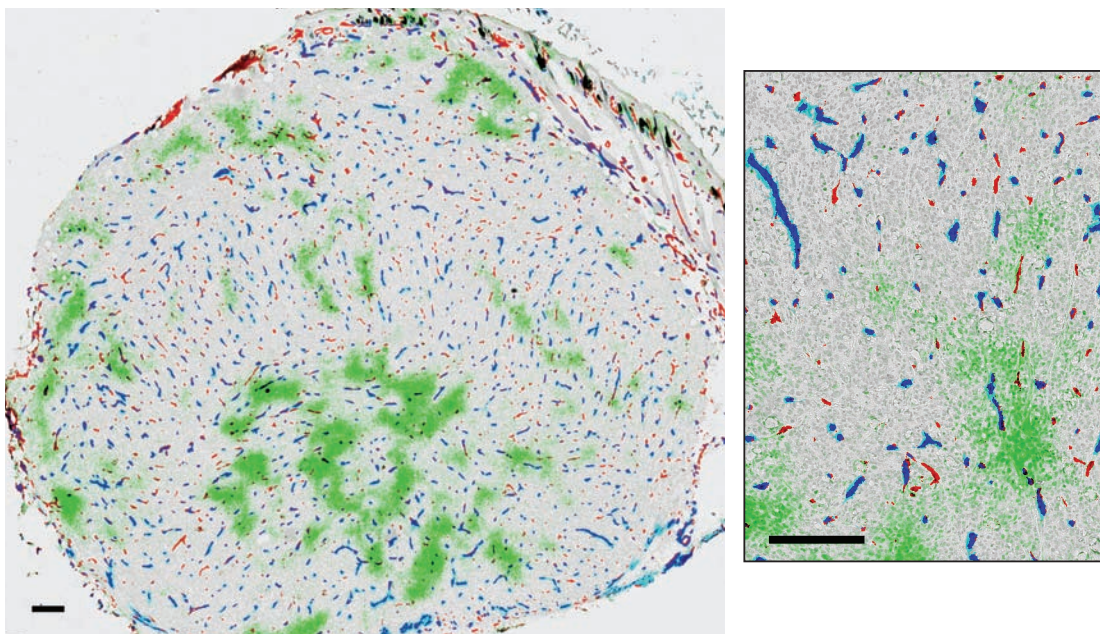


Figure 3.2 HT29 tumour maps.

Representative tumour maps of (A) control and (B) 60 mg/kg TPZ-treated HT29 colorectal xenografts at 24h. Staining shows unperfused vasculature (CD31, red), perfused blood vessels (CD31 overlapped with DiOC₇(3), blue), perfusion dye (DiOC₇(3), cyan) and hypoxia (pimonidazole, green) overlaid on hematoxylin background staining (grey). Scale bar 150 μ m.

Table 3.1 TPZ-mediated vascular dysfunction in HT29 and HCT116 colorectal xenografts.

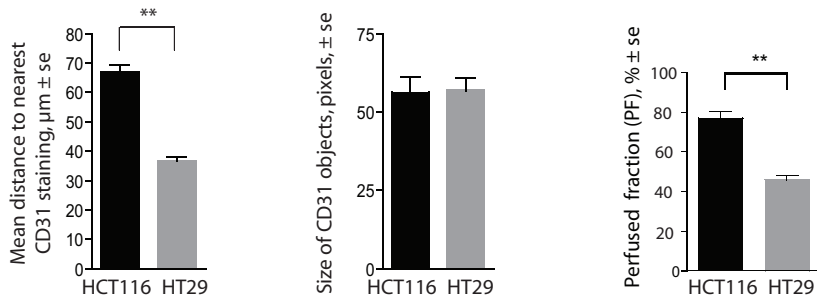
Group	PF % \pm SD	VF % \pm SD	VDS \pm SD	VDS _{min}	# tumours > VDS _{min}
HT29					
Control	65.2 \pm 10.8	97.8 \pm 3.4	0.364 \pm 0.09	0.549	n/a
60TPZ	65.3 \pm 13.4	88.4 \pm 17.9	0.406 \pm 0.20	-	1/10
HCT116					
Control	70.6 \pm 9.5	60.1 \pm 12.4	0.572 \pm 0.10	0.782	n/a
60TPZ	49.5 \pm 23.0	42.8 \pm 31.6	0.762 \pm 0.26	-	3/5

PF = perfused fraction; SD = standard deviation; VF = viable fraction; VDS = vascular dysfunction score; VDS_{min} = (mean control VDS) + (2 x SD); 60TPZ = tirapazamine at 60 mg/kg.

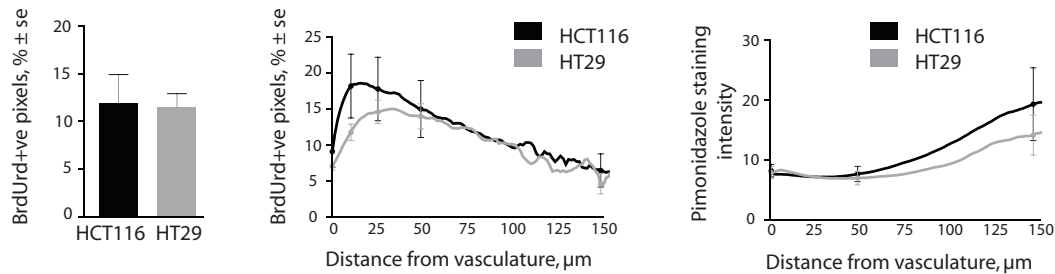
3.3.2 Microenvironmental differences between HCT116 and HT29 colorectal xenografts

Vascular density is lower in HCT116 relative to HT29 tumours, as shown by a greater mean distance of tissue to nearest CD31 object (Figure 3.3A, left). The average size of CD31+ve objects is similar in both models (Figure 3.3A, middle). The proportion of vessels positive for the perfusion marker DiOC₇(3) is significantly lower in HT29 tumours relative to HCT116 (Figure 3.3A, right). Proliferating cells and hypoxia were also mapped in untreated HCT116 and HT29 colorectal xenografts. The overall proportion of S-phase cells is reflected by the % pixels positive for incorporated BrdUrd, where no difference is seen between models (Figure 3.3B, left). However, HT29 xenografts show a trend of fewer proliferating cells proximal to vasculature compared to HCT116 (Figure 3.3B, middle). The amount of bound pimonidazole is somewhat lower in HT29 tumours, particularly at distances further from vasculature (>75 μ m) (Figure 3.3B, right). Mann-Whitney U tests were performed on BrdUrd and pimonidazole staining data at distances from vasculature as indicated on graphs by addition of s.e. bars, with no significant differences found (Figure 3.3B).

A) Vascular density & Perfusion



B) Proliferation & Hypoxia



C) Tumour Maps

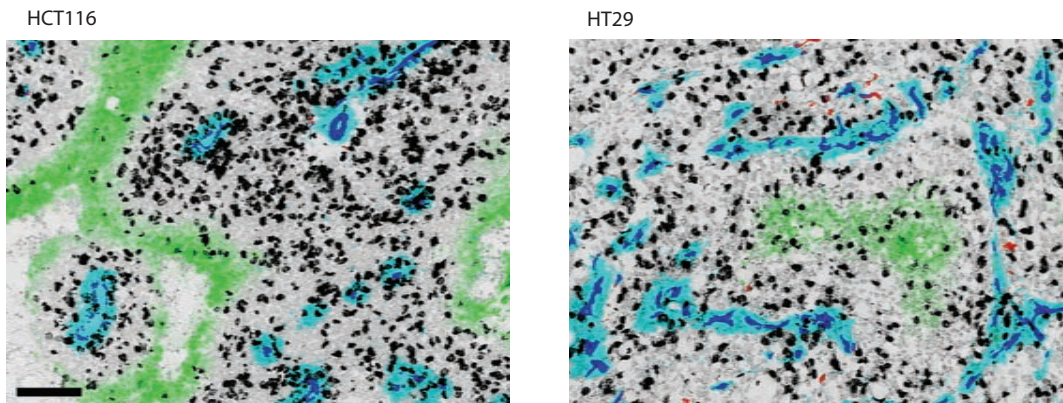


Figure 3.3 Tumour microenvironment of HCT116 and HT29 colorectal xenografts.

CD31 staining data in HCT116 and HT29 tumours reflects microvessel density as the average distance of tissue to its nearest CD31 positively stained object (A, left) and average vessel size (A, middle). The fraction of perfused vessels (PF) is calculated as the proportion of DiOC₇(3)+ve CD31 objects (A, right). Quantitative analysis of incorporated BrdUrd staining as a marker for S-phase cells is displayed as whole tumour means (B, left) or as a function of distance from nearest vasculature (B, middle). Tumour hypoxia is reflected by pimonidazole labeling as a function of distance from vasculature (B, right). Magnified tumour map images reflect representative staining patterns of HCT116 (C, left) and HT29 (C, right). Staining shows unperfused vasculature (CD31, red), perfused blood vessels (CD31 overlapped with DiOC₇(3), blue), perfusion dye (DiOC₇(3), cyan), hypoxia (pimonidazole, green) and S-phase (BrdUrd, black) overlaid on hematoxylin background staining (grey). Scale bar 150 µm; (**p<0.01).

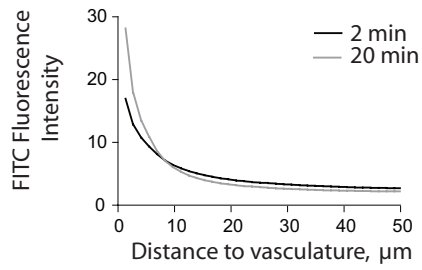
3.3.3 Differences in vascular function between HCT116 and HT29 colorectal xenografts

Quantitative analysis of the presence of 500 kDa FITC-dextran as a function of distance from nearest blood vessels in HCT116 and HT29 tumours show a difference between the two models. In HCT116 the intensity of FITC at distances far from vasculature is similar when examined at 2 and 20 min post i.v. administration (Figure 3.4A). However, in the HT29 model the marker was able to diffuse further from vasculature with time (Figure 3.4B), suggesting greater extravasation of the high MW marker in HT29 tumours.

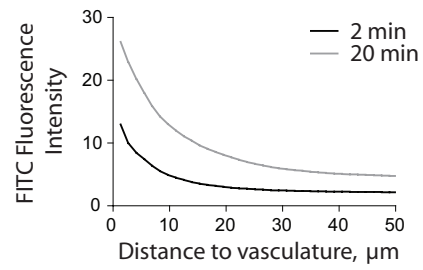
3.3.4 Differences in vascular phenotype between HCT116 and HT29 colorectal xenografts

The proportion of CD31+ve objects positive for the smooth muscle cell marker is significantly lower in the HCT116 model than in HT29 tumours, and thicker layers of α SMA are seen proximal to vasculature in HT29 tumours (Figure 3.5B). The proportion of collagen type IV basal lamina (CIV)+ve CD31 objects was similar in both HCT116 and HT29 colorectal xenograft models (Figure 3.6A). However, thicker layers of CIV are found proximal to vasculature in HT29 tumours.

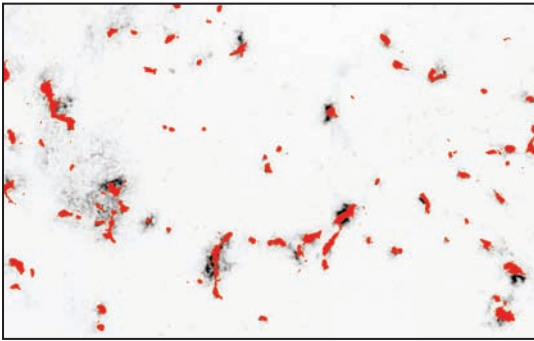
A) HCT116



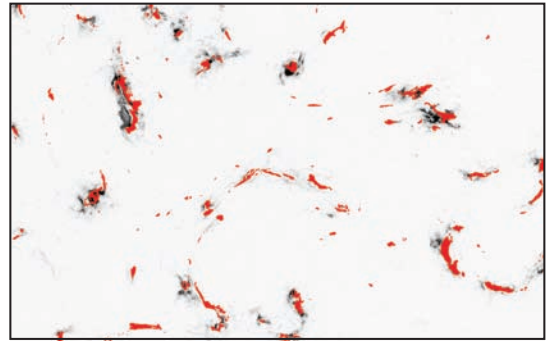
B) HT29



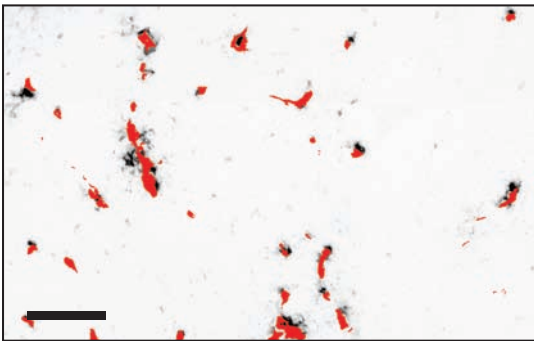
2 min



2 min



20 min



20 min

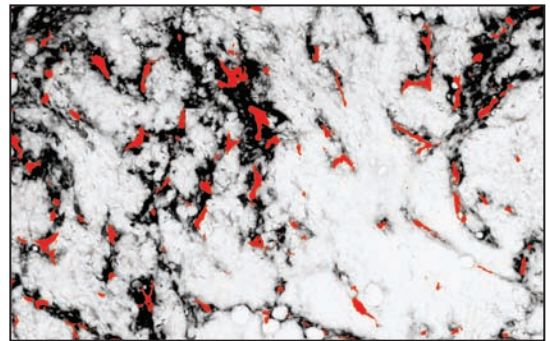
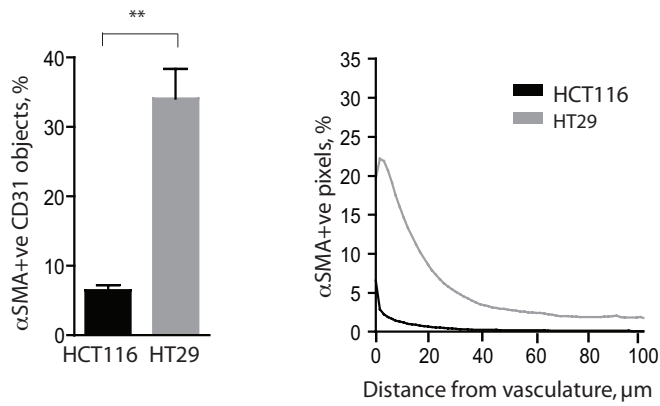


Figure 3.4 Vascular function in HCT116 and HT29 colorectal xenografts.

Fluorescence intensity of 500 kDa FITC-labeled dextran in HCT116 (B, left) and HT29 (B, Right) xenografts is displayed as a function of distance from nearest vasculature. Tumours were harvested at 2 or 20 min after intravenous injection of FITC-dextran; images show FITC fluorescence (black) and CD31 stained vasculature (red). Scale bar 150 μm .

A) Maturity, α SMA



B) Tumour maps

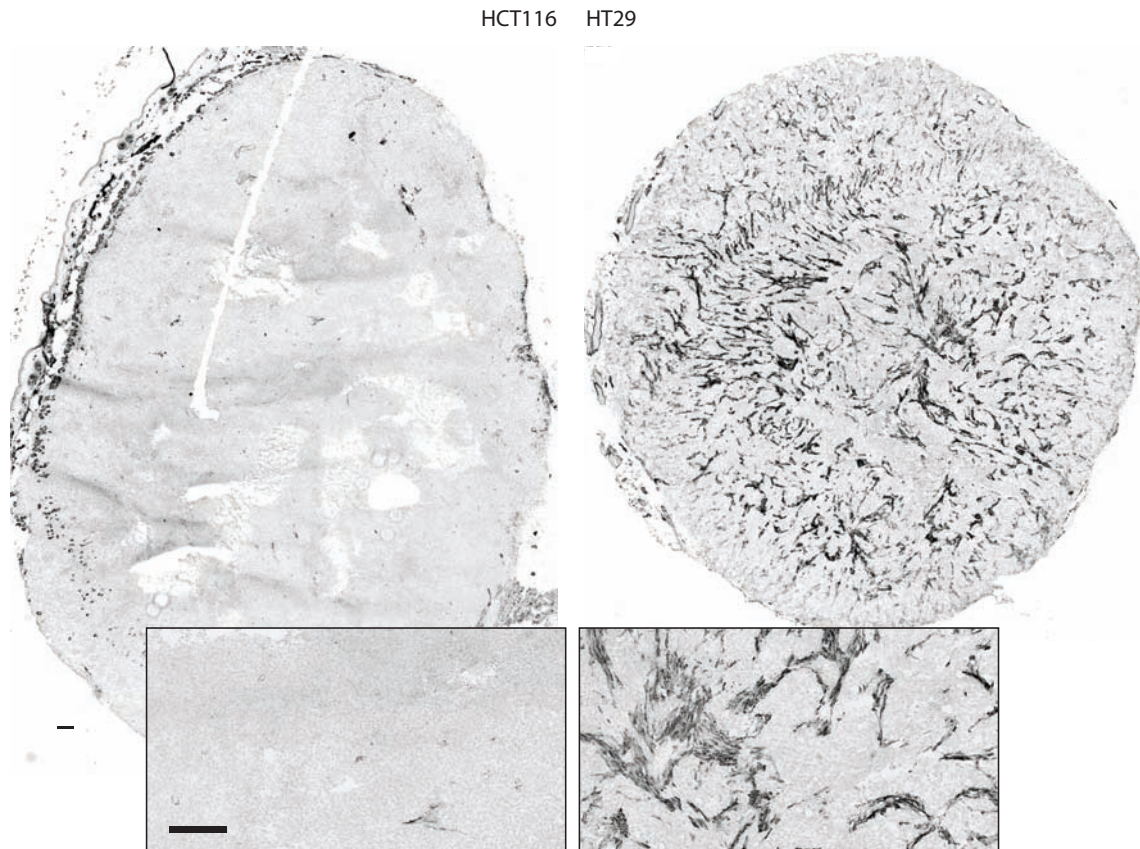
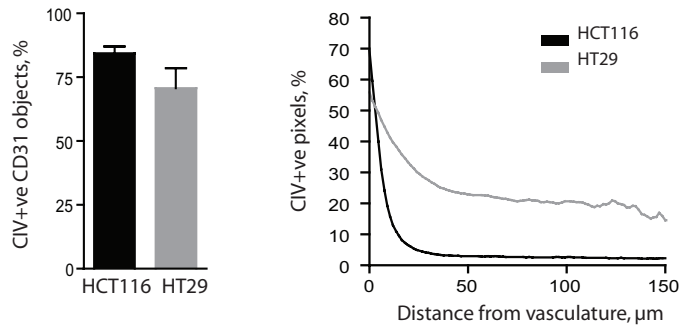


Figure 3.5 CD31 and α SMA staining in HCT116 and HT29 colorectal xenografts.

Staining of smooth muscle is shown as the proportion of CD31 objects dual labeled for α SMA (A, left) and the amount of α SMA as a function of distance from CD31+ve objects (A, right). Representative tumour maps (B) show α SMA staining (black) on hematoxylin (grey) background for HCT116 (left) and HT29 (right) tumours. Scale bars 150 μ m; (** $p < 0.01$).

A) Collagen Type IV



B) Tumour maps

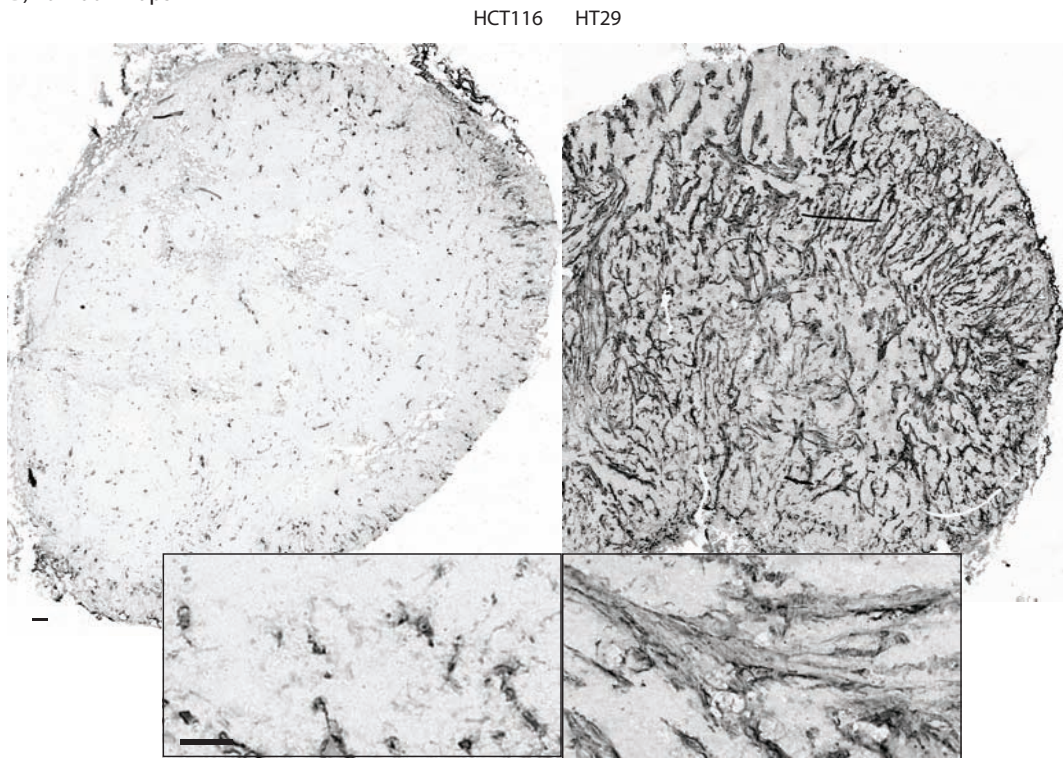


Figure 3.6 CD31 and Collagen Type IV (CIV) staining in HCT116 and HT29 colorectal xenografts.

Staining for basement membrane is shown as the proportion of CD31 objects dual labeled for CIV (A, left) and the amount of CIV staining as a function of distance from CD31 (A, right). Representative tumour maps (B) show CIV staining (black) on hematoxylin background (grey) for HCT116 (left) and HT29 (right) tumours. Scale bars 150 μm .

3.3.5 10% O₂ breathing or induction of anemia enhances the anti-vascular effects of TPZ in HCT116 colorectal xenografts

Subcutaneous HCT116 colorectal xenografts were made more hypoxic by induction of moderate anemia, where blood was removed 30 min prior to treatment with 60 mg/kg TPZ. Anemic mice had 34.0 % fewer red blood cells (RBCs) per unit volume relative to unbled animals. Bleeding-induced anemia resulted in a slightly reduced but not significant proportion of perfused vessels in the anemic group relative to unbled controls (Table 3.2). Induction of anemia did not increase hypoxia in these tumours, as indicated by the amount of bound pimonidazole (Figure 3.7A). The anemic TPZ-treatment group resulted in a higher frequency of tumours, 6 of 7 (86 %), scoring greater than the VDS_{min} (0.622) relative to tumours from unbled TPZ-treated animals where only 4 of 7 (57 %) tumours were $> VDS_{min}$ (Figure 3.8A). No significant difference was found between mean VDS for the anemic vs unbled control TPZ-treated groups.

TPZ-treated HCT116 tumours obtained from mice breathing 10 % O₂ / 5% CO₂ / balance N₂ for 30 min prior and for 6 h post TPZ-administration had a greater magnitude and frequency of vascular dysfunction relative to tumours from mice breathing room air as seen in mean VDS scores (Figure 3.8A, Table 3.2). Low (10 %) O₂ did result in increased tumour hypoxia at all distances from vasculature (Figure 3.7B).

Table 3.2. Impact of modulation of blood oxygenation on TPZ-mediated vascular dysfunction in HCT116 and HT29 colorectal xenografts.

Group	PF % \pm SD	VF % \pm SD	VDS \pm SD	VDS _{min}	# tumours > VDS _{min}
HCT116					
Air Control	67.4 \pm 6.6	68.8 \pm 10.2	0.534 \pm 0.10	0.731	n/a
Air 60TPZ	53.3 \pm 9.3	55.0 \pm 16.3	0.701 \pm 0.13	-	4/7
Low (10%) O ₂ Control	66.0 \pm 10.9	79.3 \pm 8.1	0.475 \pm 0.11	-	0/5
Low (10%) O ₂ 60TPZ	33.0 \pm 12.3	38.9 \pm 5.5	0.872 \pm 0.54	-	7/7
Anemic Control	60.4 \pm 5.5	60.9 \pm 11.0	0.628 \pm 0.09	-	1/5
Anemic 60TPZ	42.8 \pm 8.9	53.2 \pm 11.5	0.771 \pm 0.08	-	6/7
HT29					
Air Control	46.1 \pm 5.1	91.5 \pm 8.4	0.581 \pm 0.03	0.632	n/a
Air 60TPZ, 12h	60.3 \pm 6.7	99.1 \pm 1.1	0.402 \pm 0.07	-	0/5
Low (7%) O ₂ Control	55.4 \pm 10.3	95.2 \pm 4.1	0.471 \pm 0.11	-	0/5
Low (7%) O ₂ 60TPZ, 8h	28.2 \pm 17.8	60.6 \pm 19.0	0.823 \pm 0.14	-	4/5
Low (7%) O ₂ 60TPZ, 12h	49.3 \pm 17.8	85.9 \pm 19.8	0.564 \pm 0.21	-	2/5

PF = perfused fraction; SD = standard deviation; VF = viable fraction; VDS = vascular dysfunction score; VDS_{min} = (mean control VDS) + (2 x SD); 60TPZ = tirapazamine at 60 mg/kg.

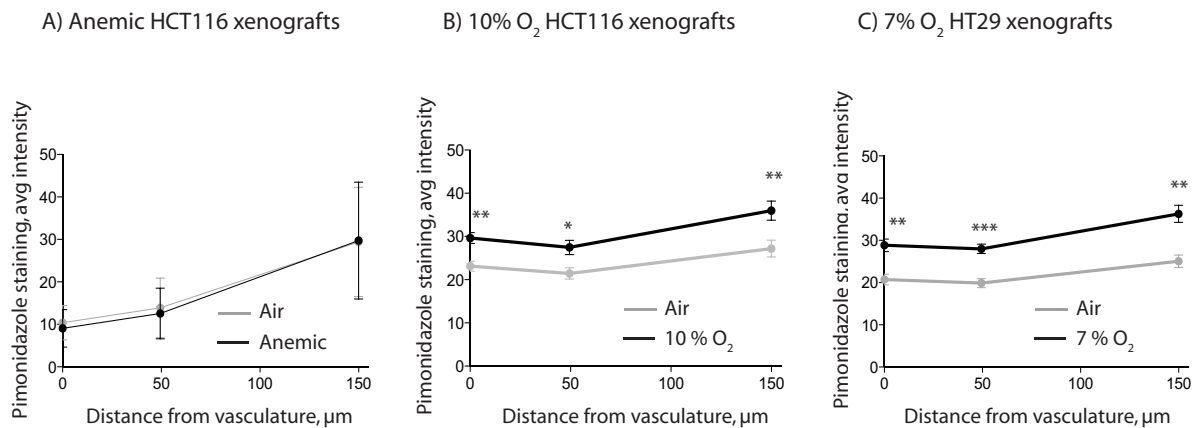
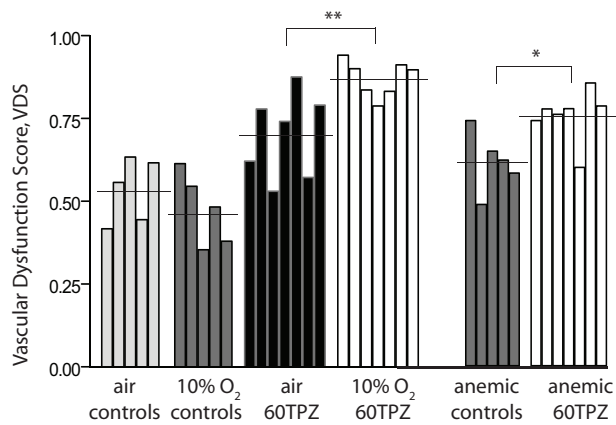


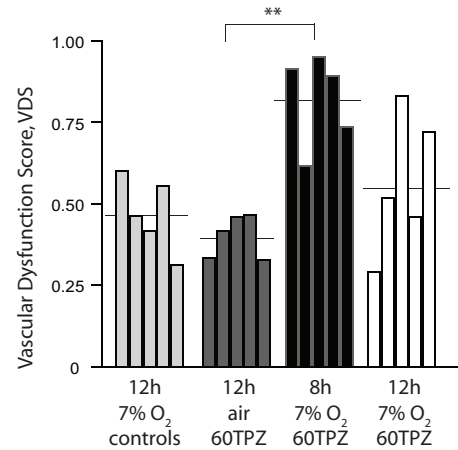
Figure 3.7 Modulation of tumour hypoxia in HCT116 and HT29 colorectal xenografts.

Tumour hypoxia detected using bound pimonidazole staining is shown as a function of distance from nearest vasculature for HCT116 xenografts in anemic mice (A) and in mice breathing 10% O₂ (B) relative to air breathing controls. Similar data is shown for HT29 tumour bearing mice breathing 7% O₂ (C); (*p < 0.05) (**p < 0.01) (**p < 0.001).

A) TPZ in low oxygen HCT116 xenografts



B) TPZ in low oxygen HT29 xenografts



C) Tumour maps

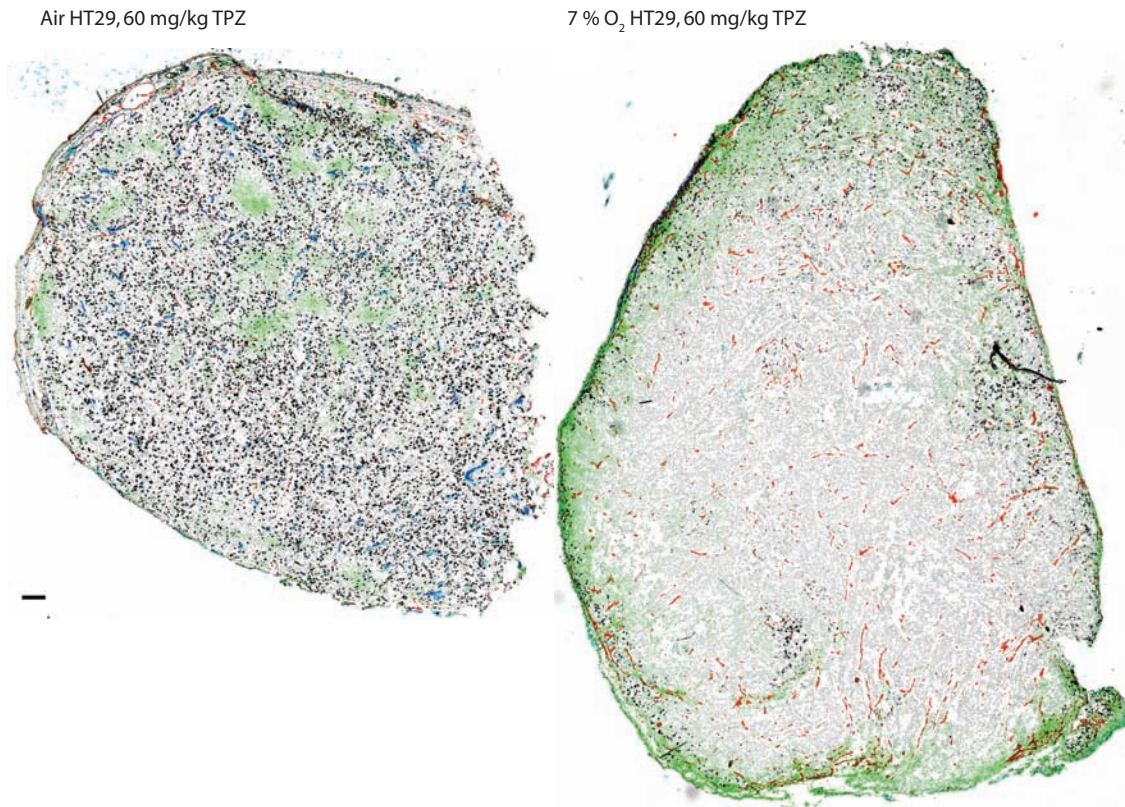


Figure 3.8 Hypoxia enhances anti-vascular effects of TPZ in HCT116 and HT29 xenografts.

Central vascular dysfunction scores (VDS) are shown for 60 mg/kg TPZ (60TPZ) treated anemic or 10% O₂ HCT116 (A) and 7% O₂ HT29 (B) colorectal xenografts relative to their control groups. Representative tumour maps of air breathing control (C, left) and 7% O₂ breathing hypoxic (C, right) HT29 tumours treated with 60 TPZ are shown; unperfused vasculature (CD31, red), perfused vasculature (DiOC₇(3) labeled CD31, blue), S-phase cells (BrdUrd, black) and hypoxia (pimonidazole, green). Scale bar 150 μ m; (*p<0.05) (**p<0.01).

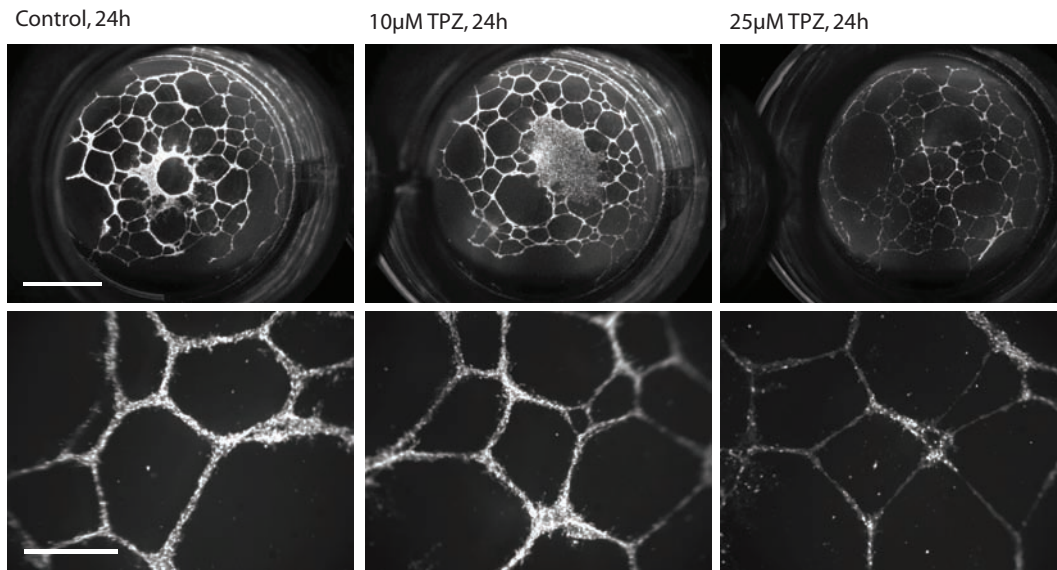
3.3.6 7% O₂ breathing enhances the anti-vascular effects of TPZ in HT29 colorectal xenografts

HT29 xenograft-bearing mice were exposed to 7% O₂ / 5% CO₂ / balance N₂ for 30 min prior and 6 h after receiving 60 mg/kg TPZ. Tumour hypoxia was increased in HT29 tumours in similar proportions to 10% oxygen breathing in HCT116 colorectal xenografts (Figure 3.7C). As seen in earlier analysis (Figure 3.1, Table 3.1), HT29 tumours treated with 60 mg/kg TPZ from mice in room air did not show any signs of vascular dysfunction, with 0 of 5 scoring greater than the VDS_{min} (0.699) (Figure 3.8B, Table 3.2). However, tumours harvested from mice in reduced oxygen conditions do show central vascular dysfunction with 4 of 5 tumours (80 %) > VDS_{min} at 8 h and 2 of 5 (40 %) > VDS_{min} at 12 h. This effect of hypoxia sensitizing HT29 tumours to the anti-vascular effects of TPZ is demonstrated in representative tumour maps (Figure 3.8C).

3.3.7 Tirapazamine mediates damage to endothelial tube structures in vitro in a time, concentration and oxygen-dependent manner

HMECs grown as tubular structures on Matrigel-coated 24 well plates were subsequently exposed to TPZ under 2% or 0.2% O₂ / 5% CO₂ / balance N₂ for 1 h, were rinsed, and then 8 or 24 h later were imaged using fluorescent Calcein AM cell viability indicator. Tubular structure networks formed prior to treatment with TPZ are comprised of multiple cells in linear structures. Exposure of the tubes to 10 µM TPZ at 2% O₂ for 1 h had minimal effect on the network or cellular makeup of the structures, whereas in 25 µM the cell density is much reduced, resulting in deteriorated networks (representative images, Figure 3.9A). At lower 0.2% pO₂, tubes exposed to 25 µM TPZ were even further deteriorated at 24 h post-treatment, however wells imaged at 8 h post-treatment show a less severe difference in cell density and network structures relative to controls (Figure 3.9B). These results demonstrate that a 1 h exposure to TPZ at clinically relevant concentrations, 25 µM, in 2 % O₂ can cause vascular damage that does not manifest for several hours post-treatment.

A) 2% Oxygen



B) 0.2% Oxygen

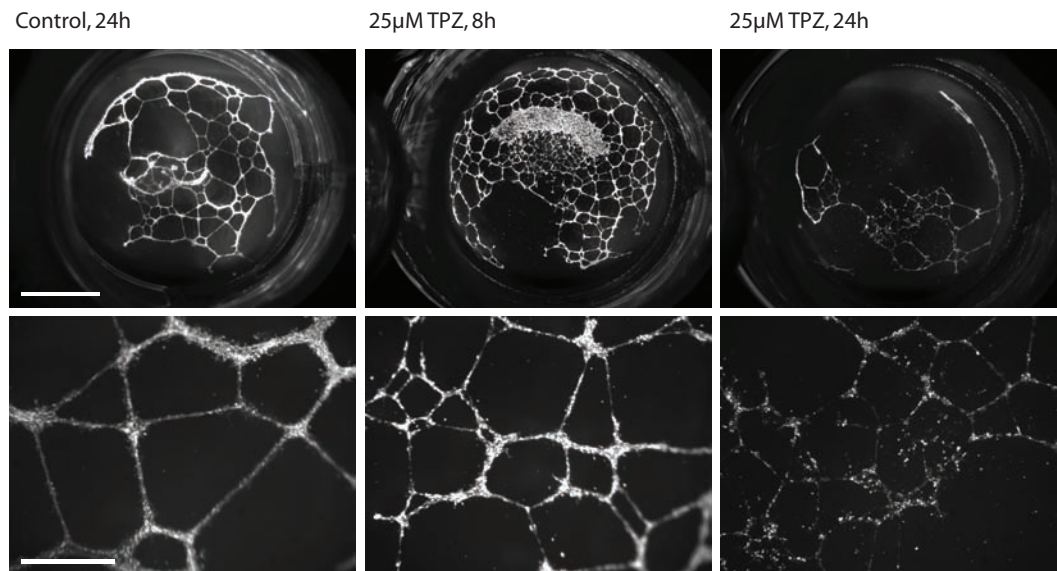


Figure 3.9 TPZ mediates damage to endothelial tube structures in a concentration, time and oxygen dependent manner.

HMECs seeded onto Matrigel-coated plates formed tubular structures by 24 h and were then treated with TPZ in 2 % (A) or 0.2 % (B) oxygen for 1 h. Tubes were then rinsed and replaced in 5 % O₂ for 8 – 24 h prior to staining and imaging. Whole wells (A and B, top rows; scale bars 500 µm) and magnified representative areas (A and B, bottom rows; scale bars 150 µm). Tubular network structures are seen in control wells, whereas in treated wells the tubes become more fragmented or contain visibly fewer cells.

3.4 DISCUSSION

TPZ mediates anti-vascular effects on the *central* blood vessels in tumours, and despite the clonogenicity of implanted tumours, some 35 % of tumours are *non-responders*. Data presented here in Chapter 3 finds features of the tumour vasculature that are distinct in tumour models that are sensitive and resistant to the anti-vascular effects of TPZ, and shows that reducing blood oxygen levels through low oxygen breathing or induction of anemia can sensitize even resistant tumours to TPZ-mediated vascular dysfunction.

HT29 colorectal xenografts are resistant to the vascular targeting effects of TPZ, while HCT116 colorectal xenografts were again shown to be sensitive (Figure 3.1) (Huxham *et al.* 2006; Bains and Baker *et al.* 2009). Other laboratories have shown HT29 sensitivity to TPZ both *in vitro* and *in vivo*, however none of the assays used directly assessed for anti-vascular effects (Siim *et al.* 1997; Hay *et al.* 2007). HCT116 and HT29 cell lines are both colorectal carcinoma models and both were grown as xenografts in genetically identical mice. The endothelial cells which comprise the vasculature in both these tumours should therefore be the same, suggesting that it is the tumour microenvironment and its impact on tumour vasculature that confer sensitivity to TPZ.

3.4.1 Tumour vasculature and TPZ sensitivity

Tumour vasculature is abnormal with respect to its organization, structure and function, with considerable heterogeneity observed in both inter- and intra-tumour comparisons (Dewhirst 2003; Baluk *et al.* 2005; Brurberg *et al.* 2008). Tumour mapping analyses presented here in Chapter 3 comparing the HT29 and HCT116 colorectal xenograft models show that HT29 tumours have greater vascular density and a lower proportion of perfused vessels (Figure 3.3). The presence of thicker layers of basement membrane, CIV, and smooth muscle, α SMA (Figure 3.5), surrounding blood vessels in HT29 tumours may be responsible for the presence of fewer proliferating tumour cells proximal to vasculature compared to HCT116 tumours (Figure 3.3). Greater amounts of smooth muscle cells or pericytes proximal to vasculature have previously been shown to correlate with resistance to both anti-angiogenic and vascular disrupting agents (Benjamin *et al.* 1998; Bergers *et al.* 2003; Tozer *et al.* 2008). However, intra-tumour heterogeneity of tumour mapping vascular analyses is low and therefore would likely not explain variation in response within the

HCT116, SiHa and SCCVII tumour models, where ~ 35 % of tumours show no centralized loss of vascular function (Huxham *et al.* 2006; Huxham *et al.* 2008; Bains and Baker *et al.* 2009).

Poor vascular function is another possible predictor for tumour sensitivity to TPZ, as demonstrated in studies presented in Chapter 2 using DCE-MRI derived biomarkers initial area under the curve (IAUC) or K^{trans} (Bains and Baker *et al.* 2009). Vascular permeability has been suggested to be a predictor for VDA sensitivity, based on studies using intravital microscopy and MRI (Beauregard *et al.* 2001; Tozer *et al.* 2008). A rationale for the correlation between pre-treatment permeability and sensitivity to VDAs is that tumour permeability permits greater delivery of the VDAs to tumours through leakage, and that loss of perfusion in response to the drugs results in even greater trapping of the drugs within tumours (Tozer *et al.* 2008). Additionally, high permeability of tumour blood vessels is at least partially responsible for greater interstitial fluid pressure (IFP) observed in solid tumours (Boucher *et al.* 1990; Leu *et al.* 2000), and greater IFP may make tumour blood vessels more vulnerable to collapse in response to VDAs (Tozer *et al.* 2001; Tozer *et al.* 2008).

Studies evaluating tumour permeability, including the DCE-MRI derived biomarkers IAUC and K^{trans} , are typically unable to determine if observations are specifically the result of differences in vascular perfusion, permeability, blood flow, vascular volume, or rates of extravasation or extravascular diffusion (O'Connor *et al.* 2007). Quantitative analysis mapping the microregional location of high molecular weight FITC-dextran suggests that the vasculature of HT29 tumours is more permeable than that of HCT116 tumours (Figure 3.4), which is consistent with previous observations using DCE-MRI where increased vascular function predicted for decreased sensitivity to TPZ. However, as is the case with most assays measuring vascular permeability, these results may also be the consequence of any of the other vascular physiological parameters previously mentioned.

3.4.2 Tumour hypoxia and TPZ sensitivity

Decreasing tumour blood oxygenation either via induction of anemia or low oxygen breathing resulted in enhancement of the *anti-vascular* effects of TPZ (Figures 3.7, 3.8). A greater magnitude and frequency of TPZ-mediated vascular dysfunction is seen in the anemic

and lower oxygen tumours, and previously resistant HT29 tumours were sensitized to TPZ-mediated vascular dysfunction. This data establishes a direct link between hypoxia and sensitivity to the anti-vascular effects of TPZ, and suggests that the bioreductive hypoxic cytotoxic mechanism of TPZ may be relevant in its ability to mediate vascular dysfunction. Evidence for a hypoxic cytotoxic mechanism of TPZ *in vivo* has previously been suggested to come from studies finding decreased clonogenic survival in tumours treated with TPZ in combination with radiotherapy (Zeman *et al.* 1988). Radiotherapy kills oxygenated cells and additional cell kill by a complementary agent is thought to have effectively targeted the hypoxic cell fraction, or to have radiosensitized cells. Low oxygen breathing has also been shown to sensitize tumours to the anti-cancer activity of TPZ (Minchinton and Brown 1992). However, these studies were not able to specifically confirm *in vivo* that TPZ kills hypoxic tumour cells and they did not assess for an anti-vascular effect.

The effects of moderate anemia and low O₂ breathing on the tumour microenvironment were evaluated using pimonidazole, which optimally labels cells at extremely low (< 10 mmHg) pO₂ (Gross *et al.* 1995; Arteel *et al.* 1998). Anemia did not change tumour hypoxia as indicated by pimonidazole binding (Figure 3.7), despite effecting a drop in perfusion that was sufficient to score > VDS_{min} for 1 of 5 tumours (Table 3.2). None of the non-TPZ treated anemic tumours with VDS > VDS_{min} showed central vascular dysfunction upon visual inspection of tumour maps. While direct measurements of tumour blood oxygenation were not obtained in these studies, the sensitizing effects of anemia and low O₂ breathing on TPZ-mediated vascular dysfunction effects suggest blood oxygenation is relevant to the activity of TPZ *in vivo*.

The anti-vascular effects of TPZ *in vitro* were shown to be oxygen dependent, with more severe effects observed at 0.2 % than 2 % oxygen, but deterioration of tubular structures is clearly seen even in 2 % oxygen conditions with 25 µM TPZ (Figure 3.9). Damage to endothelial tube structures was not as evident at 8 hours post-treatment as that seen at 24 hours. The time frame for effects is consistent with that seen in mice, where vascular dysfunction is delayed several hours from TPZ administration and exposure (Huxham *et al.* 2006; Huxham *et al.* 2008; Bains and Baker *et al.* 2009). The effects *in vitro* were also concentration-dependent, with greater damage at 25 µM vs 10 µM (4.5 µg/ml vs 1.8 µg/ml). The 4.5 µg/ml concentration is a clinically relevant exposure, as a clinical study

in humans reports that a maximum tolerated dose of 390 mg/m² yields a mean peak plasma concentration (C_{max}) of 7.1 µg/ml with an elimination half-life of 46 min (Graham *et al.* 1997). The important question of whether TPZ mediates anti-vascular effects in the clinic remains to be addressed. However, damage to endothelial tubes at clinically relevant concentrations suggests that an anti-vascular effect of TPZ is plausible and merits investigation.

Clinical trials investigating the activity of TPZ have been disappointing (for a review see (Marcu and Olver 2006)). However, Rischin *et al.* (2006) found a positive Phase III result for TPZ in patients that had greater pre-treatment hypoxia and have suggested that more trials investigating TPZ efficacy should pre-screen patients for hypoxia in tumours. If TPZ-mediated vascular dysfunction has a role in the clinical activity of TPZ, then the blood oxygenation of patients may provide a more practical and useful predictor of response. Hematocrit and hemoglobin levels of patients are routinely obtained for patients in TPZ trials; patients with hemoglobin levels that are too low are excluded from TPZ studies (Lee *et al.* 1998; Del Rowe *et al.* 2000; Rischin *et al.* 2005). Perhaps a retrospective analysis of pre-treatment hemoglobin levels for patients that did or did not respond to TPZ could provide some evidence as to whether blood oxygenation is relevant to the clinical activity of TPZ.

3.5 CONCLUSIONS

We have reported and compared tumour models that were sensitive and resistant to the anti-vascular effects of TPZ and found tumour microenvironmental differences that may confer sensitivity to TPZ. Resistant tumours have greater vascular density that is both more mature and more permeable than that of sensitive tumours. Modulation of tumour hypoxia and blood oxygen significantly enhanced the anti-vascular effects of TPZ, establishing a direct link between the hypoxic cytotoxicity of TPZ and its anti-vascular effects *in vivo*. Together, these data provide further evidence of anti-vascular activity of TPZ *in vivo* and identify some features of tumours that could be further investigated to determine if TPZ-mediated vascular dysfunction occurs in patients.

3.6 REFERENCES

- Ades, E. W., F. J. Candal, *et al.* (1992). "HMEC-1: establishment of an immortalized human microvascular endothelial cell line." J Invest Dermatol **99**(6): 683-90.
- Anderson, R. F., S. S. Shinde, *et al.* (2005). "Radical properties governing the hypoxia-selective cytotoxicity of antitumour 3-amino-1,2,4-benzotriazine 1,4-dioxides." Org Biomol Chem **3**(11): 2167-74.
- Arteel, G. E., R. G. Thurman, *et al.* (1998). "Reductive metabolism of the hypoxia marker pimonidazole is regulated by oxygen tension independent of the pyridine nucleotide redox state." Eur J Biochem **253**(3): 743-50.
- Bains, L. J., J. H. Baker, *et al.* (2009). "Detecting vascular-targeting effects of the hypoxic cytotoxin tirapazamine in tumour xenografts using magnetic resonance imaging." Int J Radiat Oncol Biol Phys **74**(3): 957-65.
- Baluk, P., H. Hashizume, *et al.* (2005). "Cellular abnormalities of blood vessels as targets in cancer." Curr Opin Genet Dev **15**(1): 102-11.
- Beauregard, D. A., S. A. Hill, *et al.* (2001). "The susceptibility of tumours to the antivascular drug combretastatin A4 phosphate correlates with vascular permeability." Cancer Res **61**(18): 6811-5.
- Benjamin, L. E., I. Hemo, *et al.* (1998). "A plasticity window for blood vessel remodelling is defined by pericyte coverage of the preformed endothelial network and is regulated by PDGF-B and VEGF." Development **125**(9): 1591-8.
- Bergers, G., S. Song, *et al.* (2003). "Benefits of targeting both pericytes and endothelial cells in the tumour vasculature with kinase inhibitors." J Clin Invest **111**(9): 1287-95.
- Boucher, Y., L. T. Baxter, *et al.* (1990). "Interstitial pressure gradients in tissue-isolated and subcutaneous tumours: implications for therapy." Cancer Res **50**(15): 4478-84.
- Brown, J. M. and W. R. Wilson (2004). "Exploiting tumour hypoxia in cancer treatment." Nature Reviews Cancer **4**(6): 437-47.
- Brurberg, K. G., J. V. Gaustad, *et al.* (2008). "Temporal heterogeneity in blood supply in human tumour xenografts." Neoplasia **10**(7): 727-35.
- Del Rowe, J., C. Scott, *et al.* (2000). "Single-arm, open-label phase II study of intravenously administered tirapazamine and radiation therapy for glioblastoma multiforme." J Clin Oncol **18**(6): 1254-9.
- Dewhirst, M. W. (2003). "Mechanisms underlying hypoxia development in tumours." Adv Exp Med Biol **510**: 51-6.
- Dewhirst, M. W., E. T. Ong, *et al.* (1992). "Perivascular oxygen tensions in a transplantable mammary tumour growing in a dorsal flap window chamber." Radiation Research **130**(2): 171-82.
- Evans, S. M., K. W. Jenkins, *et al.* (2008). "Imaging and analytical methods as applied to the evaluation of vasculature and hypoxia in human brain tumours." Radiation Research **170**(6): 677-90.
- Fenton, B. M. and D. J. Boyce (1994). "Micro-regional mapping of HbO₂ saturations and blood flow following nicotinamide administration." Int J Radiat Oncol Biol Phys **29**(3): 459-62.
- Fenton, B. M., E. K. Rofstad, *et al.* (1988). "Cryospectrophotometric determination of tumour intravascular oxyhemoglobin saturations: dependence on vascular geometry and tumour growth." J Natl Cancer Inst **80**(20): 1612-9.
- Graham, M. A., S. Senan, *et al.* (1997). "Pharmacokinetics of the hypoxic cell cytotoxic agent tirapazamine and its major bioreductive metabolites in mice and humans: retrospective analysis of a pharmacokinetically guided dose-escalation strategy in a phase I trial." Cancer Chemotherapy and Pharmacology **40**(1): 1-10.

- Gross, M. W., U. Karbach, *et al.* (1995). "Calibration of misonidazole labeling by simultaneous measurement of oxygen tension and labeling density in multicellular spheroids." Int J Cancer **61**(4): 567-73.
- Hashizume, H., P. Baluk, *et al.* (2000). "Openings between defective endothelial cells explain tumour vessel leakiness." Am J Pathol **156**(4): 1363-80.
- Hay, M. P., K. O. Hicks, *et al.* (2007). "Pharmacokinetic/pharmacodynamic model-guided identification of hypoxia-selective 1,2,4-benzotriazine 1,4-dioxides with antitumour activity: the role of extravascular transport." J Med Chem **50**(25): 6392-404.
- Helmlinger, G., F. Yuan, *et al.* (1997). "Interstitial pH and pO₂ gradients in solid tumours *in vivo*: high-resolution measurements reveal a lack of correlation." Nat Med **3**(2): 177-82.
- Huxham, L. A., A. H. Kyle, *et al.* (2006). "Tirapazamine causes vascular dysfunction in HCT-116 tumour xenografts." Radiotherapy and oncology : journal of the European Society for Therapeutic Radiology and Oncology **78**(2): 138-45.
- Huxham, L. A., A. H. Kyle, *et al.* (2008). "Exploring vascular dysfunction caused by tirapazamine." Microvasc Res **75**(2): 247-55.
- Kyle, A. H., L. A. Huxham, *et al.* (2003). "Tumour distribution of bromodeoxyuridine-labeled cells is strongly dose dependent." Cancer Res **63**(18): 5707-11.
- Kyle, A. H., L. A. Huxham, *et al.* (2007). "Limited tissue penetration of taxanes: a mechanism for resistance in solid tumours." Clin Cancer Res **13**(9): 2804-10.
- Lee, D. J., A. Trotti, *et al.* (1998). "Concurrent tirapazamine and radiotherapy for advanced head and neck carcinomas: a Phase II study." Int J Radiat Oncol Biol Phys **42**(4): 811-5.
- Leong, K. G., X. Hu, *et al.* (2002). "Activated Notch4 inhibits angiogenesis: role of beta 1-integrin activation." Mol Cell Biol **22**(8): 2830-41.
- Leu, A. J., D. A. Berk, *et al.* (2000). "Absence of functional lymphatics within a murine sarcoma: a molecular and functional evaluation." Cancer Res **60**(16): 4324-7.
- Marcu, L. and I. Olver (2006). "Tirapazamine: from bench to clinical trials." Current clinical pharmacology **1**(1): 71-9.
- Måseide, K. and E. K. Rofstad (2001). "Intratumour heterogeneity in microvessel oxyhaemoglobin saturations." Cancer Lett **162**(2): 245-51.
- Minchinton, A. I. and J. M. Brown (1992). "Enhancement of the cytotoxicity of SR 4233 to normal and malignant tissues by hypoxic breathing." Br J Cancer **66**(6): 1053-8.
- Morikawa, S., P. Baluk, *et al.* (2002). "Abnormalities in pericytes on blood vessels and endothelial sprouts in tumours." Am J Pathol **160**(3): 985-1000.
- O'Connor, J. P., A. Jackson, *et al.* (2007). "DCE-MRI biomarkers in the clinical evaluation of antiangiogenic and vascular disrupting agents." Br J Cancer **96**(2): 189-95.
- Obara, N., N. Suzuki, *et al.* (2008). "Repression via the GATA box is essential for tissue-specific erythropoietin gene expression." Blood **111**(10): 5223-32.
- Olive, P. L., J. P. Banáth, *et al.* (2002). "The range of oxygenation in SiHa tumour xenografts." Radiation Research **158**(2): 159-66.
- Rischin, D., R. J. Hicks, *et al.* (2006). "Prognostic significance of [18F]-misonidazole positron emission tomography-detected tumour hypoxia in patients with advanced head and neck cancer randomly assigned to chemoradiation with or without tirapazamine: a substudy of Trans-Tasman Radiation Oncology Group Study 98.02." J Clin Oncol **24**(13): 2098-104.
- Rischin, D., L. Peters, *et al.* (2005). "Tirapazamine, Cisplatin, and Radiation versus Fluorouracil, Cisplatin, and Radiation in patients with locally advanced head and neck cancer: a randomized phase II trial of the Trans-Tasman Radiation Oncology Group (TROG 98.02)." J Clin Oncol **23**(1): 79-87.
- Siim, B. G., D. R. Menke, *et al.* (1997). "Tirapazamine-induced cytotoxicity and DNA damage in transplanted tumours: relationship to tumour hypoxia." Cancer Res **57**(14): 2922-8.
- Thomlinson, R. H. and L. H. Gray (1955). "The histological structure of some human lung cancers and the possible implications for radiotherapy." Br J Cancer **9**(4): 539-49.

- Thorpe, P. E. (2004). "Vascular targeting agents as cancer therapeutics." Clin Cancer Res **10**(2): 415-27.
- Tozer, G. M., S. Akerman, *et al.* (2008). "Blood vessel maturation and response to vascular-disrupting therapy in single vascular endothelial growth factor-A isoform-producing tumours." Cancer Res **68**(7): 2301-11.
- Tozer, G. M., C. Kanthou, *et al.* (2005). "Disrupting tumour blood vessels." Nature Reviews Cancer **5**(6): 423-35.
- Tozer, G. M., C. Kanthou, *et al.* (2008). "Tumour vascular disrupting agents: combating treatment resistance." The British journal of radiology **81 Spec No 1**: S12-20.
- Tozer, G. M., V. E. Prise, *et al.* (2001). "Mechanisms associated with tumour vascular shut-down induced by combretastatin A-4 phosphate: intravital microscopy and measurement of vascular permeability." Cancer Res **61**(17): 6413-22.
- Trotter, M. J., D. J. Chaplin, *et al.* (1989). "Use of a carbocyanine dye as a marker of functional vasculature in murine tumours." Br J Cancer **59**(5): 706-9.
- Zeman, E. M., J. M. Brown, *et al.* (1986). "SR-4233: a new bioreductive agent with high selective toxicity for hypoxic mammalian cells." Int J Radiat Oncol Biol Phys **12**(7): 1239-42.
- Zeman, E. M., V. K. Hirst, *et al.* (1988). "Enhancement of radiation-induced tumour cell killing by the hypoxic cell toxin SR 4233." Radiotherapy and oncology : journal of the European Society for Therapeutic Radiology and Oncology **12**(3): 209-18.

CHAPTER 4

Inhibition of nitric oxide synthase enhances tirapazamine-mediated vascular dysfunction in pre-clinical tumours.³

³ A version of this chapter will be submitted for publication. Baker JHE, Kyle AH, Balbirnie A, Gabriel E, Cran J and Minchinton AI. Inhibition of nitric oxide synthase enhances tirapazamine-mediated vascular dysfunction in pre-clinical tumours.

4.1 INTRODUCTION

4.1.1 *Tirapazamine (TPZ) as a hypoxic cytotoxin with anti-vascular activity in vivo*

The presence of hypoxic cells in tumours was initially hypothesized more than 50 years ago, and tumour hypoxia has since been found to be a characteristic of many solid tumours (Thomlinson and Gray 1955). Hypoxic cells are resistant to radiation and chemotherapy, however they are also a target for anti-cancer therapies (Brown and Wilson 2004). Tirapazamine (TPZ; SR4233; 3-amino-1,2,4-benzotriazine 1,4-dioxide) is one of the most advanced hypoxic cytotoxins in clinical trial; for a review see Marcu and Olver (2006). Cellular reductases reduce and bioactivate TPZ and in the absence of oxygen TPZ is further metabolized to oxidizing radicals capable of causing DNA damage (Anderson *et al.* 2005). TPZ has greater toxicity to hypoxic cells than to oxygenated cells *in vitro* and enhances cell kill by radiotherapy and cisplatin *in vivo* (Zeman *et al.* 1986; Brown and Lemmon 1990; Dorie and Brown 1993).

TPZ also has the ability to effect dose-dependent, catastrophic vascular dysfunction in the central regions of tumours (Huxham *et al.* 2006; Huxham *et al.* 2008; Bains, Baker *et al.* 2009). TPZ-mediated vascular dysfunction is characterized by a loss of perfusion that is irreversible, occurs in only 65 % of treated tumours, and leaves a hallmark viable rim of undamaged vessels in affected tumours. In Chapter 2, DCE-MRI studies suggested that tumours with greater pre-treatment vascular function levels are less responsive to TPZ-mediated vascular damage (Bains, Baker *et al.* 2009). Follow up studies in Chapter 3 characterized vascular phenotype differences between sensitive and resistant colorectal xenografts. Decreasing blood oxygenation *in vivo* through low oxygen breathing or induction of moderate anemia increased the magnitude and frequency of anti-vascular effects of TPZ, establishing a direct link between hypoxia and TPZ mediated vascular dysfunction.

4.1.2 *TPZ reduced by Nitric Oxide Synthase (NOS)*

Sensitization of tumours to the anti-vascular effects of TPZ via decreasing blood oxygenation *in vivo* suggests that the anti-vascular effect of TPZ is related to its hypoxic cytotoxic activity, however a detailed mechanism for the effect remains unclear. The reductase enzyme responsible for bioreduction and activation of TPZ and its location in the

tumour microenvironment could be important in the observed anti-vascular activity of TPZ. There are several reductases that have been implicated in reducing TPZ, including cytosolic enzymes such as NADPH:cytochrome c reductase (P450R) (Walton *et al.* 1992; Saunders *et al.* 2000) and intranuclear enzymes (Evans *et al.* 1998). Work by Garner *et al.* (1999) has shown nitric oxide synthase (NOS), which has a reductase domain with homology to that of P450R, is also capable of reducing TPZ and can result in DNA damage (Garner *et al.* 1999; Chinje *et al.* 2003). A constitutively expressed isoform of NOS is expressed in vascular endothelial cells and is also known as endothelial NOS (eNOS).

Enzymatic reduction of TPZ by the NOS enzyme competitively inhibits NOS production of nitric oxide (NO) (Garner *et al.* 1999). NO is an important messenger molecule synthesized by NOS in a two-step oxidation of L-arginine to L-citrulline in the presence of oxygen (Moncada and Higgs 1993). For a comprehensive review of the role of NO in tumour biology, see Fukumura *et al.* (2006). A reduction in NO levels can have acute effects on tumour vasculature, including decreasing tumour blood flow and vessel diameter (Andrade *et al.* 1992; Horsman *et al.* 1996; Fukumura *et al.* 1997; Tozer *et al.* 1997; Ng *et al.* 2007). Inhibition of NOS has been observed to increase tumour hypoxia and has therefore been suggested as a suitable complementary treatment for hypoxic cytotoxins (Wood *et al.* 1994; Butler *et al.* 1997). The proposed mechanism for this combined treatment is that NOS inhibition causes an increase in tumour hypoxia that results in greater bioactivation of hypoxic cytotoxic prodrugs to their cytotoxic form for greater tumour cell kill. Given the observation that TPZ is a competitive inhibitor of NOS, Garner *et al.* (1999) have proposed that TPZ may potentiate itself via this mechanism.

The purpose of studies in this Chapter 4 is to investigate the potential effects of NO modulation on the response of tumours to TPZ.

4.2 METHODS

4.2.1 Reagents

Tirapazamine was synthesized by Dr. L.A. Huxham (Huxham *et al.* 2006) and administered at 60 or 40 mg/kg (0.34 or 0.23 mmol/kg) by intraperitoneal (i.p.) injection. L-NNA (Sigma) was administered at 180 mg/kg by i.p. injection (Huxham *et al.* 2008). NO donor spermine NONOate (Invitrogen) was prepared in 10 mM NaOH and diluted in PBS to 0.2 mM NaOH immediately prior to intravenous (i.v.) injection according to manufacturer instructions. Intravenous injections of 10 mg/kg NONOate were done simultaneously with and every 30 min following TPZ administration, for a total of 4 NONOate injections (Peralta *et al.* 1997). The S-phase marker 5-Bromo-2-deoxyuridine (BrdUrd, Sigma Chemical) was administered at 1000 mg/kg along with 60 mg/kg of the hypoxia marker pimonidazole (provided by Dr. J Raleigh) as an i.p. injection 2 h prior to tissue harvest. The fluorescent dye DiOC₇(3) (Molecular Probes), 0.6 mg/ml dissolved in 75 % (v/v) dimethyl sulfoxide / 25 % sterile H₂O, was administered intravenously as a marker of vessel perfusion 5 min prior to tissue harvest.

4.2.2 Mice and tumours

Female NOD/SCID and C3H/HeN mice were bred and maintained in our institutional SPF animal facility in accordance with the Canadian Council on Animal Care guidelines. Experiments in this chapter were approved by the University of British Columbia and its Animal Care Committee (Appendices B, C, D). Mice were allowed free access to standard laboratory rodent food and water. Cells were maintained as monolayers using minimum essential media, MEM/EBSS (HyClone) supplemented with 10 % bovine growth serum (HyClone) and passaged every 3 to 4 days. HCT116 (8×10^6 cells, in NOD/SCID mice), HT29 (5×10^6 cells, in NOD/SCID) and SCCVII (5×10^5 cells, in C3H/HeN) were implanted subcutaneously into the sacral region of mice. For tumour mapping experiments mice were randomly assigned to experimental groups when average tumour volumes reached 100 to 150 mm³ as measured using calipers of three orthogonal diameters (a, b and c) using the formula $\text{volume} = \pi/6(abc)$. For growth assessment tumours were randomly assigned for treatment 14

days post-implantation when tumours measured $59.0 \pm 7 \text{ mm}^3$; repeat measurements were performed blind.

4.2.3 Immunohistochemistry

Immediately after excision, tumours were frozen on an aluminum block held at -20 °C, embedded in cutting medium (OCT, Tissue-TEK) and stored at -20 °C until sectioning. The general immunohistochemical procedure used has been previously reported (Huxham *et al.* 2006). Briefly, $10 \mu\text{m}$ tumour cryosections were obtained 2-3 mm from the tumour edge, were air-dried, imaged for native DiOC₇(3) fluorescence and fixed in 50 % (v/v) acetone/methanol for 10 min at room temperature. Vasculature was identified using an antibody to PECAM/CD31 (BD PharMingen), bound pimonidazole using HypoxyprobeTM-1 MAb1, eNOS using a mouse MAb (PharMingen), and non-isoform specific NOS using a rabbit PAb to universal NOS (uNOS; NeoMarkers) and incorporated BrdUrd using a mouse MAb to clone BU33 (Sigma) (Kyle *et al.* 2003). Slides were counterstained with 25 % hematoxylin (Sigma) in dH₂O, dehydrated and mounted using Permount (Fisher Scientific).

4.2.4 Image acquisition and overlay

The imaging system has been previously described (Kyle *et al.* 2007). Images of entire tumour cryosections up to 1 cm^2 were captured at a resolution of $0.75 \mu\text{m}$ per pixel. Grayscale CD31 and DiOC₇(3) images were thresholded and a composite colour image was produced (CD31 alone in red, or overlapped with DiOC₇(3) in dark blue prioritized over DiOC₇(3) alone in cyan) using Adobe Photoshop CS (version 8.0). The combined vascular image was then overlaid onto grayscale images of BrdUrd and hematoxylin, where converted grayscale images of pimonidazole (green channel) were then added using the *multiply* mask. Similarly, grayscale images of eNOS and CD31 were thresholded and a composite color image produced (CD31 alone in red, or overlapped with eNOS as black prioritized over eNOS alone as blue) and overlaid on grayscale images of uNOS.

4.2.5 Image analysis

Using the ImageJ software application and user-supplied algorithms, fluorescent images were inverted and combinations of images of DiOC₇(3), CD31, pimonidazole, eNOS, uNOS, BrdUrd and hematoxylin staining from each tumour section were aligned, cropped to

tumour tissue boundaries and staining artifacts removed. Necrosis was cropped away based on hematoxylin stained sections; non-perfused tissue was cropped away based on overlaid images of CD31, DiOC₇(3) and hematoxylin. The viable fraction (VF) of tumours was calculated based on the ratio of the total number of pixels in cropped images by the total number of pixels in whole tumour areas.

Percent positive staining was obtained using the proportion of pixels at intensities meeting or exceeding a threshold value above background. For distribution analysis of pimonidazole relative to vasculature, each pixel in a pimonidazole image was sorted based on its distance relative to CD31-positive vasculature and the average tissue intensity in 1.5 µm increments from vasculature was determined. For dual positive staining analysis of CD31 in combination with additional markers, thresholds were set to identify staining above background and a minimum 20 % overlap was required to classify CD31 objects as dual labeled. The proportion of perfused (PF) and eNOS +ve vessels was obtained by dividing the total number of CD31 objects positive for DiOC₇(3) or eNOS respectively by the total number of CD31 objects.

4.2.6 Vascular Dysfunction Score (VDS)

The VDS score has previously been reported in Chapter 2 (Bains and Baker *et al.* 2009) and was used again here with a modification as reported:

$$\text{VDS} = 1 - (\text{VF} \times \text{PF})$$

where VF (viable fraction) and PF (perfused fraction) are calculated as described above. Decreased perfusion (low PF) may be insufficient to report vascular dysfunction in cases where tissue has already proceeded to necrosis and inadequate numbers of CD31 stained vessels remain to reflect loss of functional vasculature (Figure 2.3). Therefore it is necessary to include both the VF and PF in the VDS due to the pathophysiology of vascular dysfunction. Instead of calculating individual tumour VDS using maximal control values (as in Chapter 2), VDS in Chapters 3 and 4 is calculated independently for each tumour using only PF and VF. These independent values are then compared to the VDS_{min} calculated as the control mean plus 2 x SD. A value of 1 indicates complete vascular dysfunction, where both the VF and PF are 0. Tumours from treatment groups scoring higher than their control

VDS_{min} and that showed focused areas of vascular dysfunction in tumour maps were considered positive for vascular dysfunction.

4.2.7 Statistics

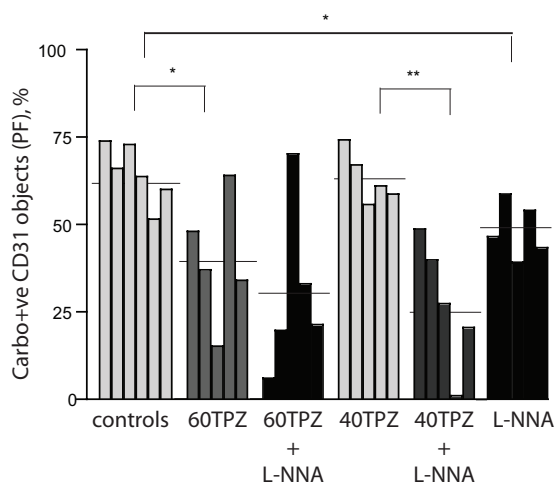
All statistical analyses were performed using GraphPad Prism software (version 4.0e for Macintosh). Nonparametric Mann-Whitney U tests were used for comparisons between groups; p values $* < 0.05$, $** < 0.01$ and $** < 0.001$ are reported. Where appropriate charts display values for individual tumours as means for analysis of whole tumour sections; combined means are reported for 4-8 tumours per group \pm standard error (s.e.).

4.3 RESULTS

4.3.1 *L-NNA enhances TPZ-mediated vascular dysfunction in HCT116 xenografts*

Combined administration of non-specific NOS inhibitor L-NNA with 40 mg/kg TPZ resulted in a significantly increased magnitude and greater frequency of anti-vascular response in HCT116 tumour xenografts examined at 24 h relative to 40 mg/kg TPZ alone (Figure 4.1, Table 4.1). VDS values were greatest in tumours treated with 180 mg/kg L-NNA in combination with either 60 mg/kg or 40 mg/kg TPZ. 180 mg/kg L-NNA + 60 mg/kg TPZ had 4 of 5 (80 %) of tumours scoring $>VDS_{min}$, and L-NNA + 40 mg/kg TPZ also had 4 of 5 (80 %) response rate (Figure 4.1, 4.2, Table 4.1). L-NNA administered alone at 180 mg/kg reduced the perfused fraction (PF) relative to untreated controls, giving some individual tumours in this group a VDS score greater than the VDS_{min} (control mean + 2SDs) (Table 4.1). However, *none* of the L-NNA treated tumours showed a centralized loss of perfusion in tumour maps and were therefore *not classed as responders* (representative tumour map shown in Figure 4.2iii). TPZ treatment alone at 60 mg/kg caused 4 of 5 tumours (80 %) to score $> VDS_{min}$ and demonstrate focused areas of anti-vascular effects in tumour maps. A lower dose of 40 mg/kg TPZ did not result in any individual tumours scoring greater than the VDS_{min} .

A) Perfused vasculature in HCT116 tumours



B) Vascular Dysfunction Score (VDS) in HCT116 tumours

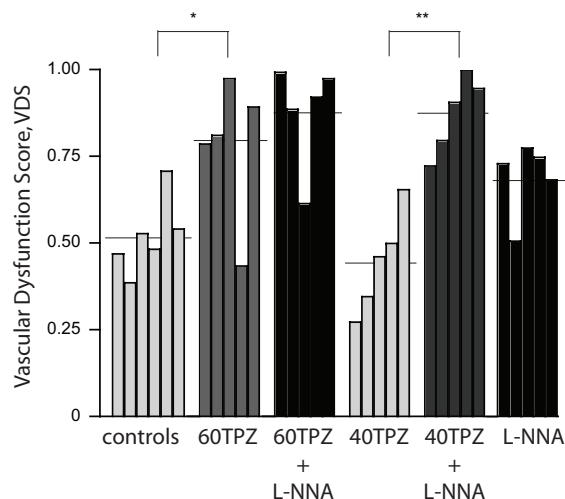


Figure 4.1 NOS inhibition enhances anti-vascular effects of TPZ in HCT116 tumours; quantitative data.

The perfused fraction (PF) (A) and VDS (B) are reported for individual tumours (bars); group means are represented by horizontal lines. (* $p < 0.05$) (** $p < 0.01$).

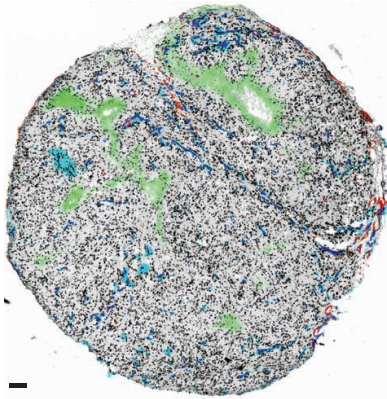
Table 4.1. Impact of modulation of NO on TPZ-mediated vascular dysfunction in HCT116 colorectal xenografts.

Group	PF % \pm SD	VF % \pm SD	VDS \pm SD	VDS _{min}	# tumours > VDS _{min}
Control	64.7 \pm 8.4	74.0 \pm 12.7	0.519 \pm 0.11	0.734	n/a
60TPZ	39.7 \pm 18.0	46.5 \pm 26.8	0.779 \pm 0.21	-	4/5
60TPZ + 180L-NNA	30.1 \pm 24.3	32.0 \pm 22.9	0.878 \pm 0.15	-	4/5
40TPZ	63.4 \pm 7.4	86.6 \pm 16.9	0.446 \pm 0.15	-	0/5
40TPZ + 180L-NNA	27.5 \pm 18.3	35.5 \pm 19.4	0.873 \pm 0.11	-	4/5
180L-NNA	48.4 \pm 7.9	63.9 \pm 14.6	0.688 \pm 0.11	-	2/5
NONOate	57.8 \pm 9.4	80.2 \pm 10.7	0.513 \pm 0.10	-	0/4
60TPZ + NONOate	28.4 \pm 18.9	33.8 \pm 23.0	0.872 \pm 0.15	-	5/6

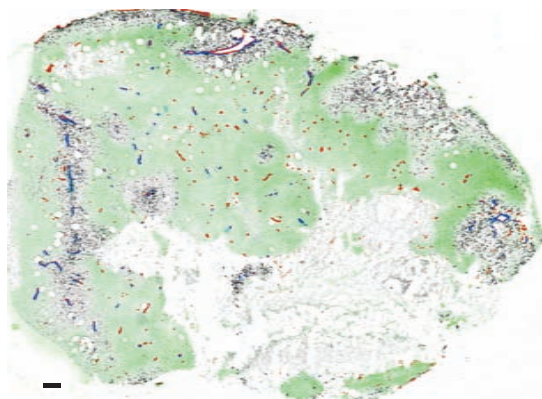
PF = perfused fraction; SD = standard deviation; VF = viable fraction; VDS = vascular dysfunction score; VDS_{min} = (mean control VDS) + (2 x SD); 60TPZ = tirapazamine at 60 mg/kg; 40TPZ = tirapazamine at 40 mg/kg; 180L-NNA = l-nitro-l-arginine at 180 mg/kg; NONOate = spermine NONOate at 10 mg/kg every 30 min for total 4 injections.

HCT116 Tumour maps

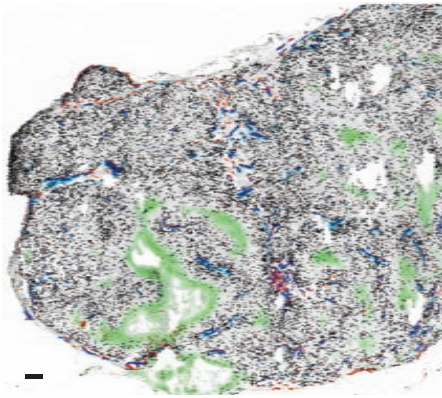
i) Control



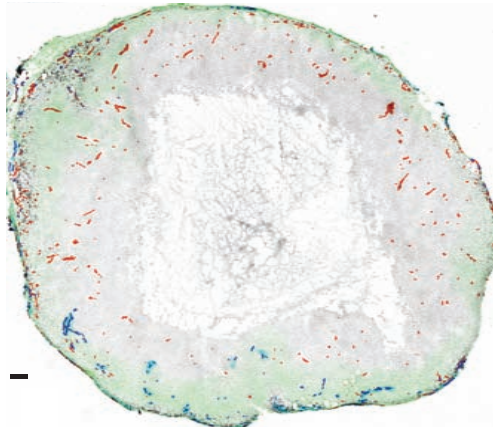
ii) 60 mg/kg TPZ



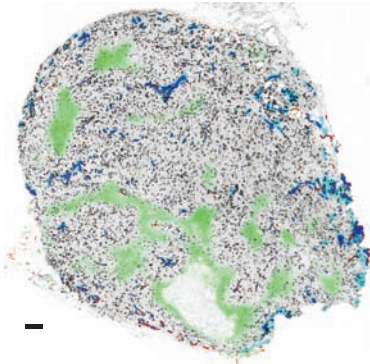
iii) 180 mg/kg L-NNA



iv) 60 mg/kg TPZ + 180 mg/kg L-NNA



v) 40 mg/kg TPZ



vi) 40 mg/kg TPZ + 180 mg/kg L-NNA

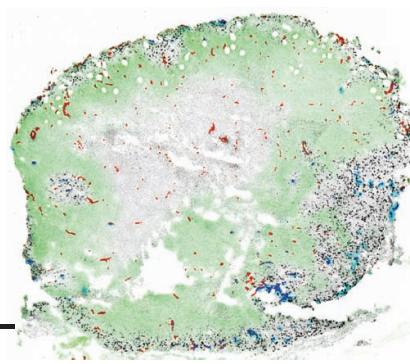


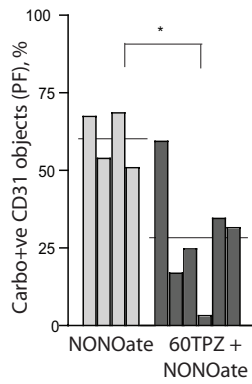
Figure 4.2 NOS inhibition enhances anti-vascular effects of TPZ in HCT116 tumours; tumour maps.

Tumours maps show staining for unperfused vasculature (CD31, red), perfused vasculature (DiOC₇(3)+ve CD31, blue), S-phase cells (BrdUrd, black) and hypoxia (pimonidazole, green). Representative tumours are shown for each group, with exception to ii), iv) and vi) where displayed tumour maps are representative of central vascular dysfunction effects observed within indicated treatment groups. Scale bars 150 μ m.

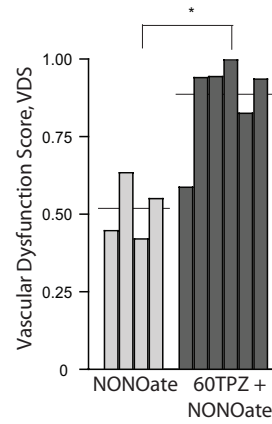
4.3.2 Excess NO enhances the vascular dysfunction effects of TPZ in HCT116 xenografts

Excess NO provided by 4 x 10 mg/kg i.v. spermine NONOate did not significantly change the perfused fraction (PF) in HCT116 tumours relative to controls (Table 4.1). Although not statistically significant, NONOate in combination with 60 mg/kg TPZ did increase the mean VDS score and the frequency of tumours $>VDS_{min}$ relative to TPZ treatment alone (Figure 4.3B, Table 4.1). Tumour maps show the effect as a striking loss of perfusion in the central regions of affected tumours (Figure 4.3C). Excess NO therefore did not protect against the anti-vascular effects of TPZ and instead appeared to enhance the effects similarly to NOS inhibition by L-NNA.

A) Perfused vasculature in HCT116 tumours

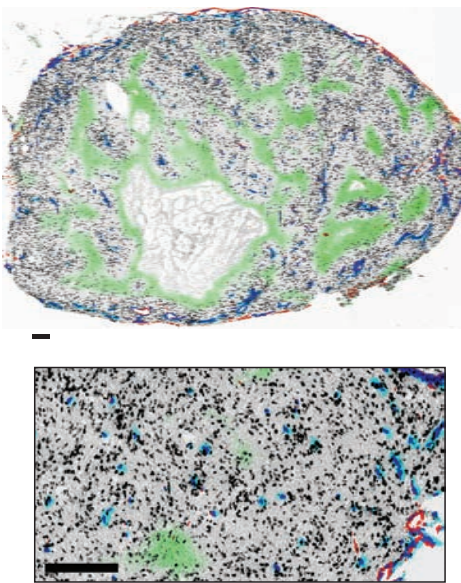


B) Vascular Dysfunction Score (VDS) in HCT116 tumours



C) HCT116 tumour maps

i) 4 x 10 mg/kg NONOATE



ii) 60 mg/kg TPZ + (4 x 10 mg/kg NONOATE)

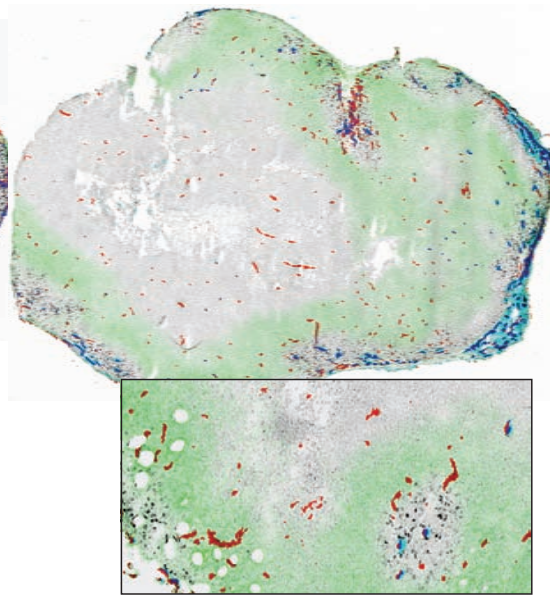


Figure 4.3 Excess NO enhances anti-vascular effects of TPZ in HCT116 tumours.

The perfused fraction (PF) (A) and VDS (B) are reported for individual tumours (bars); group means are represented by horizontal lines. Tumours maps (C) show staining for unperfused vasculature (CD31, red), perfused vasculature (DiOC₇(3)+ve CD31, blue), S-phase cells (BrdUrd, black), hypoxia (pimonidazole, green) and tissue background (hematoxylin, grey). Scale bars 150 μ m; (*p<0.05).

4.3.3 Decrease in proliferating cells in response to NOS inhibition in combination with TPZ

The relative proportion of S-phase cells in HCT116 tumours was measured using the exogenous marker BrdUrd, administered to each animal 2 h prior to tumour harvest at a dose of 1000 mg/kg. Tumour cryosections cropped to remove non-perfused and necrotic areas were analysed for BrdUrd staining and show that 60 mg/kg TPZ is able to reduce proliferation in these areas, but when combined with the NOS inhibitor L-NNA the effect is increased to significance (Figure 4.4). Similarly, 40 mg/kg TPZ does not significantly reduce proliferation whereas in combination with the 180 mg/kg L-NNA there is a significant reduction relative to controls or L-NNA alone. The NO donor spermine NONOate also has no effect on proliferation when administered as a single agent, whereas in combination with TPZ it reduces proliferation to rates significantly lower than those seen with TPZ alone or TPZ in combination with L-NNA.

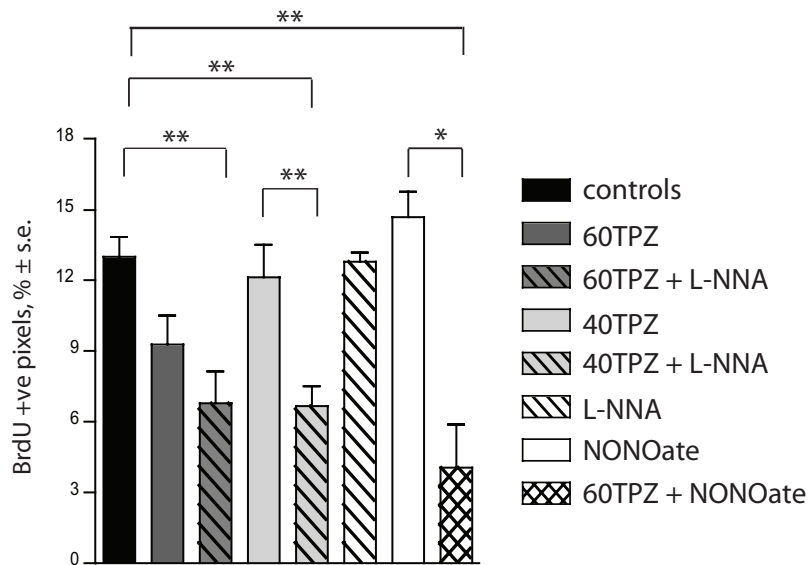


Figure 4.4 Decrease in S-phase cells when TPZ combined with NO modulation.

Staining for S-phase marker BrdUrd is reported as a group mean \pm s.e. Analysis was performed only in tumour regions that contained perfused vasculature; * $p < 0.05$.

4.3.4 L-NNA enhances growth inhibition effects of TPZ in HCT116 xenografts

L-NNA in combination with TPZ results in inhibited tumour growth relative to that seen for either treatment alone (Figure 4.5). HCT116 tumours were treated with 40 mg/kg TPZ, 180 mg/kg L-NNA or a combination of both drugs on day 0 when tumours reached an average size of $59.0 \pm 7 \text{ mm}^3$. Repeat volume measurements show separation of the combined treatment from all groups, with significant differences relative to untreated controls on days 5, 7 and 9. Mean weight loss was greater in the combination treatment ($9.9 \pm 2.3\%$) relative to 40 mg/kg TPZ alone ($6.7 \pm 1.7\%$) but this difference was not significant. Data represented as means for minimum $n = 7$ tumours per group, \pm standard error.

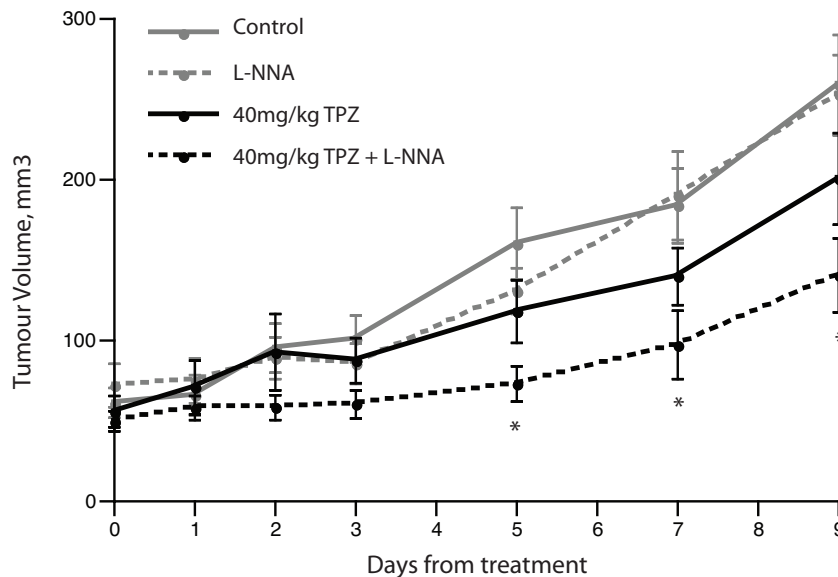


Figure 4.5 Inhibition of NOS by L-NNA enhances growth inhibition effects of TPZ in HCT116 tumours.

HCT116 tumours were treated on day 0 with 180 mg/kg L-NNA, 40 mg/kg TPZ or a combination of both drugs. Statistically significant differences in tumour volumes are indicated for the (40 mg/kg TPZ + 180 mg/kg L-NNA) group (black, dashed), relative to untreated controls (grey, solid); (* $p < 0.05$). Volumes shown \pm s.e.

4.3.5 L-NNA enhances the vascular dysfunction effects of TPZ in SCCVII murine but not in HT29 xenografts

Treatment with L-NNA causes a drop in both the perfused fraction (PF) and viable fraction (VF) of SCCVII tumours and produces some focused areas of vascular dysfunction seen in tumour maps; 3 of 4 L-NNA treated tumours had $VDS > VDS_{min}$. The anti-vascular effect is less severe than in TPZ-treated SCCVII tumours, where 60 mg/kg TPZ resulted in 3 of 5 tumours (60 %) scoring $>VDS_{min}$ and tumour maps depicting larger focused areas of vascular dysfunction (Figure 4.6, Table 4.2). Combining 180 mg/kg L-NNA with 60 mg/kg TPZ dramatically increases the vascular dysfunction response in SCCVII tumours, with 5 of 5 (100 %) of tumours $>VDS_{min}$ and the mean VDS score for the group essentially at the maximum of 1. Enhancement of TPZ-mediated vascular response by L-NNA in SCCVII tumours also occurs at lower doses, where 40 mg/kg TPZ alone results in 0 of 4 tumours $>VDS_{min}$, however when combined with 180 mg/kg L-NNA this response increases to 3 of 4 tumours (75 %).

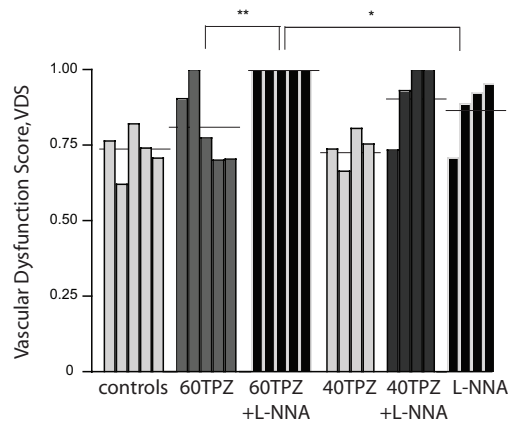
In HT29 colorectal xenografts no enhancement of TPZ mediated vascular dysfunction by L-NNA is seen in tumour maps (Figure 4.7, Table 4.2). However, quantitative analysis results in 1 of 5 TPZ-treated tumours, 2 of 6 L-NNA treated tumours, and 4 of 5 combination treated tumours scoring a $VDS > VDS_{min}$. No focused areas of unperfused or necrotic tissues were observed in these tumours, and they are therefore classed as non-responders (Figure 4.7). Treatment was apparently able to effect loss of vascular function in large numbers of vessels within the tumours, but these effects were not substantial enough, or were not sufficiently proximal to each other to cause central vascular dysfunction and subsequent tumour tissue death.

Table 4.2. Impact of NOS inhibition on TPZ-mediated vascular dysfunction in SCCVII and HT29 tumours.

Group	PF % \pm SD	VF % \pm SD	VDS \pm SD	VDS_{min}	# tumours > VDS_{min}
SCCVII					
Control	27.1 \pm 7.5	99.3 \pm 1.5	0.731 \pm 0.07	0.878	n/a
60TPZ	20.0 \pm 12.1	73.3 \pm 39.2	0.817 \pm 0.13	-	2/5
60TPZ + 180L-NNA	0.62 \pm 0.61	1.2 \pm 1.2	0.999 \pm 0.00	-	5/5
40TPZ	27.3 \pm 7.1	95.7 \pm 3.3	0.740 \pm 0.06	-	0/4
40TPZ + 180L-NNA	16.6 \pm 18.9	26.1 \pm 28.9	0.916 \pm 0.12	-	3/4
180L-NNA	17.1 \pm 9.1	77.7 \pm 35.1	0.868 \pm 0.11	-	3/4
HT29					
Control	57.5 \pm 4.0	100 \pm 0	0.425 \pm 0.40	0.505	n/a
60TPZ	62.6 \pm 11.3	92.4 \pm 8.1	0.415 \pm 0.15	-	1/5
60TPZ + 180L-NNA	45.5 \pm 11.5	98.8 \pm 2.8	0.551 \pm 0.11	-	4/5
180L-NNA	54.8 \pm 10.5	98.3 \pm 3.2	0.459 \pm 0.11	-	2/6

PF = perfused fraction; SD = standard deviation; VF = viable fraction; VDS = vascular dysfunction score; VDS_{min} = mean control VDS + 2 x SD; 60TPZ = tirapazamine at 60 mg/kg; 40TPZ = tirapazamine at 40 mg/kg; 180L-NNA = l-nitro-l-arginine at 180 mg/kg.

A) Vascular Dysfunction Score (VDS) in SCCVII tumours



B) SCCVII tumour maps

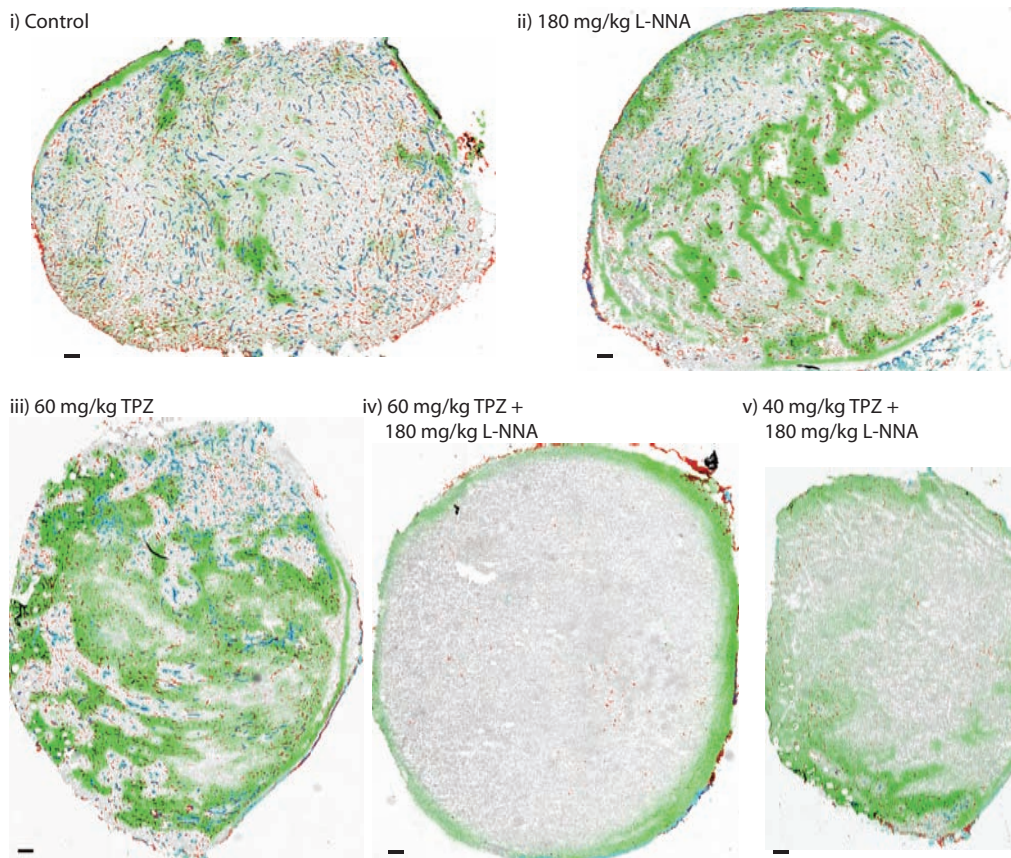
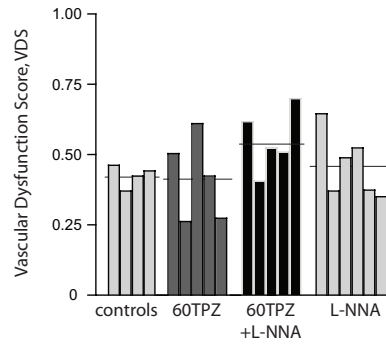


Figure 4.6 NOS inhibition enhances the anti-vascular effect of TPZ in SCCVII tumours.

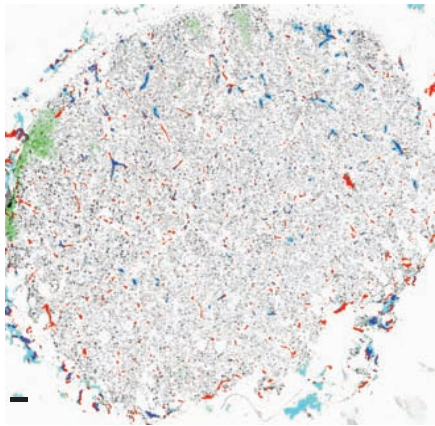
Vascular dysfunction scores (VDS) are reported for TPZ-treated SCCVII tumours (A); individual tumours represented by bars, group means by horizontal lines. Tumour maps (B) show staining for unperfused vasculature (CD31, red), perfused vasculature (DiOC₇(3)+ve CD31, blue), tissue background (hematoxylin, grey) and hypoxia (pimonidazole, green). Representative tumours are shown for each group, with exception to ii), iii), iv) and v) where displayed tumour maps are representative of vascular dysfunction effects observed within indicated treatment groups. Scale bars 150 μ m; (* p <0.05) (** p <0.01).

A) Vascular Dysfunction Score (VDS) in HT29 tumours

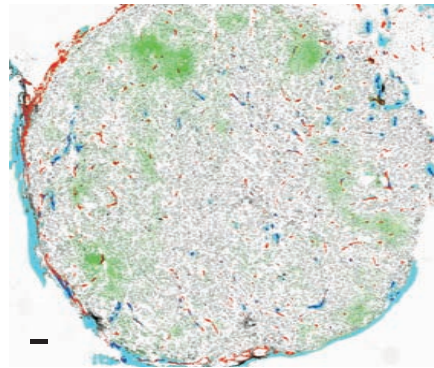


B) HT29 tumour maps

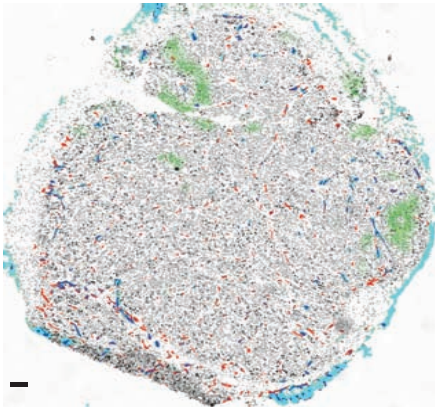
i) Control



ii) 180 mg/kg L-NNA



iii) 60 mg/kg TPZ



iv) 60 mg/kg TPZ + 180 mg/kg L-NNA



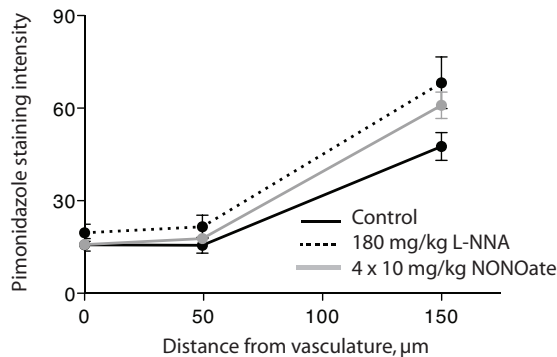
Figure 4.7 NOS inhibition does *not* enhance anti-vascular effects of TPZ in HT29 tumours.

VDS scores are reported for TPZ-treated HT29 tumours (A); individual tumours represented by bars, group means by horizontal lines. Tumours maps (B) show staining for unperfused vasculature (CD31, red), perfused vasculature (DiOC₇(3)+ve CD31, blue), hypoxia (pimonidazole, green) and tissue background (hematoxylin, grey). Representative tumours are shown for each group. Scale bars 150 μ m.

4.3.6 L-NNA and spermine NONOate effects on hypoxia in colorectal xenografts

Immunohistochemical staining for pimonidazole labeling in untreated control and 180 mg/kg L-NNA treated HCT116 and HT29 colorectal xenografts is shown as a function of distance to the nearest CD31+ve object (Figure 4.8). Although values do not reach statistical significance, the trend shows that pimonidazole is greater, particularly at distances further from vessels, for both NOS inhibition by L-NNA and excess NO by spermine NONOate in HCT116 colorectal xenografts. HT29 colorectal xenografts also have greater pimonidazole binding when treated with L-NNA, however this effect appears to be slightly less than that seen in HCT116 tumours.

A) HCT116 colorectal xenografts



B) HT29 colorectal xenografts

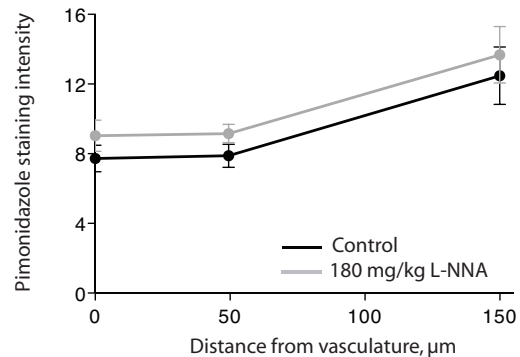


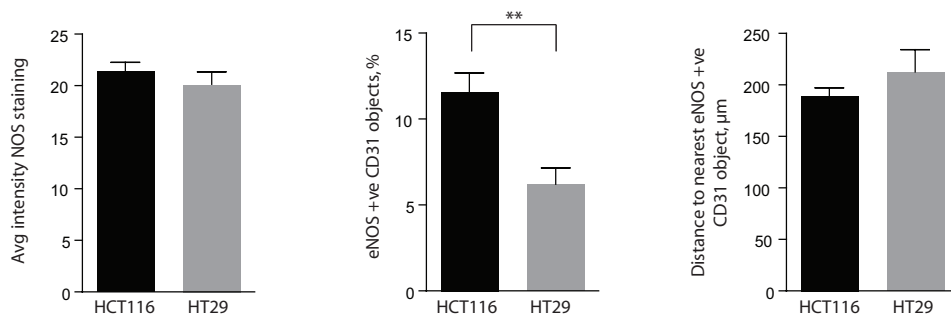
Figure 4.8 Modulation of NO effects on hypoxia in HCT116 and HT29 tumours.

Pimonidazole labeling of hypoxic cells is displayed as a function of distance from nearest CD31 stained blood vessel for HCT116 (A) and HT29 (B) colorectal xenografts. NOS inhibition using 180 mg/kg L-NNA (black, dashed) increases hypoxia in both tumour models, relative to controls (black, solid) (A, B). Excess NO using 4 doses of spermine NONOate also results in an increase in pimonidazole labeling in HCT116 tumours (A).

4.3.7 Differential NOS expression in colorectal xenografts that are sensitive (HCT116) and resistant (HT29) to TPZ mediated vascular dysfunction

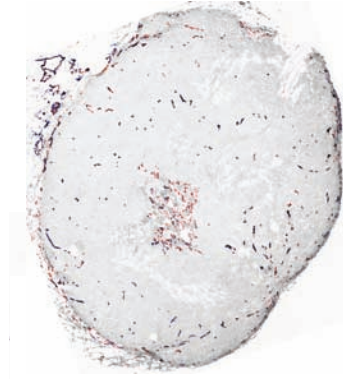
Untreated HCT116 and HT29 colorectal xenografts grown subcutaneously in NOD/SCID mice were immunohistochemically stained for CD31 and the NOS enzyme using both a non-specific pan-NOS antibody (uNOS) and an antibody specifically labeling endothelial NOS (eNOS). Expression of all isoforms of NOS, reflected by staining intensity data for uNOS, is similar in HCT116 and HT29 (Figure 4.9A, left). Specific expression of eNOS staining is expressed as the proportion of CD31 +ve vessels that are at minimum 20 % dual labeled for eNOS staining. HT29 tumours have significantly fewer eNOS+ve CD31 vessels relative to HCT116 tumours (Figure 4.9A, middle). However, there is no significant difference in the overall eNOS+ve CD31 vessel density between tumours, as reflected by the average distance of tissue to the nearest dual eNOS and CD31 +ve object in HCT116 and HT29 (Figure 4.9A, right).

A) Quantitative assessment of NOS expression in HCT116 and HT29 colorectal xenografts



B) Tumour maps of vasculature and NOS expression in HCT116 and HT29 colorectal xenografts

i) HCT116



ii) HT29

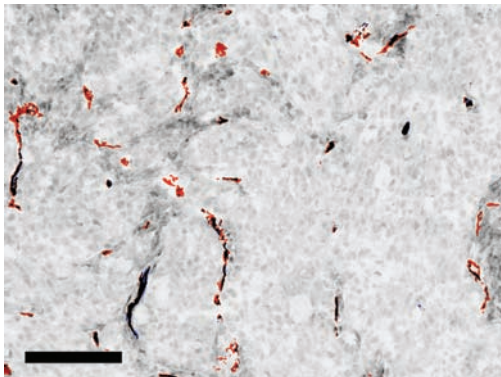


Figure 4.9 NOS expression variation between HCT116 and HT29 tumours.

No significant differences in overall NOS expression are seen between the HCT116 and HT29 colorectal xenograft models (A, left). Specific assessment of eNOS+ve CD31 staining shows that a greater proportion of HCT116 vessels are positive for eNOS (A, middle). However, the overall density of eNOS +ve CD31 vasculature is similar in both HCT116 and HT29 (A, right). Representative images of HCT116 and HT29 colorectal xenografts illustrate CD31 staining (alone, red; overlapped with eNOS, black), non-specific NOS (grey) and eNOS (overlapped with CD31, black). Scale bars 150 μm ; (** $p < 0.01$)

4.4 DISCUSSION

Studies in Chapter 4 have shown that inhibition of the enzyme nitric oxide synthase (NOS) can enhance the *anti-vascular activity* of TPZ in some tumours, including HCT116 xenografts. Combining NOS inhibition with TPZ translates to reduced tumour growth in HCT116 tumours, suggesting NOS inhibition in combination with TPZ is a therapeutically useful strategy.

4.4.1 *Effects of NO modulation in tumours*

Administration of the NOS inhibitor L-NNA alone reduced the perfused fraction (PF) in HCT116 and SCCVII tumour models, and increased pimonidazole-labeled tumour hypoxia in HCT116 tumours (Tables 4.1, 4.2; Figure 4.8). Although none of the HCT116 or HT29 tumours treated with L-NNA showed evidence of a central vascular dysfunction effect, L-NNA alone did effect some small regions of focused vascular dysfunction in SCCVII tumours (Figure 4.6). A lower 20 mg/kg dose of L-NNA has previously been shown to effect a growth delay in SCCVII tumours (Korbelik *et al.* 2000). In a limited, previous study in the Minchinton laboratory, 180 mg/kg L-NNA in HCT116 tumours resulted in greater proportions of central necrosis at 24 h after administration of the NOS inhibitor (Huxham *et al.* 2008). However, several follow up studies were unable to observe central areas of decreased perfusion as a prelude to necrosis in L-NNA treated tumours, and central vascular dysfunction, either as decreased perfused or viable fractions in HCT116 tumours, has never subsequently been observed. L-NNA therefore appears to be able to decrease the perfused fraction in some tumours, but is not as potent at initiating a large, central anti-vascular effect that would translate to reduced tumour growth. The combined effect of L-NNA and TPZ in the current studies is not suggestive of an additive effect in HCT116 tumours, as L-NNA alone had no significant reductions in tumour growth, or in the proliferating fraction of tumour cells. A 40 mg/kg dose of TPZ alone did not result in lower perfused fractions (PFs), but when combined with L-NNA the PFs were significantly lower than for L-NNA alone (Tables 4.1, 4.2). Instead it appears that either drug alone may have some effects on vascular function, but when combined create a greater than additive impact on tumour perfusion and subsequent necrosis.

Inhibition of NOS has been shown to enhance the anti-vascular effects of vascular disrupting agents (VDAs) and photodynamic therapy (PDT) (Korbelik *et al.* 2000; Parkins *et al.* 2000; Cullis *et al.* 2006; Tozer *et al.* 2009). VDAs are a relatively new class of compounds that are designed to specifically target existing tumour vasculature for destruction in a similar, but much faster pattern than that seen with TPZ *in vivo* (Thorpe 2004; Tozer *et al.* 2005). PDT uses light to activate prodrug compounds to their toxic forms when located within tumour vasculature (Korbelik *et al.* 2000). Both VDAs and PDT effect loss of perfusion that leads to necrosis in the central regions of tumours. The mechanisms for synergistic activity of VDAs with NOS inhibition are varied, but it has been suggested that nitric oxide (NO) produced by NOS functions as an anti-oxidant and neutralizes reactive oxygen species that may be produced by VDAs (Davis *et al.* 2002).

NO interactions with reactive oxygen species (ROS) are complex and often contradictory, having been implicated for both damage and cytoprotection depending on the physiological situation (Beckman *et al.* 1990; Gaboury *et al.* 1994; Stamler 1994). NO interacts with superoxide ($O_2^{\bullet-}$) to form peroxynitrite, which may undergo further reactions to form even more reactive intermediates. However, $O_2^{\bullet-}$ itself has been implicated in vascular damage, as the primary enzyme responsible for neutralizing $O_2^{\bullet-}$, superoxide dismutase (SOD), protects vascular endothelium from damage (Parkins *et al.* 1995; Parkins *et al.* 1998). In these ischemia / reperfusion studies, cytotoxic damage to an ischemic tumour was potentiated by the NOS inhibitor L-NNA and was protected by a NO donor or excess supply of SOD, emphasizing the role of NO in protecting vasculature from oxidative stress, and of $O_2^{\bullet-}$ in effecting vascular damage (Parkins *et al.* 1995; Parkins *et al.* 1998). TPZ produces oxidizing species under both aerobic and anaerobic conditions, as cycling of the prodrug in the presence of oxygen results in $O_2^{\bullet-}$ as a by-product (see Figure 1.2). In the absence of oxygen, the TPZ radical undergoes further metabolism. The radical intermediate responsible for mediating hypoxic cytotoxicity via topoisomerase II poisoning or DNA double strand breaks is thought to be an oxidizing hydroxyl (OH^{\bullet}) or benzotriazinyl radical (BTZ $^{\bullet}$) (Peters and Brown 2002; Anderson *et al.* 2005). Inhibition of the enzyme NOS either by TPZ alone or by co-administered L-NNA can produce conditions of reduced NO availability; a decrease in locally available anti-oxidant NO could prolong the presence of

$O_2\cdot^-$ in oxygenated conditions, or other reactive oxygen species in hypoxic conditions, to result in vascular damage.

TPZ inhibits NOS production of NO, and data presented here in Chapter 4 shows that inhibition of NOS enhances the anti-vascular effects of TPZ. A rational hypothesis is therefore that TPZ causes a decrease in microregional NO availability and consequently causes damage to the tumour vasculature.

4.4.2 Hypothesis for role of NOS in mechanism for TPZ mediated vascular dysfunction

A critical step in validating this hypothesis is determining if the vascular targeting effects of TPZ are attenuated by the presence of excess NO. This was not the case in studies combining 60 mg/kg TPZ with repeat doses of spermine NONOate. Instead of protecting tumour vasculature from damage, exogenous NO appeared to *sensitize* tumours to the anti-vascular effects of TPZ. NO was provided in excess for up to 2 h in the plasma and should have well exceeded 4 x TPZ plasma half-lives, which is thought to be about 27 minutes in rodents (Minchinton *et al.* 2002). This prolonged exposure could have exceeded that needed to protect vasculature from oxidative stress initiated by TPZ and may actually have destabilized the vasculature such that it was made vulnerable or less able to recover from damage inflicted by TPZ. In addition, NO donors have previously been found to result in an ‘oxygen steal effect’ where NO decreases systemic blood pressure and consequently tumour blood flow is decreased in a dose-dependent manner, producing a net drop in tumour oxygenation despite the vasodilatory effects of NO in normal tissues (Shan *et al.* 1997). Pimonidazole labeling of hypoxic cells in HCT116 tumours treated with spermine NONOate did show slightly increased staining at distances far from vasculature, though the difference was not significant and was less than that seen with the NOS inhibitor, L-NNA (Figure 4.8).

Therefore data from the studies presented here in Chapter 4 cannot confirm a specific mechanism for TPZ mediated vascular dysfunction, but do suggest that NOS and NO may play roles in its effects on tumour vasculature. It remains unclear if this is due to localized activation of TPZ by NOS in endothelial cells and consequently greater amounts of $O_2\cdot^-$ and reduced TPZ (TPZ \cdot) within the endothelium. However, HCT116 tumours with greater sensitivity to TPZ were shown to have greater expression of eNOS in their vascular endothelium relative to resistant HT29 tumours (Figure 4.9). Alternatively, reduced levels of

the antioxidant NO as a result of NOS inhibition by TPZ may prolong the effects of ROS produced by TPZ. Or, modulation of NO levels by inhibition of NOS by TPZ may result in destabilized and sensitized vasculature, which could also occur through excess supply of NO. Lastly, hypoxia plays an important role in TPZ activity and reduced blood oxygenation has been shown to enhance the anti-vascular activity of TPZ, as shown in Chapter 3. Inhibition of NOS may reduce blood flow rates, causing decreased blood oxygenation or increased tumour hypoxia to result in enhancement of TPZ mediated vascular dysfunction. Further work is required to determine which of these effects, or what combination of these effects, is relevant to the mechanism for TPZ mediated vascular dysfunction.

Combinations of TPZ with NOS inhibition or excess NO also resulted in a decreased fraction of S-phase tumour cells (Figure 4.4). The reduced tumour growth observed with TPZ and NOS inhibition in combined treatment may therefore be a consequence of both reduced proliferation and enhanced anti-vascular effects.

Despite both HCT116 and SCCVII showing striking enhancement of the anti-vascular effects of TPZ when combined with NOS inhibitor L-NNA (Figure 4.1, Figure 4.6), the HT29 tumour remained resistant (Figure 4.7). The relative insensitivity of HT29 colorectal xenografts to TPZ-mediated vascular dysfunction has been demonstrated in Chapter 3, where their resistance was overcome by sensitization via 7% O₂ breathing. Hypoxia, but not NOS inhibition alone, can enhance the anti-vascular effects of TPZ in HT29 tumours. If the role of NOS inhibition in enhancing TPZ-mediated vascular dysfunction is increasing tumour hypoxia, then perhaps NOS inhibition is not able to produce the same effects in HT29 tumours as in other models. Alternatively, perhaps the presence or absence of NO is less important than the ability of vasculature to respond to NO fluctuations. This observation is supported by the findings in Chapter 3 of relatively thick coatings of CIV and α SMA in HT29 colorectal xenografts, which may make them less sensitive or more able to recover from vascular damage relative to the sensitive HCT116 colorectal xenografts that had less CIV and α SMA. The variation in microregional NOS expression in these contrasting tumour models (Figure 4.9) also offers a potential explanation as to why HT29 tumours may be less sensitive to NO levels, as HT29 tumours have a lower frequency of vasculature staining positive for eNOS.

4.4.3 Bioreductive hypoxic cytotoxic targeting of tumour vasculature enhanced by NOS inhibition

Combining NOS inhibition with hypoxic cytotoxins for enhanced anti-cancer activity has been previously suggested and has been shown as a therapeutically beneficial strategy (Wood *et al.* 1994; Butler *et al.* 1997). However, most studies examining the effects of bioreductive hypoxic cytotoxins have not examined whole tumour sections histologically and may therefore miss opportunities to observe anti-vascular activity. Butler *et al.* (1997) observed that the hypoxic cytotoxin RB6145, when combined with NOS inhibitor L-NNA, produced an effect that far exceeded that expected for a bioreductive agent selectively killing hypoxic tumour cells. The clonogenic cell survival was decreased if tissues were harvested at > 12 h post administration (Butler *et al.* 1997). Earlier studies using clonogenic survival studies in SCCVII/Ha tumours showed that L-NNA enhanced the anti-cancer activity of RB6145 and caused extensive necrosis in treated tumours when examined at 24 h post-treatment (Wood *et al.* 1994). The timing of tissue harvest in clonogenic survival studies is crucial when detecting an anti-vascular effect (see section 1.2). If tissues are harvested too early following anti-vascular treatment the tumour cells that would otherwise be doomed to die due to lost blood vessels would be effectively rescued by the excision and plating of cells in clonogenic survival assays. The time-dependent survival effects observed when combining hypoxic cytotoxin RB6145 with NOS inhibition may have occurred due to an anti-vascular effect, which would also account for the greater than expected cell kill in those studies (Wood *et al.* 1994; Butler *et al.* 1997). RB6145 was also combined with the NOS inhibitor L-NNA in subcutaneous SaF tumours to produce a growth delay that, although only a 1.5 day effect, was significantly greater than that seen for RB6145 alone (Horsman *et al.* 1996). No assessment for anti-vascular effects were undertaken in studies examining NOS inhibition treatment combined with RB6145, but we propose that a large, irreversible anti-vascular effect may have occurred that would explain enhancement of the bioreductive hypoxic cytotoxin RB6145 by the NOS inhibitor L-NNA.

4.5 CONCLUSIONS

TPZ is reduced by NOS to result in reduced available NO and increased oxidative stress. Tumour vasculature is already under greater oxidative stress than most tissues due to sluggish and intermittent blood flow. In addition, tumour vasculature may be selectively unable to withstand or recover from vascular damage. Therefore, it seems plausible that targeting tumour vasculature with bio-reductive cytotoxins that can competitively inhibit NOS may represent a viable therapeutic approach with an advantageous mechanism for selectively targeting tumour tissue for damage.

The studies presented here in Chapter 4 demonstrate a therapeutic benefit for combining TPZ with NOS inhibition and emphasize the importance of ascertaining whether the vascular dysfunction effects of TPZ occur in clinically treated patients. In addition, assessment of an anti-vascular effect is strongly suggested for other hypoxic cytotoxins alone or in combination with NOS inhibition.

4.6 REFERENCES

- Anderson, R. F., S. S. Shinde, *et al.* (2005). "Radical properties governing the hypoxia-selective cytotoxicity of antitumor 3-amino-1,2,4-benzotriazine 1,4-dioxides." Org Biomol Chem **3**(11): 2167-74.
- Andrade, S. P., I. R. Hart, *et al.* (1992). "Inhibitors of nitric oxide synthase selectively reduce flow in tumor-associated neovasculature." British Journal of Pharmacology **107**(4): 1092-5.
- Bains, L. J., J. H. Baker, *et al.* (2009). "Detecting vascular-targeting effects of the hypoxic cytotoxin tirapazamine in tumor xenografts using magnetic resonance imaging." Int J Radiat Oncol Biol Phys **74**(3): 957-65.
- Beckman, J. S., T. W. Beckman, *et al.* (1990). "Apparent hydroxyl radical production by peroxynitrite: implications for endothelial injury from nitric oxide and superoxide." Proc Natl Acad Sci USA **87**(4): 1620-4.
- Brown, J. M. and M. J. Lemmon (1990). "Potentiation by the hypoxic cytotoxin SR 4233 of cell killing produced by fractionated irradiation of mouse tumors." Cancer Res **50**(24): 7745-9.
- Brown, J. M. and W. R. Wilson (2004). "Exploiting tumour hypoxia in cancer treatment." Nature Reviews Cancer **4**(6): 437-47.
- Butler, S. A., P. J. Wood, *et al.* (1997). "Enhancement of bioreductive drug toxicity in murine tumours by inhibition of the activity of nitric oxide synthase." Br J Cancer **76**(4): 438-44.
- Chinje, E. C., R. L. Cowen, *et al.* (2003). "Non-nuclear localized human NOSII enhances the bioactivation and toxicity of tirapazamine (SR4233) in vitro." Mol Pharmacol **63**(6): 1248-55.
- Cullis, E. R., T. L. Kalber, *et al.* (2006). "Tumour overexpression of inducible nitric oxide synthase (iNOS) increases angiogenesis and may modulate the anti-tumour effects of the vascular disrupting agent ZD6126." Microvasc Res **71**(2): 76-84.
- Davis, P. D., G. M. Tozer, *et al.* (2002). "Enhancement of vascular targeting by inhibitors of nitric oxide synthase." Int J Radiat Oncol Biol Phys **54**(5): 1532-6.
- Dorie, M. J. and J. M. Brown (1993). "Tumor-specific, schedule-dependent interaction between tirapazamine (SR 4233) and cisplatin." Cancer Res **53**(19): 4633-6.
- Evans, J. W., K. Yudoh, *et al.* (1998). "Tirapazamine is metabolized to its DNA-damaging radical by intranuclear enzymes." Cancer Res **58**(10): 2098-101.
- Fukumura, D., S. Kashiwagi, *et al.* (2006). "The role of nitric oxide in tumour progression." Nature Reviews Cancer **6**(7): 521-34.
- Fukumura, D., F. Yuan, *et al.* (1997). "Role of nitric oxide in tumor microcirculation. Blood flow, vascular permeability, and leukocyte-endothelial interactions." Am J Pathol **150**(2): 713-25.
- Gaboury, J. P., D. C. Anderson, *et al.* (1994). "Molecular mechanisms involved in superoxide-induced leukocyte-endothelial cell interactions in vivo." Am J Physiol **266**(2 Pt 2): H637-42.
- Garner, A. P., M. J. Paine, *et al.* (1999). "Nitric oxide synthases catalyze the activation of redox cycling and bioreductive anticancer agents." Cancer Res **59**(8): 1929-34.
- Horsman, M. R., D. J. Chaplin, *et al.* (1996). "Effect of nitro-L-arginine on blood flow, oxygenation and the activity of hypoxic cell cytotoxins in murine tumours." Br J Cancer Suppl **27**: S168.
- Huxham, L. A., A. H. Kyle, *et al.* (2006). "Tirapazamine causes vascular dysfunction in HCT-116 tumour xenografts." Radiotherapy and oncology : journal of the European Society for Therapeutic Radiology and Oncology **78**(2): 138-45.
- Huxham, L. A., A. H. Kyle, *et al.* (2008). "Exploring vascular dysfunction caused by tirapazamine." Microvasc Res **75**(2): 247-55.
- Korbelik, M., C. S. Parkins, *et al.* (2000). "Nitric oxide production by tumour tissue: impact on the response to photodynamic therapy." Br J Cancer **82**(11): 1835-43.
- Kyle, A. H., L. A. Huxham, *et al.* (2003). "Tumor distribution of bromodeoxyuridine-labeled cells is strongly dose dependent." Cancer Res **63**(18): 5707-11.

- Kyle, A. H., L. A. Huxham, *et al.* (2007). "Limited tissue penetration of taxanes: a mechanism for resistance in solid tumors." Clin Cancer Res **13**(9): 2804-10.
- Larrivée, B., K. Niessen, *et al.* (2005). "Minimal contribution of marrow-derived endothelial precursors to tumor vasculature." J Immunol **175**(5): 2890-9.
- Marcu, L. and I. Olver (2006). "Tirapazamine: from bench to clinical trials." Current clinical pharmacology **1**(1): 71-9.
- Minchinton, A. I., D. A. Tonn, *et al.* (2002). "Carbogen breathing after irradiation enhances the effectiveness of tirapazamine in SiHa tumors but not SCCVII tumors in mice." Radiat Res **158**(1): 94-100.
- Moncada, S. and A. Higgs (1993). "The L-arginine-nitric oxide pathway." N Engl J Med **329**(27): 2002-12.
- Ng, Q., V. Goh, *et al.* (2007). "Effect of nitric-oxide synthesis on tumour blood volume and vascular activity: a phase I study." The Lancet Oncology **8**(2): 111-118.
- Parkins, C. S., M. F. Dennis, *et al.* (1995). "Ischemia reperfusion injury in tumors: the role of oxygen radicals and nitric oxide." Cancer Res **55**(24): 6026-9.
- Parkins, C. S., A. L. Holder, *et al.* (1998). "Involvement of oxygen free radicals in ischaemia-reperfusion injury to murine tumours: role of nitric oxide." Free Radic Res **28**(3): 271-81.
- Parkins, C. S., A. L. Holder, *et al.* (2000). "Determinants of anti-vascular action by combretastatin A-4 phosphate: role of nitric oxide." Br J Cancer **83**(6): 811-6.
- Patterson, L. H. and S. R. McKeown (2000). "AQ4N: a new approach to hypoxia-activated cancer chemotherapy." Br J Cancer **83**(12): 1589-93.
- Peralta, C., G. Hotter, *et al.* (1997). "Protective effect of preconditioning on the injury associated to hepatic ischemia-reperfusion in the rat: role of nitric oxide and adenosine." Hepatology **25**(4): 934-7.
- Peters, K. B. and J. M. Brown (2002). "Tirapazamine: a hypoxia-activated topoisomerase II poison." Cancer Res **62**(18): 5248-53.
- Saunders, M. P., A. V. Patterson, *et al.* (2000). "NADPH:cytochrome c (P450) reductase activates tirapazamine (SR4233) to restore hypoxic and oxycytotoxicity in an aerobic resistant derivative of the A549 lung cancer cell line." Br J Cancer **82**(3): 651-6.
- Shan, S. Q., G. L. Rosner, *et al.* (1997). "Effects of diethylamine/nitric oxide on blood perfusion and oxygenation in the R3230Ac mammary carcinoma." Br J Cancer **76**(4): 429-37.
- Stamler, J. S. (1994). "Redox signaling: nitrosylation and related target interactions of nitric oxide." Cell **78**(6): 931-6.
- Thomlinson, R. H. and L. H. Gray (1955). "The histological structure of some human lung cancers and the possible implications for radiotherapy." Br J Cancer **9**(4): 539-49.
- Thorpe, P. E. (2004). "Vascular targeting agents as cancer therapeutics." Clin Cancer Res **10**(2): 415.
- Tozer, G. M., C. Kanthou, *et al.* (2005). "Disrupting tumour blood vessels." Nature Reviews Cancer **5**(6): 423-35.
- Tozer, G. M., V. E. Prise, *et al.* (1997). "Inhibition of nitric oxide synthase induces a selective reduction in tumor blood flow that is reversible with L-arginine." Cancer Res **57**(5): 948-55.
- Tozer, G. M., V. E. Prise, *et al.* (2009). "Nitric oxide synthase inhibition enhances the tumor vascular-damaging effects of combretastatin a-4 3-o-phosphate at clinically relevant doses." Clin Cancer Res **15**(11): 3781-90.
- Walton, M. I., C. R. Wolf, *et al.* (1992). "The role of cytochrome P450 and cytochrome P450 reductase in the reductive bioactivation of the novel benzotriazine di-N-oxide hypoxic cytotoxin 3-amino-1,2,4-benzotriazine-1,4-dioxide (SR 4233, WIN 59075) by mouse liver." Biochem Pharmacol **44**(2): 251-9.
- Wood, P. J., J. M. Sansom, *et al.* (1994). "Induction of hypoxia in experimental murine tumors by the nitric oxide synthase inhibitor, NG-nitro-L-arginine." Cancer Res **54**(24): 6458-63.
- Zeman, E. M., J. M. Brown, *et al.* (1986). "SR-4233: a new bioreductive agent with high selective toxicity for hypoxic mammalian cells." Int J Radiat Oncol Biol Phys **12**(7): 1239-42.

CHAPTER 5

Conclusions

5.1 Research hypothesis

The purpose of this research was to investigate the *in vivo* mechanism for anti-cancer activity of the bioreductive hypoxic cytotoxin tirapazamine (TPZ). TPZ has greater toxicity to hypoxic cells than oxygenated cells *in vitro*, but can damage the central blood vessels of tumours grown in mice *in vivo*. There is considerable inter- and intra-tumour heterogeneity in tumour response to TPZ, with ~35 % of treated tumours showing no anti-vascular effects when treated with near maximum tolerated doses. Even in responding tumours, a viable rim of undamaged vessels and tissue persists following treatment with TPZ. The main hypothesis of the work in this thesis is that features of the tumour microenvironment confer tumour sensitivity to the anti-vascular effects of tirapazamine. The microenvironmental features of tumours that were sensitive or resistant to the anti-vascular effects of TPZ were compared. Strategies for sensitizing tumours to the anti-vascular effects of TPZ were also assessed in this effort to characterize the mechanism for TPZ-mediated vascular dysfunction in solid tumours.

5.2 Assessing the anti-vascular effects of TPZ

The anti-vascular effects of TPZ were primarily assessed in this thesis work using IHC-based tumour mapping analysis. Layered IHC staining of multiple markers creates opportunity for multiple features to be assessed in relation to one another. Images of whole tumour sections were generated by tiling microscopy where adjacent fields are automatically stitched together. Overlaid, composite images of multiple markers, described as *tumour maps*, create visual representations of the effects of drugs in tumours, and quantitative data may also be obtained. This approach is gaining popularity for investigations of many anti-cancer drugs *in vivo*, and robotic microscopes with automated features are continuing to improve the accessibility and application of tumour mapping for many laboratories (Kaanders *et al.* 2002; Fenton *et al.* 2004; Franco *et al.* 2006; Tredan *et al.* 2009). In addition to examining the microregional effects of TPZ, tumour mapping has been used successfully in our laboratory to assess the *in vivo* effects of several therapeutics including trastuzumab (Baker *et al.* 2008a), liposomal irinotecan (Baker *et al.* 2008b), anti-metabolites (Huxham *et al.* 2004), the taxanes (Kyle *et al.* 2007) and S-phase marker BrdUrd (Kyle *et al.* 2003).

Assessment of the anti-vascular effects of TPZ described in this thesis using tumour mapping analyses was done by staining cryosections of tumours grown subcutaneously in mice. Prior to tissue harvest mice were administered exogenous markers, which labeled hypoxic (pimonidazole) and S-phase (BrdUrd) cells. A fluorescent dye (carbocyanine, DiOC₇(3)) was administered intravenously to label functioning, perfused vasculature. Staining and fluorescent imaging of these markers, in combination with labeling of tumour vasculature (CD31) and tissue (hematoxylin), all on the same sections generated the tumour maps where central vascular dysfunction could easily be identified (see Figure 1.3). Quantitative analysis was achieved similarly to previous reports of TPZ mediated vascular dysfunction (Huxham *et al.* 2006; Huxham *et al.* 2008), by determining the fraction of blood vessels that were perfused (perfused fraction, PF) as well as the amount of remaining viable tissue (viable fraction, VF). In the work reported in this thesis, PF and VF were combined to create an objectively quantifiable vascular dysfunction score (VDS). The VDS reflects the overall vascular damage in individual tumours that is subsequently compared to untreated control tumours.

The VDS is a valuable tool for objectively quantifying vascular damage in tumours and could be widely applicable for evaluating other compounds that have similar effects in tumours. In the case of central vascular dysfunction effects of TPZ and other VDAs, the tumour response may be described as all-or-nothing. For this reason it is relevant to describe the frequency of tumours that may be classed as having 'responded' vs those that did not, despite this approach resulting in fragmentation of already small group sizes. Throughout this thesis and in prior reporting of the central vascular dysfunction effects of TPZ, the response values both for individual tumours and for group means are reported such that a detailed observation of response may be made (Huxham *et al.* 2006; Huxham *et al.* 2008). In addition, individual tumours are compared to control means to determine a frequency for the number of tumours that sustained catastrophic central vascular dysfunction. Both the frequency and magnitude of response are used in this thesis to investigate whether modification of treatment conditions, dose or administering in combination with complementary drugs can increase or decrease the central vascular dysfunction effects of TPZ. A total of 25 HCT116 tumour xenografts were treated with 60 mg/kg TPZ and are reported in this thesis, of which 16 had VDS scores greater than their experimental VDS_{min},

an average response rate of 64%. This rate of response is similar to those previously reported for TPZ (Huxham *et al.* 2006; Huxham *et al.* 2008).

While the VDS was successful for evaluating the anti-vascular effects of TPZ in tumours, tumour mapping data are by nature static, with samples only analyzable at one time point in an experiment. Additionally, the exogenous markers and large samples required make application of this technique limited in the clinical setting. Magnetic resonance imaging (MRI) technology is used in clinical oncology applications for diagnosis and monitoring response to treatment, with dynamic contrast-enhanced (DCE-MRI) being increasingly used for the assessment of vascular function (Jackson *et al.* 2007; O'Connor *et al.* 2007). Drug effects on tumour blood volume, flow and permeability can be accomplished non-invasively using MRI. Several pre-clinical studies have used MRI in the investigation of other vascular disrupting agents, including examinations of ZD6126 (Robinson *et al.* 2003), DMXAA (McPhail *et al.* 2006) and CA-4-P (Beauregard *et al.* 2001). MRI has also been employed in clinical investigations of vascular disrupting agents; for a review see O'Connor *et al.* (2007).

Chapter 2 presents a method for evaluating the effects of TPZ non-invasively using two DCE-MRI derived biomarkers for assessment of vascular function: initial area under the curve (IAUC) and K^{trans} . IAUC and K^{trans} were determined for tumours before treatment with TPZ and these values were retrospectively correlated with histological determinations of tumour sensitivity to TPZ-mediated vascular dysfunction (Figure 2.11). These data show that pre-treatment measures of vascular function IAUC and K^{trans} may be useful predictors of sensitivity to TPZ. Both IAUC and K^{trans} are related measures of vascular function. IAUC is a model-free value that reflects uptake of Gd-DTPA, the contrast agent used in these studies. The volume transfer coefficient (K^{trans}) reflects transfer of the contrast agent from the blood vessels to the extravascular space. K^{trans} may be interpreted as an indication of vascular permeability or tumour blood flow depending on whether contrast agent delivery is limited by blood flow or permeability in the individual sample being analyzed (Figure 2.4) (Tofts *et al.* 1999). Therefore, discrimination between blood flow and permeability are difficult using these analyses due to the small molecule nature of the Gd-DTPA tracer that may not be completely intravascular due to the high permeability of tumour blood vessels (Leach *et al.* 2005). Further studies using macromolecular contrast agents may be able to determine more

specifically which aspects of vascular function can predict for tumour sensitivity to the anti-vascular effects of TPZ. Measures of vascular function may indirectly reflect levels of oxygenation which may be of more direct physiological relevance for predicting sensitivity to TPZ-mediated vascular dysfunction. Positron emission tomography (PET) scanning using radio-labeled hypoxia indicators is an alternative method for non-invasively monitoring hypoxia levels in tumours, and has been successfully used in studies attempting to predict which tumours may have greater sensitivity to TPZ (Rischin *et al.* 2006). It is unclear if this type of study would be sufficiently sensitive to detect differences in the levels of intermediately oxygenated tumour blood vessels, or if overall tumour hypoxia levels would be a useful predictor for sensitivity to TPZ-mediated vascular dysfunction. Due to the vascular damage effects of TPZ, PET imaging of radio-labeled tracers may have limited application in monitoring increases in tumour hypoxia following treatment, as loss of perfusion in the tumour would lead to reduced delivery of the tracer molecules.

In addition to their potential as predictors for sensitivity to TPZ, the DCE-MRI derived biomarkers IAUC and K^{trans} were demonstrated as useful measures of tumour response to TPZ (Figures 2.7, 2.9). Determining if the anti-vascular effects of TPZ observed in pre-clinical models occurs in clinically treated patients is of high importance. In Chapter 2, the use of DCE-MRI to non-invasively detect the effects of TPZ in tumours was validated. A clinical trial based on the MRI protocol presented in Chapter 2 has been undertaken by the gynecological oncology group (GOG) at the BC Cancer Agency in Vancouver, where patients with cervical cancer are being recruited for a randomized Phase III trial examining radiotherapy and cisplatin alone or in combination with TPZ. Patients recruited to the DCE-MRI trial are being imaged prior to their therapy that may include TPZ, with follow up DCE-MRI scans obtained at two timepoints following treatment. Results from this trial may indicate whether TPZ is able to mediate central vascular dysfunction in clinical cervical cancers. Further studies examining TPZ or other hypoxic cytotoxins in clinical trials could also investigate the potential of DCE-MRI as a tool for either assessment of response, or for predicting response to therapies that may have anti-vascular activity.

5.3 Tumour Blood Vessels – impact on sensitivity to TPZ

In Chapter 2, MRI-derived biomarkers IAUC and K^{trans} were useful in predicting which HCT116 tumours would be more sensitive to the anti-vascular effects of TPZ. Tumour blood vessel phenotype as a predictor for sensitivity to TPZ was further explored and is described in Chapter 3. HCT116 colorectal xenografts are sensitive to the anti-vascular effects of TPZ and appear to be less permeable to extravasation of high MW FITC-dextran than HT29 colorectal xenografts, which are resistant to TPZ. This result is consistent with DCE-MRI data from Chapter 2, where greater vascular function predicts for less sensitivity to TPZ. However, the distance of the FITC-dextran from vasculature could be the result of many features, including vascular permeability, extravasation rates, blood flow rates and tumour microenvironment-specific features that regulate extravascular diffusion of agents in solid tissue. The same confounding variables exist in most permeability assessments, including DCE-MRI and intravital microscopy. Interpretation of these results must therefore be carefully considered in context of further data.

Additional data described in Chapter 4 suggests that poor tumour vascular function can predict for tumour sensitivity to TPZ-mediated vascular dysfunction. Decreasing levels of NO via inhibition of NOS caused a drop in perfusion in HCT116 and SCCVII tumours and sensitized them to greater damage by TPZ. However, inhibition of NOS did not effect a significant change in the perfused fraction of HT29 tumour blood vessels, and these tumours remained resistant to the anti-vascular effects of TPZ. The vasculature in HT29 tumours also have thicker layers of α SMA and collagen type IV relative to HCT116 tumours, which may suggest a greater capacity to regulate blood flow or decreased sensitivity to modulation of signaling molecules such as NO.

While a detailed mechanism remains unclear, it appears that poor vascular function can predict for tumour sensitivity to the anti-vascular effects of TPZ. Greater vascular permeability has been suggested to be a predictor for *sensitivity* to other vascular disrupting agents (VDAs) based on studies using intravital microscopy and MRI (Beauregard *et al.* 2001; Tozer *et al.* 2008). A rationale for the correlation between greater pre-treatment permeability and greater sensitivity to VDAs is that tumor vascular permeability permits greater delivery of the VDAs to tumors through leakage, and loss of perfusion in response to the VDAs results in even greater trapping of the drugs within tumors (Tozer *et al.* 2008).

Additionally, high permeability of tumor blood vessels is at least partially responsible for greater interstitial fluid pressure (IFP) observed in solid tumors (Boucher *et al.* 1990; Leu *et al.* 2000), and greater IFP may make tumor blood vessels more vulnerable to collapse in response to VDAs (Tozer *et al.* 2001; Tozer *et al.* 2008).

In future studies it would be valuable to try and use alternate DCE-MRI tools such as higher molecular weight contrast agents to determine more specifically whether it is blood flow or vascular permeability that can predict for TPZ sensitivity. DCE-MRI is of particularly high value due to its potential to be applied as a predictor of response in clinical patients. Additional efforts could look at more tumour models with differential sensitivity to TPZ, examining whether there are histological features such as the presence of α SMA that consistently correlate with sensitivity to TPZ. Tumour blood vessel markers of phenotype and function, while not previously evaluated as relevant for TPZ or other hypoxic cytotoxins, may provide useful indicators of tumour sensitivity to these drugs. Identification and characterization of predictors of response to anti-cancer therapy are of great value. When accurate predictors of response to treatment are available, patients may be more carefully selected for treatments that could be beneficial and can avoid fruitless toxic or expensive therapies that they would not benefit from.

5.4 Hypoxia – impact on sensitivity to TPZ

TPZ has greater toxicity to hypoxic cells than oxygenated cells *in vitro* and its *in vivo* toxicity has been assumed to be of a similar mechanism (see section 1.2). Evidence for a hypoxic cytotoxic mechanism of TPZ *in vivo* has previously been suggested to come from studies finding decreased clonogenic survival in tumors treated with TPZ in combination with radiotherapy. Radiotherapy kills oxygenated cells and additional cell kill by a complementary agent is thought to have effectively targeted the hypoxic cell fraction, or to have radiosensitized cells (Zeman *et al.* 1988). Low oxygen breathing has also been shown to sensitize tumors to the anti-cancer activity of TPZ (Minchinton and Brown 1992). However, these studies were not able to specifically confirm *in vivo* that TPZ kills hypoxic tumor cells and they did not assess for an anti-vascular effect.

Data from this thesis suggests that poor oxygenation of the tumour vasculature sensitizes tumours to the *anti-vascular* effects of TPZ. As shown in Chapter 3, endothelial

tube structures *in vitro* showed damage in response to clinically relevant TPZ concentrations at 2% oxygen, showing that the endothelium is sensitive to TPZ damage at intermediate oxygen levels (Figure 3.9). Induction of moderate anemia or low oxygen breathing increased the magnitude and frequency of vascular dysfunction in sensitive HCT116 tumours and low oxygen breathing sensitized otherwise resistant HT29 tumours to catastrophic central vascular damage in response to TPZ (Figure 3.8, Table 3.2). Further evidence from Chapter 4 showed that both excess NO and decreased NO resulted in somewhat greater HCT116 tumour hypoxia, and both strategies resulted in enhanced anti-vascular activity of TPZ (Figures 4.1 - 4.3, Table 4.1). In addition, the suggestion that poor tumour vascular function (further described above in section 1.3) predicts for tumour sensitivity to TPZ-mediated vascular dysfunction may be indirect support for lower tumour oxygenation as a predictor or sensitizer to the effect.

Intravascular hypoxia was not directly measured in studies in this thesis, but could provide valuable data and may be useful in further investigations regarding TPZ mediated vascular dysfunction. Pimonidazole labeling was used in this thesis as an indicator of tumour hypoxia, but pimonidazole has been suggested to be most effective at labeling cells at < 10 mmHg (1 % O₂) (Gross *et al.* 1995; Arteel *et al.* 1998) and therefore may not be able to reflect tumour or blood oxygenation at intermediate oxygen levels (> 1 % O₂). It would be useful to know whether microregional blood oxygenation varies in a pattern that correlates with TPZ sensitivity in HCT116 tumours, particularly with respect to intra-tumour heterogeneity. This would help confirm whether tumour blood oxygenation is primarily responsible for tumour sensitivity to the anti-vascular effects of TPZ. Other reports of intra- and inter-tumour heterogeneity with respect to blood vessel oxygenation suggest a consistent pattern of lower oxygenation in the central regions of tumours relative to the more oxygenated peripheral margins. This pattern reflects the pattern of TPZ-mediated vascular dysfunction, providing additional evidence that the anti-vascular effects of TPZ *in vivo* are related to its status as a hypoxic cytotoxin. Microregional variation can be amplified in the presence of low or sluggish blood flow, as M. Dewhirst *et al.* (1999) have shown that fluctuating blood flow can induce a disproportionate increase in regional hypoxia in areas of low vascular density (Kimura *et al.* 1996; Dewhirst *et al.* 1999; Lanzen *et al.* 2006). The microregional pattern of tumour hypoxia suggests a possible mechanism for TPZ selectivity

for the central regions of tumours. Further theoretical studies by Dewhirst *et al.* (2007) assessed the potential impact of intermediate or fluctuating oxygen on bioreductive agents, and the authors suggest that this heterogeneous tumour microenvironmental feature may be partially responsible for poor hypoxic cytotoxin penetration through solid tumour tissue and for the anti-vascular effects of TPZ *in vivo* (Cárdenas-Navia *et al.* 2007).

Support for a hypoxia-associated predictor for the clinical success of TPZ treatment comes from Rischin *et al.* (2006), where patients with greater ^{18}F -fluoromisonidazole binding detected using PET were more likely to benefit from TPZ than patients with non-hypoxic primary tumours. Many of the clinical trials performed with TPZ have been unable to pre-screen patient tumours for hypoxia. Identifying sensitive tumours for TPZ treatment based on hypoxic status typically assumes that greater tumour hypoxia will result in increased TPZ-mediated hypoxic cytotoxicity to *hypoxic tumour cells*. Previous studies showing improved anti-cancer effects due to low oxygen breathing did not assess the mechanism for the enhanced TPZ activity and assumed the up to 10X greater clonogenic cell kill was due to increased cytotoxicity of TPZ to tumour cells (Minchinton and Brown 1992; Minchinton and Brown 1992). If tumour blood oxygenation has an impact on tumour sensitivity to TPZ, as suggested by pre-clinical studies in Chapter 3, it may be beneficial to look at the blood oxygenation of patients in trials with TPZ. Patients with anemia or low blood pO_2 levels for other reasons may have greater sensitivity to TPZ, and detection of patient blood oxygenation may aid in selecting patients likely to be most responsive to treatment. Screening for anemia or blood oxygen carrying capacity would perhaps be a more effective and more practical screen for TPZ patients, in lieu of the often more complicated approach of imaging for tumour hypoxia. Future studies and clinical trials with TPZ or other hypoxic cytotoxins may intentionally assess blood oxygenation as a possible predictor for response. In addition, retrospective analyses of concluded clinical trial data may be practical. Trials assessing patient response to TPZ typically evaluate blood hematocrit in order to eliminate patients who are deemed too anemic to be admitted to the trials. It may therefore be possible to do retrospective correlative evaluations of these studies to investigate whether pre-treatment patient hematocrit correlates with tumour responses to TPZ treatment.

5.5 NO - Impact on sensitivity to TPZ

In addition to tumour blood vessels and tumour blood oxygenation, the impact of nitric oxide (NO) was examined as a potential feature of the microenvironment that may impact tumour sensitivity to TPZ. Data presented in Chapter 4 suggests that decreased NO availability may sensitize tumour blood vessels to the anti-vascular effects of TPZ. Evidence from the literature demonstrates that TPZ competitively inhibits NOS to reduce its production of NO. TPZ is also bioactivated by NOS. When TPZ is administered in combination with a non-specific NOS inhibitor such as L-NNA, the vascular dysfunction effects of TPZ are enhanced in HCT116 and SCCVII tumour models (Figures 4.1, 4.6). This enhancement is particularly evident at lower 40 mg/kg doses of TPZ that do not typically cause vascular dysfunction, but that can result in catastrophic anti-vascular effects when combined with L-NNA. The combination results in reduced tumour growth in HCT116 xenografts (Figure 4.5). However, NOS inhibition in combination with TPZ was not able to cause central vascular dysfunction in the resistant HT29 model. Staining for the endothelial isoform of NOS, eNOS, in HT29 colorectal xenografts showed that a lower proportion of HT29 tumour vasculature was positive for eNOS staining relative to HCT116 tumours (Figure 4.9). This data suggests that perhaps TPZ is bioactivated by NOS at greater frequency in the endothelium of HCT116 tumours, or that inhibiting the production of NO may have a more dramatic effect in HCT116 tumours to result in their greater sensitivity relative to HT29 tumours. Interestingly, inhibition of NOS by L-NNA alone does produce some moderate vascular dysfunction, particularly in SCCVII tumours (Figure 4.6), but appears to be less potent than the effects seen with TPZ. Low doses of L-NNA have resulted in growth delay effects in SCCVII tumours in other laboratories (Horsman *et al.* 1996). Perhaps NOS inhibition can cause some vascular dysfunction and TPZ is more potent than non-specific NOS inhibitors such as L-NNA, but when combined the TPZ and NOS inhibition can produce stronger anti-cancer effects.

It is unclear if it is bioactivation of TPZ by NOS or reduced levels of NO in the tumour vasculature, or both effects in combination, that is responsible for the anti-vascular activity of TPZ in tumours. Provision of excess NO in combination with TPZ did not protect tumour vasculature from the anti-vascular effects of TPZ (Figure 4.3). This lack of protection may not reflect the desired control conditions where excess NO provides the opposite of

NOS inhibition. Instead, excess NO may have an alternate effect where systemic blood pressure drops so much that blood flow is actually removed from the tumour in contrast to extra blood flow elsewhere (Shan *et al.* 1997). Therefore, in the tumour, excess NO actually results in increased hypoxia, which can enhance the effects of TPZ. This may suggest that hypoxia is a more potent sensitizer than inhibition of NOS, which is also supported by the finding that in resistant HT29 tumours low oxygen breathing produced a sensitizing effect whereas inhibition of NOS in combination with TPZ was unable to have this effect.

Future studies investigating other hypoxic cytotoxins may find benefits in combinations with NOS inhibitors and should be investigated for anti-vascular effects as well as anti-cancer effects. It would also be interesting to look at isoform-specific inhibitors of NOS and their individual abilities to effect vascular dysfunction in tumours alone or in combination with TPZ. Perhaps analogues of TPZ or other hypoxic cytotoxins could be assessed for their ability to be reduced by NOS, their ability to inhibit NOS production of NO and their ability to effect central vascular dysfunction. These data would help select drugs that may have greater efficacy.

5.6 Conclusions

While a clear mechanism for activity of TPZ in the tumour vasculature remains elusive, the work described in this thesis has provided evidence that TPZ mediates anti-vascular effects in specific microregions of tumours. The anti-vascular effects of TPZ are detectable using DCE-MRI, and some tumour models are inherently resistant to its effects. Modulation of blood oxygenation levels had the most potent impact on conferring sensitivity to otherwise resistant tumours, and tumour vascular function and pre-treatment hypoxia may be useful predictors for response to TPZ. Combining TPZ with a NOS inhibitor enhances tumour vascular dysfunction, which translates to reduced tumour growth in HCT116 tumour xenografts.

The direct impacts of microenvironmental features such as hypoxia and vascular phenotype on tumour sensitivity to the anti-vascular effects of TPZ are difficult to prove with certainty. Experimental data confirms the relevance and impact that tumour hypoxia may have with respect to the anti-vascular effects of TPZ. Vulnerable, destabilized or hypoxic vasculature that is prevalent in solid tumours may be responsible for conferring the selective activity of TPZ and for the inter- and intra-tumour heterogeneity of response to TPZ. Further work with TPZ should focus on determining whether anti-vascular effects occur in clinical tumours. Assessment of effective pre-treatment predictors of sensitivity would be of high value. These suggestions also apply to other bioreductive hypoxic cytotoxins that have not previously been investigated for anti-vascular activity.

Ultimately the target cell for TPZ in mediating vascular dysfunction remains to be identified. TPZ may inhibit NOS production by tumour cells, or may have direct cytotoxic effects to intermediately oxygenated, or intermittently hypoxic tumour cells located proximal to the tumour vasculature. Damage to these cells may result in vascular damage sufficient to cause the losses in perfusion seen in these studies. Alternatively the target cell for damage by TPZ may be the endothelial cells or vascular support cells lining intermediately oxygenated, or intermittently perfused tumour blood vessels. Cellular damage and stress may be a consequence of mitochondrial dysfunction, the presence of reactive oxygen species and oxidative stress due to redox cycling of TPZ and production of the byproduct superoxide, or direct damage sustained in response to reduced and bioactivated TPZ. Further work

investigating the mechanism for anti-vascular activity may focus around identifying the target cell and the chemical species responsible for damage.

Based on the studies described in this thesis, it is recommended that TPZ treatment in the clinic should endeavour to assess vascular function prior and post-treatment using MRI or another indicator. In addition, the combination of NOS inhibition with TPZ may be a beneficial treatment strategy and is worth investigating further. Finally, a comprehensive examination of the whole tumour microenvironment using tumour mapping or other laboratory techniques is recommended for investigation of the effects of anti-cancer drugs in solid tumours.

5.7 REFERENCES

- Arteel, G. E., R. G. Thurman, *et al.* (1998). "Reductive metabolism of the hypoxia marker pimonidazole is regulated by oxygen tension independent of the pyridine nucleotide redox state." Eur J Biochem **253**(3): 743-50.
- Baker, J. H., K. E. Lindquist, *et al.* (2008). "Direct visualization of heterogeneous extravascular distribution of trastuzumab in human epidermal growth factor receptor type 2 overexpressing xenografts." Clin Cancer Res **14**(7): 2171-9.
- Baker, J. H., J. Lam, *et al.* (2008). "Irinophore C, a novel nanof ormulation of irinotecan, alters tumor vascular function and enhances the distribution of 5-fluorouracil and doxorubicin." Clin Cancer Res **14**(22): 7260-71.
- Beauregard, D. A., S. A. Hill, *et al.* (2001). "The susceptibility of tumors to the antivascular drug combretastatin A4 phosphate correlates with vascular permeability." Cancer Res **61**(18): 6811-5.
- Boucher, Y., L. T. Baxter, *et al.* (1990). "Interstitial pressure gradients in tissue-isolated and subcutaneous tumors: implications for therapy." Cancer Res **50**(15): 4478-84.
- Breidahl, T., F. U. Nielsen, *et al.* (2006). "The effects of the vascular disrupting agents combretastatin A-4 disodium phosphate, 5,6-dimethylxanthenone-4-acetic acid and ZD6126 in a murine tumour: a comparative assessment using MRI and MRS." Acta Oncol **45**(3): 306-16.
- Cárdenas-Navia, L. I., T. W. Secomb, *et al.* (2007). "Effects of fluctuating oxygenation on tirapazamine efficacy: Theoretical predictions." Int J Radiat Oncol Biol Phys **67**(2): 581-6.
- Cooper, R. A., B. M. Carrington, *et al.* (2000). "Tumour oxygenation levels correlate with dynamic contrast-enhanced magnetic resonance imaging parameters in carcinoma of the cervix." Radiotherapy and oncology : journal of the European Society for Therapeutic Radiology and Oncology **57**(1): 53-9.
- Dewhurst, M. W., E. T. Ong, *et al.* (1999). "Quantification of longitudinal tissue pO₂ gradients in window chamber tumours: impact on tumour hypoxia." Br J Cancer **79**(11-12): 1717-22.
- Fenton, B. M., S. F. Paoni, *et al.* (2004). "Effect of VEGF receptor-2 antibody on vascular function and oxygenation in spontaneous and transplanted tumors." Radiotherapy and oncology : journal of the European Society for Therapeutic Radiology and Oncology **72**(2): 221-30.
- Franco, M., S. Man, *et al.* (2006). "Targeted anti-vascular endothelial growth factor receptor-2 therapy leads to short-term and long-term impairment of vascular function and increase in tumor hypoxia." Cancer Res **66**(7): 3639-48.
- Gross, M. W., U. Karbach, *et al.* (1995). "Calibration of misonidazole labeling by simultaneous measurement of oxygen tension and labeling density in multicellular spheroids." Int J Cancer **61**(4): 567-73.
- Horsman, M. R., D. J. Chaplin, *et al.* (1996). "Effect of nitro-L-arginine on blood flow, oxygenation and the activity of hypoxic cell cytotoxins in murine tumours." Br J Cancer Suppl **27**: S168-71.
- Huxham, L. A., A. H. Kyle, *et al.* (2006). "Tirapazamine causes vascular dysfunction in HCT-116 tumour xenografts." Radiotherapy and oncology : journal of the European Society for Therapeutic Radiology and Oncology **78**(2): 138-45.
- Huxham, L. A., A. H. Kyle, *et al.* (2008). "Exploring vascular dysfunction caused by tirapazamine." Microvasc Res **75**(2): 247-55.
- Huxham, L. A., A. H. Kyle, *et al.* (2004). "Microregional effects of gemcitabine in HCT-116 xenografts." Cancer Res **64**(18): 6537-41.
- Jackson, A., J. P. O'Connor, *et al.* (2007). "Imaging tumor vascular heterogeneity and angiogenesis using dynamic contrast-enhanced magnetic resonance imaging." Clin Cancer Res **13**(12): 3449-59.

- Kaanders, J. H., K. I. Wijffels, *et al.* (2002). "Pimonidazole binding and tumor vascularity predict for treatment outcome in head and neck cancer." Cancer Res **62**(23): 7066-74.
- Kimura, H., R. D. Braun, *et al.* (1996). "Fluctuations in red cell flux in tumor microvessels can lead to transient hypoxia and reoxygenation in tumor parenchyma." Cancer Res **56**(23): 5522-8.
- Kyle, A. H., L. A. Huxham, *et al.* (2003). "Tumor distribution of bromodeoxyuridine-labeled cells is strongly dose dependent." Cancer Res **63**(18): 5707-11.
- Kyle, A. H., L. A. Huxham, *et al.* (2007). "Limited tissue penetration of taxanes: a mechanism for resistance in solid tumors." Clin Cancer Res **13**(9): 2804-10.
- Lanzen, J., R. D. Braun, *et al.* (2006). "Direct demonstration of instabilities in oxygen concentrations within the extravascular compartment of an experimental tumor." Cancer Res **66**(4): 2219-23.
- Leach, M. O., K. M. Brindle, *et al.* (2005). "The assessment of antiangiogenic and antivascular therapies in early-stage clinical trials using magnetic resonance imaging: issues and recommendations." Br J Cancer **92**(9): 1599-610.
- Leu, A. J., D. A. Berk, *et al.* (2000). "Absence of functional lymphatics within a murine sarcoma: a molecular and functional evaluation." Cancer Res **60**(16): 4324-7.
- Loncaster, J. A., B. M. Carrington, *et al.* (2002). "Prediction of radiotherapy outcome using dynamic contrast enhanced MRI of carcinoma of the cervix." Int J Radiat Oncol Biol Phys **54**(3): 759-67.
- McPhail, L. D., D. J. McIntyre, *et al.* (2006). "Rat tumor response to the vascular-disrupting agent 5,6-dimethylxanthenone-4-acetic acid as measured by dynamic contrast-enhanced magnetic resonance imaging, plasma 5-hydroxyindoleacetic acid levels, and tumor necrosis." Neoplasia **8**(3): 199-206.
- Minchinton, A. I. and J. M. Brown (1992). "Enhancement of the cytotoxicity of SR 4233 to normal and malignant tissues by hypoxic breathing." Br J Cancer **66**(6): 1053-8.
- Minchinton, A. I. and J. M. Brown (1992). "Improving the effectiveness of the bioreductive antitumor agent SR 4233 by induced hypoxia." Adv Exp Med Biol **317**: 177-81.
- O'Connor, J. P., A. Jackson, *et al.* (2007). "DCE-MRI biomarkers in the clinical evaluation of antiangiogenic and vascular disrupting agents." Br J Cancer **96**(2): 189-95.
- Rischin, D., R. J. Hicks, *et al.* (2006). "Prognostic significance of [18F]-misonidazole positron emission tomography-detected tumor hypoxia in patients with advanced head and neck cancer randomly assigned to chemoradiation with or without tirapazamine: a substudy of Trans-Tasman Radiation Oncology Group Study 98.02." J Clin Oncol **24**(13): 2098-104.
- Robinson, S. P., D. J. McIntyre, *et al.* (2003). "Tumour dose response to the antivascular agent ZD6126 assessed by magnetic resonance imaging." Br J Cancer **88**(10): 1592-7.
- Shan, S. Q., G. L. Rosner, *et al.* (1997). "Effects of diethylamine/nitric oxide on blood perfusion and oxygenation in the R3230Ac mammary carcinoma." Br J Cancer **76**(4): 429-37.
- Tofts, P. S., G. Brix, *et al.* (1999). "Estimating kinetic parameters from dynamic contrast-enhanced T(1)-weighted MRI of a diffusable tracer: standardized quantities and symbols." Journal of magnetic resonance imaging : JMRI **10**(3): 223-32.
- Tozer, G. M., C. Kanthou, *et al.* (2008). "Tumour vascular disrupting agents: combating treatment resistance." The British journal of radiology **81 Spec No 1**: S12-20.
- Tozer, G. M., V. E. Prise, *et al.* (2001). "Mechanisms associated with tumor vascular shut-down induced by combretastatin A-4 phosphate: intravital microscopy and measurement of vascular permeability." Cancer Res **61**(17): 6413-22.
- Tredan, O., A. Garbens, *et al.* (2009). "The Hypoxia-Activated ProDrug AQ4N Penetrates Deeply in Tumor Tissues and Complements the Limited Distribution of Mitoxantrone." Cancer Res **69**(3): 940-947.
- Zeman, E. M., V. K. Hirst, *et al.* (1988). "Enhancement of radiation-induced tumor cell killing by the hypoxic cell toxin SR 4233." Radiotherapy and oncology : journal of the European Society for Therapeutic Radiology and Oncology **12**(3): 209-18.

APPENDIX

A. List of Publications - Manuscripts

*Denotes publications that are included as part of the thesis.

***Baker JHE**, Kyle AH, Balbirnie A, Cran J, Gabriel E and Minchinton AI. Inhibition of nitric oxide synthase enhances tirapazamine-mediated vascular dysfunction in pre-clinical solid tumours. In preparation for submission for publication.

***Baker JHE**, Kyle AH, Bartels KL, Flanagan EJ, Methot SP and Minchinton AI. Decreased blood oxygen tension sensitizes tumors to the anti-vascular effects of tirapazamine. Submitted for publication October 27, 2009.

Wong LY, Franssen Y, Qadir M, **Baker JHE**, Kapanen A, Masin D, Minchinton AI, Gorski S, Gelmon K, Dr. Bally M and Dragowska V. Gefinitib and RAD001 in combination enhance cytostasis and impede tumor growth in trastuzumab sensitive and resistant HER2 overexpressing breast cancers. Submitted for publication October 2, 2009.

Bains LJ, **Baker JHE***, Kyle AK, Minchinton AI and Reinsberg ST. (2009). Detecting vascular-targeting effects of hypoxic cytotoxin tirapazamine in tumour xenografts using MRI. *Radiation Oncology Biology Physics*, 74 957-965. *Co-first authors.

Baker JHE, Lam J, Kyle AH, Sy JT, Oliver T, Co S, Dragowska W, Ramsay E, Anantha M, Ruth T, Adam M, Yung A, Kozlowski P, Minchinton AI, Ng S, Bally M, Yapp DTT. (2008). Irinophore CTM, a novel nano-formulation of irinotecan, alters tumor vascular function and enhances the distribution of 5-FU and doxorubicin. *Clinical Cancer Research*, 14 7260-7271.

Baker JHE, Lindquist KE, Huxham LAH, Kyle AK, Sy JT and Minchinton AI. (2008). Direct visualization of heterogeneous distribution of trastuzumab in human epidermal growth factor receptor type 2 overexpressing xenografts. *Clinical Cancer Research*, 14 2171-2179.

Huxham LAH, Kyle AK, **Baker JHE**, McNicol KL and Minchinton AI. (2008). Exploring vascular dysfunction of tirapazamine. *Microvascular Research*, 75 247-255.

Baker JHE, Huxham LAH, Kyle AK, Lam K and Minchinton AI. (2006). Vascular - specific quantification in an *in vivo* Matrigel chamber angiogenesis assay. *Microvascular Research*, 71 69-75.

Huxham LAH, Kyle AK, **Baker JHE**, McNicol KL and Minchinton AI. (2006). Tirapazamine causes vascular dysfunction. *Radiotherapy and Oncology*, 78 138-145.

List of Publications - Manuscripts, continued....

Tozer GM, Ameer-Beg SM, **Baker JHE**, Barber PR, Hill SA, Hodgkiss RJ, Locke R, Prise VE, Wilson I and Vojnovic B. (2005). Intravital imaging of tumour vasculature networks using multi-photon fluorescence microscopy. *Advanced Drug Delivery Reviews*, 57 135-152.

Huxham LA, Kyle AH, **Baker JHE**, Nykilchuk LK and Minchinton AI. (2004). Microregional effects of gemcitabine in HCT-116 xenografts. *Cancer Research*, 64 6537-6541.

Kyle AH, Huxham LA, **Baker JHE**, Burston HE and Minchinton AI. (2003). Tumour distribution of bromodeoxyuridine labeled cells is strongly dose dependent. *Cancer Research*, 63 5707-5711.

List of Publications - Selected Meeting Abstracts (presented by Baker JHE)

*Denotes presented abstracts that are **relevant** to the thesis.

*Targeting the tumour microenvironment: anti-vascular effects of the hypoxic cytotoxin tirapazamine.

Baker JHE, Kyle AH, Bartels KL, Flannagan EJ, Methot SP, Balbirnie A, Cran J, Gabriel E, Bains LJ, Reinsberg SA and Minchinton AI.

Presented as a poster, EORTC-AACR-NCI Annual Meeting, Boston MA, 2009.

*Investigating the vascular targeting effects of the bioreductive radiosensitizer tirapazamine.

Baker JHE, Kyle AH, Flannagan E, Methot S, Balbirnie A and Minchinton AI.

Presented as a poster, Radiation Research Annual Meeting, Savannah GA, 2009.

*Mechanisms associated with vascular targeting in cancer mediated by tirapazamine

Baker JHE, Kyle AH, Flannagan E, Methot S, Balbirnie A and Minchinton AI.

Presented as a poster, Keystone Dissecting the Vasculature Meeting, Vancouver, 2009.

*Lower tumour perfusion and permeability in tumours with stronger sensitivity to vascular targeting effects of tirapazamine

Baker JHE, Bains L, Reinsberg ST, Kyle AH, Methot S, Flannagan E and Minchinton AI.

Presented as a talk, Tumour Microenvironment Meeting, Miami, 2008.

*Differential sensitivity to vascular targeting effects of tirapazamine in HCT116 and HT29 xenografts

Baker JHE, Bains L, Huxham LAH, Kyle AH, Lindquist KE, Reinsberg S, Minchinton AI.

Presented as a talk, Vascular Targeted Therapies in Oncology (European Society of Hematology), France, 2007.

Liposomal CPT-11 changes the vasculature and oxygenation status of HT29 tumours

Baker JHE, Sy J, Co S, Yung A, Dragowska W, Ruth T, Adam M, Ng S, Minchinton A, Kozlowski P, Ramsay E, Bally M, Yapp D.

Poster, Tumour Microenvironment: Progression, Therapy and Prevention, Florence, 2007.

Distribution of Herceptin in tumour xenografts overexpressing HER2/neu.

Baker JHE, Lindquist KE, Huxham LAH, Kyle AH, Sy J, Minchinton AI.

Poster, AACR Annual Meeting, Washington DC, 2006.

Characterization of *in vivo* anti-angiogenic activity using the Matrigel Chamber Angiogenesis Assay and Tumour Blood Vessel Mapping.

Baker JHE, Huxham LA, Kyle AH, Lam K, Minchinton AI.

Poster, Pathobiology of Cancer Workshop hosted by AACR, Aspen, 2006.

A quantitative *in vivo* Matrigel chamber angiogenesis assay: Anti-angiogenic activity of thalidomide and LL/M27 primary tumours.

Baker JHE, Huxham LA, Kyle AH, Lam K, Minchinton AI.

Presented as a talk, Tumour Microenvironment Meeting, Oxford, 2005.

B. Biohazard Approval Certificate: B06-0187



The University of British Columbia



Biohazard Approval Certificate

PROTOCOL NUMBER: **B06-0187**

INVESTIGATOR OR COURSE DIRECTOR: Andrew I. Minchinton

DEPARTMENT: **Pathology & Laboratory Medicine**

PROJECT OR COURSE TITLE: **Benzotriazines as Antivascular Anticancer Drugs**

APPROVAL DATE: **June 18, 2009**

START DATE: **October 4, 2006**

APPROVED CONTAINMENT LEVEL: **2**

FUNDING TITLE: **Benzotriazines as Antivascular Anticancer Drugs**
FUNDING AGENCY: **Canadian Institutes of Health Research (CIHR)**

UNFUNDED TITLE: **Benzotriazines as Antivascular Anticancer Drugs**

The Principal Investigator/Course Director is responsible for ensuring that all research or course work involving biological hazards is conducted in accordance with the University of British Columbia Policies and Procedures, Biosafety Practices and Public Health Agency of Canada guidelines.

This certificate is valid for one year from the above start or approval date (whichever is later) provided there are no changes. Annual review is required.

A copy of this certificate must be displayed in your facility.

Office of Research Services
102, 6190 Agromomy Road, Vancouver, V6T 1Z3
Phone: 604-827-5111 FAX: 604-822-5093

C. Animal Care Certificate: A06-1454



THE UNIVERSITY OF BRITISH COLUMBIA

ANIMAL CARE CERTIFICATE

Application Number: A06-1454					
Investigator or Course Director: Andrew L. Minchinton					
Department: Pathology & Laboratory Medicine					
Animals:					
<table border="1"><tr><td>Mice C3H/HeN 40</td></tr><tr><td>Mice C57/Bl6 40</td></tr><tr><td>Mice eNOS 280</td></tr><tr><td>Mice NOD/SCID 225</td></tr></table>		Mice C3H/HeN 40	Mice C57/Bl6 40	Mice eNOS 280	Mice NOD/SCID 225
Mice C3H/HeN 40					
Mice C57/Bl6 40					
Mice eNOS 280					
Mice NOD/SCID 225					
Start Date:	October 1, 2006	Approval Date:	December 18, 2008		
Funding Sources:					
Funding Agency:	Canadian Institutes of Health Research (CIHR)				
Funding Title:	Bensotriazines as antivasular anticancer drugs				
Funding Agency:	Natural Sciences and Engineering Research Council of Canada (NSERC)				
Funding Title:	Dynamic Contrast-Enhanced MR Imaging				
Funding Agency:	Canadian Cancer Society Research Institute				
Funding Title:	Quantifying response to anticancer therapy - linking histopathology with MRI				
Funding Agency:	UBC Dean of Science				
Funding Title:	Startup Funding: Stefan A Reinsberg				
Unfunded title:	N/A				

The Animal Care Committee has examined and approved the use of animals for the above experimental project.

This certificate is valid for one year from the above start or approval date (whichever is later) provided there is no change in the experimental procedures. Annual review is required by the CCAC and some granting agencies.

A copy of this certificate must be displayed in your animal facility.

Office of Research Services and Administration
102, 6190 Agronomy Road, Vancouver, BC V6T 1Z3
Phone: 604-827-5111 Fax: 604-822-5093

D. Animal Care Certificate: A07-0404



THE UNIVERSITY OF BRITISH COLUMBIA

ANIMAL CARE CERTIFICATE

Application Number: A07-0404				
Investigator or Course Director: Andrew L. Minchinton				
Department: Pathology & Laboratory Medicine				
Animals:				
<table border="1"><tr><td>Mice C3H/HeN 500</td></tr><tr><td>Mice C57/Bl6 500</td></tr><tr><td>Mice Nod/SCID 700</td></tr></table>		Mice C3H/HeN 500	Mice C57/Bl6 500	Mice Nod/SCID 700
Mice C3H/HeN 500				
Mice C57/Bl6 500				
Mice Nod/SCID 700				
Start Date:	October 1, 2007	Approval Date:	November 19, 2008	
Funding Sources:				
Funding Agency:	Canadian Institutes of Health Research (CIHR)			
Funding Title:	Extravascular distribution of anticancer drugs			
Unfunded title:	N/A			

The Animal Care Committee has examined and approved the use of animals for the above experimental project.

This certificate is valid for one year from the above start or approval date (whichever is later) provided there is no change in the experimental procedures. Annual review is required by the CCAC and some granting agencies.

A copy of this certificate must be displayed in your animal facility.

Office of Research Services and Administration
102, 6190 Agronomy Road, Vancouver, BC V6T 1Z3
Phone: 604-827-5111 Fax: 604-822-5093